AFFDL-TR-68-150

PROGRESS REPORT ON DISCRETE-ELEMENT ELASTIC AND ELASTIC-PLASTIC ANALYSES OF SHELLS OF REVOLUTION SUBJECTED TO AXISYMMETRIC AND ASYMMETRIC LOADING

Emmett A. Witmer* and James J. Kotanchik**

Massachusetts Institute of Technology

The small-deflection, linear-elastic analysis of meridionally-curved branched shells of revolution which consist of single layers, bonded double layers, and/or foam stiffening is carried out by employing single layer and bonded double layer shell discrete elements of revolution and by using solid elements of revolution of triangular or quadrilateral cross section for the core material. The characteristics of these discrete elements are reviewed and illustrative examples involving a variety of geometric and loading conditions are presented. In addition, the small deflection elastic-plastic analysis of axi- and asymmetrically-loaded shells of revolution is described, and both experimental and theoretical results are shown for an asymmetrically-loaded structure.

*Associate Professor, Department of Aeronautics and Astronautics
**Senior Research Engineer, Aeroelastic and Structures Research Laboratory

SECTION I

INTRODUCTION

The objective of this paper is to present a brief review of developments carried out at the MIT Aeroelastic and Structures Research Laboratory over the past few years* for the discrete-element elastic analysis of thin shells of revolution and of asymmetric shells (i.e., shells with cutouts and/or circumferential variations of material properties and thickness); some of the features of a typical problem are shown in Figure 1. Among the configuration and material property features included in the shell-of-revolution analysis are single layers, soft-bonded double layers, variable thickness, meridional curvature, multiple branches, isotropic and orthotropic material, thermal stresses, and core stiffening. Accordingly, the types of discrete elements developed include (a) meridionally-curved shell element of revolution (SOR element), (b) element having a shell midsurface of revolution but with other geometric and material parameters represented by circumferential Fourier harmonics (HSOR element), (c) solid of revolution element with triangular and quadrilateral cross sections (SOLOR elements), and (d) doubly-curved quadrilateral shell elements (QUASH); these discrete elements are depicted schematically in Figure 2. The salient features of these developments will be described. Because of time and space limitations, an adequate review of relevant similar developments by other researchers cannot be included in this paper; only brief reference is made to typical work in this category.

Discrete-element analyses of shells of revolution have been carried out using the conical frustum as the basic discrete element by Meyer and Harmon (Reference 1), Grafton and Strome (Reference 2), Klein (Reference 3), Lu, Penzien, and Popov** (Reference 4), and Percy, Pian, Klein, and Navaratna (Reference 5), among others. The procedures used in References 1 and 4 to compute the discrete-element stiffness matrix encounter convergence difficulties, especially where conical elements are mated with either cylindrical or flat-plate

*This research has been carried out (1) largely under sponsorship from the Air Force Space and Missile Systems Organization under Contracts AF04(694)-857 and F04694-67-C-0039, and (2) with support from the Engineering Sciences Laboratory, Picatinny Arsenal, Dover, New Jersey under Contract DA-28-017-AMC-2158(A).

**These authors also used a spherical segment element of revolution for pole regions.

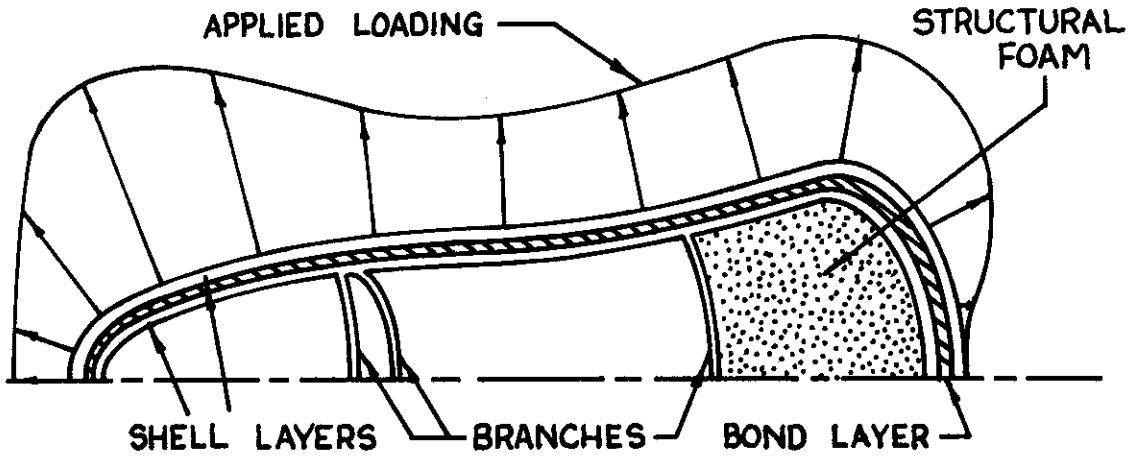

(a) Configuration and Loading

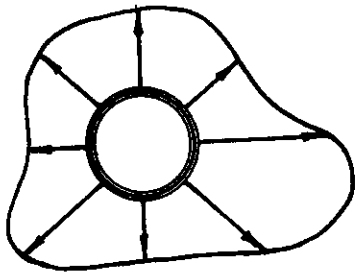

(b) Example Circumferential Variation of External Loading

Figure 1. Features of a Typical Problem

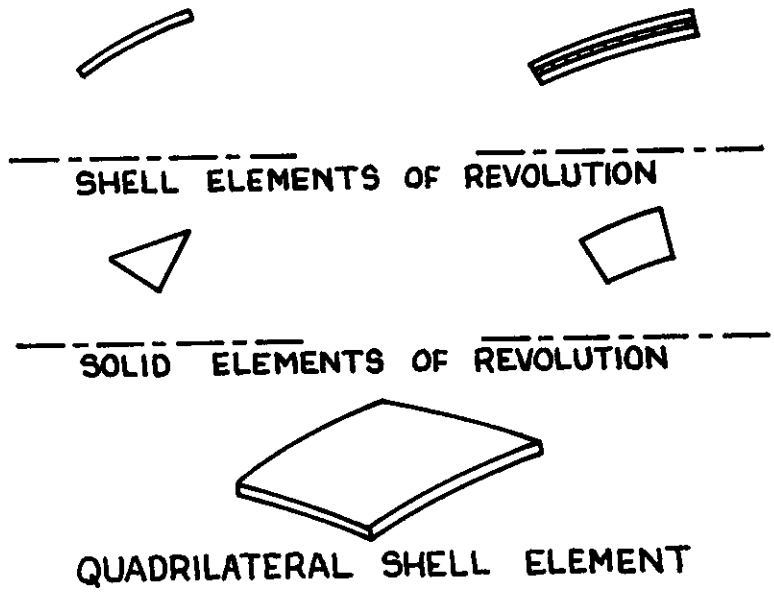

Figure 2. Schematic of Discrete Elements Analyzed

elements. Grafton and Strome used energy methods to derive the stiffness matrix, but unfortunately incurred some inaccuracy in the method used to evaluate the energy integral. This procedure was improved in References 3 and 5 where both axisymmetric and asymmetric loading conditions were included.

The application of (the better of) these conical discrete elements to the analysis of shells of revolution subjected to axisymmetric and/or asymmetric loading showed good agreement (References 5 through 7) with independent analytical and/or numerical solutions, even using relatively few discrete elements if the shell of revolution being analyzed did not have meridional curvature. However, for meridionally-curved shells of revolution, many conical discrete elements are generally required to produce an accurate solution (References 5 through 7). Since computer storage is limited and one seeks to minimize the computing time (or cost), it is desirable to keep the number of degrees of freedom to a minimum for a given desired solution accuracy. Thus, since it was expected that this improved efficiency could be realized by using a meridionally-curved discrete element for the analysis of meridionally-curved shells of revolution, the development of the stiffness and (and mass) properties of such an element was undertaken.

The results obtained by using meridionally-curved discrete elements have been reported by various authors (References 6 through 14). Although the discrete element descriptions and properties are somewhat different in the three approaches reported (References 10, 11, and 14, for example), the expected solution efficiency and accuracy by using meridionally-curved vs conical elements has been demonstrated.

For a shell having a midsurface of revolution but with circumferentially-varying structural and material parameters, the use of Fourier series to represent those circumferential variations has been employed by various investigators; for example, this type of representation has been reported in Reference 15 where finite-difference methods have been applied to the analysis of such structures. This procedure has also been used in developing the properties of the HSOR discrete element (Reference 16).

Among the analyses of bonded double-layer shells of revolution is the finite-difference analysis of Reference 17. Some predictions from that analysis are compared in this paper with the present discrete-element predictions (References 18 and 19).

Since certain shells of revolution are core stiffened (for example, being partially filled with structural foam), the use of ring elements of revolution of various cross sections to analyze this core material is a natural choice. Such elements have been developed and used by Wilson (Reference 20), Becker and Brisbane (Reference 21), Wilson and Jones (Reference 22), and Dunham and Nickell (Reference 23). The work being reported here in this category (References 24 and 25) includes results for both axisymmetric and asymmetric loading, and more comprehensive discrete-element behavior.

For analyzing asymmetric shells, quadrilateral and/or triangular curved discrete shell elements are often appropriate. Among research reported on the development of curved shell elements are that of Bogner, Fox, and Schmit (Reference 26) for a cylindrical-shell discrete element, that of Utku (Reference 27) for a doubly-curved triangular element using shallow-shell theory, and that of Cantin and Clough (Reference 28) for a cylindrical shell element which includes a proper accounting for rigid-body displacement effects. The developments reported in the present paper apply to quadrilateral shell elements whose sides are the circumferential and meridional lines of a shell of revolution; shell thickness variation and orthotropic material behavior are included in the present formulation.

In the remainder of this paper, the general formulation procedure employed is described. Then, for linear-elastic behavior, the essential aspects of the formulations for the three categories of discrete elements used for analyzing shells of revolution are given, and some illustrative results are presented. Also for the linear elastic regime, the formulation of the doubly-curved quadrilateral shell element is described. Then, the elastic-plastic static analysis of axisymmetrically- and asymmetrically-loaded shells of revolution is outlined (Reference 29), and predictions are compared with experimental results for an asymmetrically-loaded structure.

SECTION II

FORMULATION PROCEDURE

The application of variational principles to formulate discrete-element analyses of complex structures is used widely and is recognized as a very powerful approach (Reference 30). Numerous variational formulations have been devised; many of them are reviewed and classified logically in Reference 31. For the small displacement formulations which will be reviewed in this paper, the Principle of Stationary Total Potential Energy (PSTPE) together with the concept of initial strain are employed to form the governing load-deflection equations of equilibrium for analyzing (a) isothermal structures, (b) thermal stress problems, and (c) elastic-plastic structural problems.* Within this framework, the assumed-displacement version of the stiffness method is employed. This formulation is reviewed briefly in the following.

Consider the small-deflection static behavior of a structure which is represented by n discrete elements and which is subjected to body forces B_i and surface tractions T_i. Thermal strains and/or plastic strains are treated as known initial strains ϵ^o_{ij} which cause no stress. The total strains, thus, may be divided into two parts:

$$\epsilon_{ij} = \epsilon^e_{ij} + \epsilon^o_{ij} \tag{1}$$

where superscripts "e" and "o" represent (a) the elastic strain resulting from the change in stress and (b) the initial strain, respectively. Note also that $\delta\epsilon_{ij} = \delta\epsilon^e_{ij}$ since ϵ^o_{ij} is prescribed, and that the variation of the strain energy density $\hat{U}$ is given by $\delta\hat{U} = \sigma_{ij}\,\delta\epsilon^e_{ij}$. But since

$$\sigma_{ij} = E_{ijk\ell}\,\epsilon^e_{k\ell} \tag{2}$$

it follows that

$$\delta\hat{U} = E_{ijk\ell}\,\epsilon_{k\ell}\,\delta\epsilon^e_{ij} \tag{3}$$

*A similar formulation using Hamilton's Principle (or Lagrange's equations for discretized systems) can be carried out for the dynamic response problem.

Hence,

$$\hat{U} = \frac{1}{2} E_{ijk\ell}\, \epsilon^{e}_{ij}\, \epsilon^{e}_{k\ell}$$

$$= \frac{1}{2} E_{ijk\ell}\, \epsilon_{ij}\, \epsilon_{k\ell} - E_{ijk}\, \epsilon^{o}_{ij}\, \epsilon_{k\ell} + \underbrace{\frac{1}{2} E_{ijk\ell}\, \epsilon^{o}_{ij}\, \epsilon^{o}_{k\ell}}_{\text{Constant}} \tag{4}$$

Thus, for a structure consisting of n discrete elements, the total potential energy may be written as,

$$\pi_p = \sum_n \left[\int_{V_n} (\hat{U} - B_i\, u_i)\, dV - \int_S T_i\, u_i\, dS \right] \tag{5}$$

or

$$\pi_p = \sum_n \left[\int_{V_n} \left(\frac{1}{2} E_{ijk\ell}\, \epsilon_{ij}\, \epsilon_{k\ell} - E_{ijk\ell}\, \epsilon^{o}_{ij}\, \epsilon_{k\ell} - B_i\, u_i \right) dV \right.$$

$$\left. - \int_S T_i\, u_i\, dS \right] + \text{constant} \tag{6}$$

In Equation 6, the body force B_i, the surface traction T_i, and the initial strain ϵ^{o}_{ij} are all prescribed (or otherwise are known). By invoking appropriate displacement assumptions (Kirchhoff, for example), choosing appropriate assumed-displacement fields and associated generalized displacements, and employing appropriate strain-displacement relations, one can express the total strain ϵ_{ij} in terms of the generalized displacements q. Then by invoking generalized displacement compatibility between adjacent discrete elements and applying the PSTPE

$$\delta \pi_p = 0$$

where only displacement variations are permitted, the load-deflection equations of static equilibrium are obtained and are found to be of the form:

$$\mathbf{K}\,\mathbf{q} = \mathbf{F} + \mathbf{F}^{o} \tag{7}$$

where

$\mathbf{K}$ = usual stiffness matrix for the complete assembled discretized structure

$\mathbf{q}$ = generalized displacements of the discretized structure

$\mathbf{F}$ = load vector of prescribed applied generalized nodal forces

$\mathbf{F}^{o}$ = load vector of equivalent generalized nodal forces due to the initial strains

Applying this initial-strain approach to the small-deflection behavior of a nonuniformly-heated, statically-loaded structure, one proceeds by treating the thermal strains

$$\epsilon^{t}_{ij} = \delta_{ij} \alpha \Delta T \tag{8}$$

as initial strains. Thus,

$$\epsilon^{o}_{ij} \equiv \epsilon^{t}_{ij} = \delta_{ij} \alpha \Delta T \tag{9}$$

Then Equation 6 for the Total Potential Energy of the system becomes

$$\pi_p = \sum_n \left[\int_{V_n} \left(\frac{1}{2} E_{ijk\ell} \epsilon_{ij} \epsilon_{k\ell} - E_{ijk\ell} \epsilon^{t}_{ij} \epsilon_{ij} - B_i u_i \right) dV \right.$$

$$\left. - \int_S T_i u_i \, dS \right] + \text{constant} \tag{10}$$

Now, let it be assumed, for convenience of discussion, that there are no body forces acting and that the externally-applied loads have been discretized into virtual-work-equivalent generalized nodal loads $\mathbf{Q}_M$. Also for simplicity and convenience, consider initially a single isolated discrete element.

For that isolated discrete element, one may choose an assumed displacement field, invoke appropriate deformation assumptions (Kirchhoff, for example), and use the strain-displacement relations to express the strain throughout the discrete element in terms of the generalized nodal displacements $\mathbf{q}$ by

$$\epsilon_{k\ell} = \mathbf{A}\,\mathbf{q} \tag{11}$$

Similarly, the thermal (initial) strains throughout that discrete element may be expressed by:

$$\epsilon^{t}_{k\ell} = \mathbf{H}\,\epsilon^{t} \tag{12}$$

where $\mathbf{H}$ is a thermal strain distribution matrix and ϵ^{t} represents the known thermal strains at a finite number of reference points in the element. In matrix form Equation 10 applied to this isolated discrete element becomes

$$\pi_p = \int_V \left(\frac{1}{2} \mathbf{q}^T \mathbf{A}^T \mathbf{E} \mathbf{A} \mathbf{q} - \mathbf{q}^T \mathbf{A}^T \mathbf{E} \mathbf{H} \epsilon^{t} \right.$$

$$\left. + \frac{1}{2} \epsilon^{tT} \mathbf{H}^T \mathbf{E} \mathbf{H} \epsilon^{t} \right) dV - \mathbf{q}^T \mathbf{Q}_M \tag{13}$$

Applying the PSTPE by setting $\delta \pi_p = 0$, and since the δ_q^T are independent and arbitrary, one obtains:

$$\mathbf{k}\,\mathbf{q} = \mathbf{Q}_M + \mathbf{T}\,\boldsymbol{\epsilon}^t \tag{14}$$

where

$$\mathbf{k} = \int_V \mathbf{A}^T\,\mathbf{E}\,\mathbf{A}\,dV = \text{usual stiffness matrix} \tag{15}$$

$$\mathbf{T} = \int_V \mathbf{A}^T\,\mathbf{E}\,\mathbf{H}\,dV \tag{16}$$

$$\mathbf{T}\,\boldsymbol{\epsilon}^t = \text{thermal force vector} \tag{17}$$

This variational formulation can be carried through readily from Equation 10 to obtain the following corresponding load-deflection equation of static equilibrium for the complete assembled discretized structure:

$$\mathbf{K}\,\mathbf{q} = \mathbf{F}_M + \mathbf{F}_t \tag{18}$$

where $\mathbf{K}$, $\mathbf{F}_n$ and $\mathbf{F}_t$ represent the assembled stiffness matrix, the assembled generalized mechanical load vector, and the assembled thermal force vector for the complete assembled discretized structure.

Alternatively, the effects of heating ΔT (in shells, for example) may be taken into account in the discrete-element method by employing the well-known approach wherein equivalent midsurface loads are used to represent ΔT effects (References 32 and 33). These equivalent loads may be defined and determined by requiring that static equilibrium of an infinitesimal segment $r\,d\theta\,ds$ of the shell element be satisfied. However, employing these equivalent loads in the assumed displacement version of the stiffness method will be somewhat inconsistent (although often convenient) since in the assumed displacement method, equilibrium of the discrete element as a whole is assured but local equilibrium in the interior of the discrete element will not, in general, be satisfied. This inconsistency is avoided in the variational formulation described above.

Finally, by writing the kinetic energy in terms of the generalized velocities while using velocity distributions which are consistent with the assumed displacement distributions, one may determine consistent generalized mass matrices for each discrete element. Although this has been done for each discrete element in the cited References, no further mention is made of mass matrices in this paper because of space limitations.

SECTION III

LINEAR ELASTIC ANALYSES

Consider a statically-loaded, heated or unheated, shell which is in equilibrium under externally-applied loads. Let it be assumed that the structure has been appropriately discretized as depicted, for example, in Figure 3. Also, let it be assumed that all of the externally-applied distributed and/or concentrated loads have been converted into virtual-work equivalent generalized nodal loads such as indicated in Figure 4; this determination will involve the assumed-displacement field (to be discussed) associated with each type of discrete element used.* The essential remaining steps pertain to the development of the stiffness, mass, and load matrices for each type of discrete element.

The determination of the stiffness and load matrices (identified in Equation 14 for individual discrete elements and in Equation 15 for the complete assembled discretized structure) is routine with the initial-strain, variational formulation after having chosen, for each type of discrete element employed:

(a) appropriate displacement assumptions,

(b) appropriate assumed-displacement fields and associated generalized displacements,

(c) appropriate strain-displacement relations, and

(d) appropriate stress-strain laws.

Hence, the remainder of this section will be devoted to describing items (a), (b), and (c) for each type of element** treated. The determination of (1) virtual-work-equivalent generalized nodal loads and (2) consistent mass matrices is both straightforward and well known; hence, discussion of these quantities is omitted in the following.

---

*For all elements of revolution, it is assumed that all applied loads, temperature fields, displacements, strains, and stresses at any given axial station may be represented by Fourier series in the circumferential coordinate θ.

**It should be noted that each discrete element has its own notation; the notation used herein from element to element is not always consistent, but is made clear from the context and the pertinent illustrations.

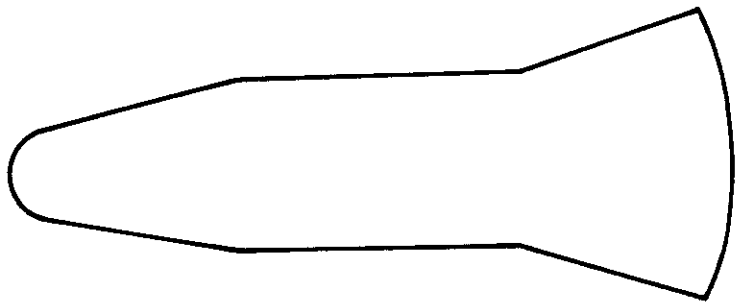

(a) Actual Structure

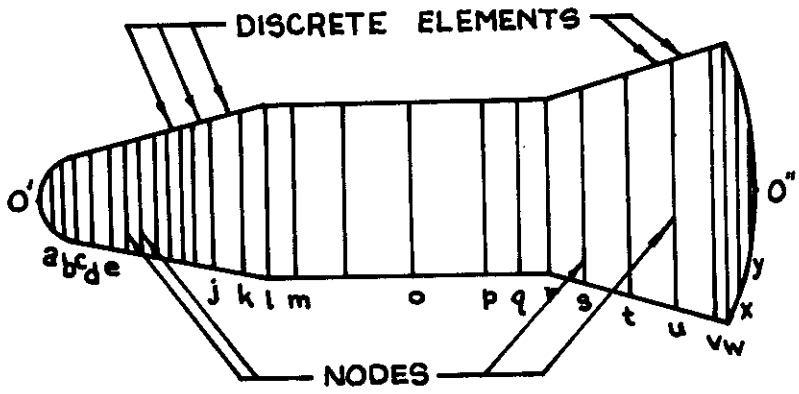

(b) Idealized Structure

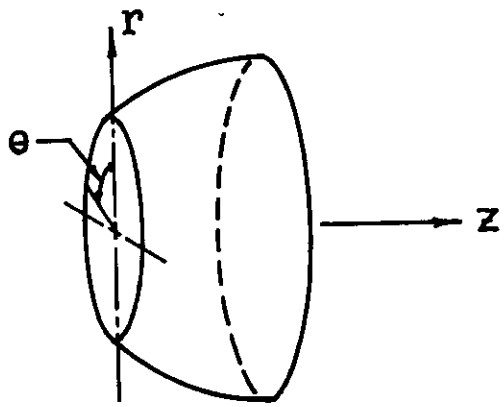

(c) Typical Meridionally-Curved Discrete Element

Figure 3. Discretization of the Structure

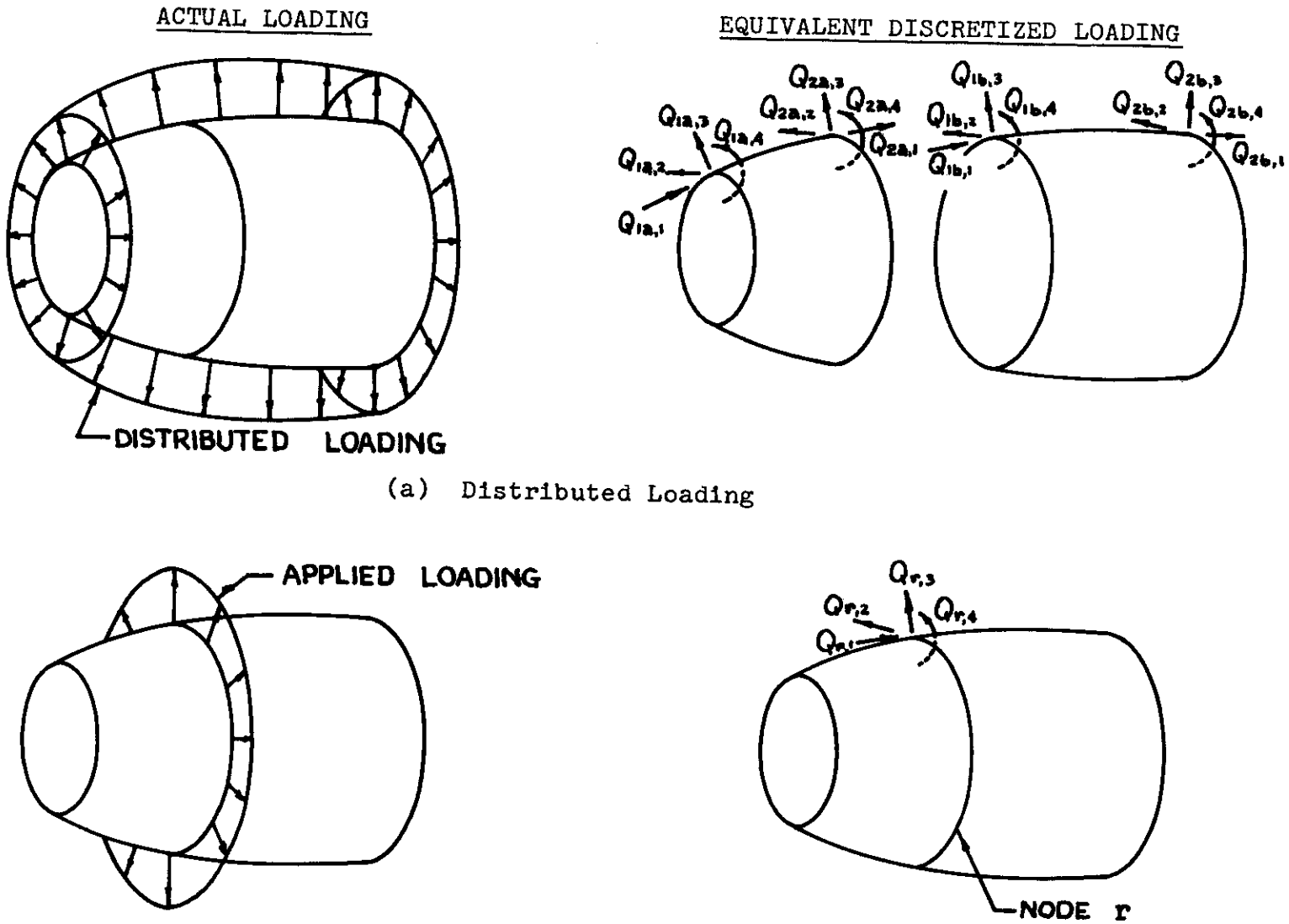

Figure 4. Schematic of Load Discretization

STRESS-STRAIN RELATIONS

For conciseness, however, the stress-strain laws to which convenient reference can be made for each type of element are now identified. Let the meridional direction (or coordinate) and the circumferential direction along the midsurface of a shell of revolution be denoted by s and θ, respectively. Considering the shell to be in a state of plane stress and to consist of orthotropic material whose principal material axes (ξ,η) are aligned at an angle β with respect to the s, θ coordinates, the stress-strain law for this material may be expressed as:

$$\begin{Bmatrix} \sigma_s \\ \sigma_\theta \\ \sigma_{s\theta} \end{Bmatrix} = \begin{vmatrix} B_{11} & B_{12} & B_{13} \\ & B_{22} & B_{23} \\ \text{Symm.} & & B_{33} \end{vmatrix} \begin{Bmatrix} \epsilon_s \\ \epsilon_\theta \\ \epsilon_{s\theta} \end{Bmatrix} - \begin{Bmatrix} C_{11}\,\Delta T \\ C_{22}\,\Delta T \\ 0 \end{Bmatrix} \tag{19}$$

where

$$\begin{aligned}
B_{11} &= E_{11}\cos^4\beta + E_{22}\sin^4\beta + 2\sin^2\beta\cos^2\beta\,(E_{12}+2E_{33}) \\
B_{12} &= E_{12}(1-2\sin^2\beta\cos^2\beta) + \sin^2\beta\cos^2\beta\,(E_{11}+E_{22}-4E_{33}) \\
B_{13} &= \sin\beta\cos\beta\left[E_{11}\cos^2\beta - E_{22}\sin^2\beta - (\cos^2\beta-\sin^2\beta)(E_{12}+2E_{33})\right]
\end{aligned} \tag{20}$$

$$\begin{aligned}
B_{22} &= E_{22}\cos^4\beta + E_{11}\sin^4\beta + 2\sin^2\beta\cos^2\beta\,(E_{12}+2E_{33}) \\
B_{23} &= -\sin\beta\cos\beta\left[E_{22}\cos^2\beta - E_{11}\sin^2\beta - (\cos^2\beta-\sin^2\beta)(E_{12}+2E_{33})\right] \\
B_{33} &= (1-4\sin^2\beta\cos^2\beta)E_{33} + \sin^2\beta\cos^2\beta(E_{11}+E_{22}-2E_{12}) \\
C_{11} &= B_{11}\alpha_\xi + B_{12}\alpha_\eta \\
C_{22} &= B_{12}\alpha_\xi + B_{22}\alpha_\eta
\end{aligned}$$

and

$$E_{11} = \frac{E_\xi}{1-\nu_\xi\nu_\eta}\;;\; E_{12} = \frac{\nu_\eta E_\xi}{1-\nu_\xi\nu_\eta}\;;\; E_{22} = \frac{E_\eta}{1-\nu_\xi\nu_\eta}\;;\; E_{33} = G_{\xi\eta} \tag{21}$$

and where

E_ξ = elastic modulus in the ξ direction

E_η = elastic modulus in the η direction

ν_ξ = Poisson's ratio in the ξ direction = $\dfrac{-\epsilon_\eta}{\epsilon_\xi}$

ν_η = Poisson's ratio in the η direction = $\dfrac{-\epsilon_\xi}{\epsilon_\eta}$

$G_{\xi\eta}$ = shear modulus (in the ξ, η plane)

α_ξ = coefficient of thermal expansion in the ξ direction

α_η = coefficient of thermal expansion in the η direction

For the non-skew orthotropic case (i. e., for $\beta = 0$), this stress-strain law reduces to

$$\begin{Bmatrix} \sigma_s \\ \sigma_\theta \\ \sigma_{s\theta} \end{Bmatrix} = \begin{bmatrix} E_{11} & E_{12} & 0 \\ & E_{22} & 0 \\ \text{Symm.} & & E_{33} \end{bmatrix} \begin{Bmatrix} \epsilon_s \\ \epsilon_\theta \\ \epsilon_{s\theta} \end{Bmatrix} - \begin{Bmatrix} \dfrac{E_s(\alpha_s + \nu_\theta \alpha_\theta)}{1 - \nu_s \nu_\theta} \Delta T \\ \dfrac{E_\theta(\alpha_\theta + \nu_s \alpha_s)}{1 - \nu_s \nu_\theta} \Delta T \\ 0 \end{Bmatrix} \tag{22}$$

where

$$E_\xi = E_s,\ E_\eta = E_\theta,\ \nu_\xi = \nu_s,\ \nu_\eta = \nu_\theta,\ \alpha_\xi = \alpha_s,\ \alpha_\eta = \alpha_\theta \text{ and } G_{\xi\eta} = G_{s\theta} \equiv G$$

Finally, for isotropic material where $E_s = E_\theta = E$; $\alpha_s = \alpha_\theta = \alpha$, and $\nu_\theta = \nu$, Equation 22 reduces to the familiar form:

$$\begin{Bmatrix} \sigma_s \\ \sigma_\theta \\ \sigma_{s\theta} \end{Bmatrix} = \begin{bmatrix} \dfrac{E}{1-\nu^2} & \dfrac{\nu E}{1-\nu^2} & 0 \\ & \dfrac{E}{1-\nu^2} & 0 \\ \text{Symm.} & & \dfrac{E}{2(1+\nu)} \end{bmatrix} \begin{Bmatrix} \epsilon_s \\ \epsilon_\theta \\ \epsilon_{s\theta} \end{Bmatrix} - \begin{Bmatrix} \dfrac{E\alpha\Delta T}{1-\nu} \\ \dfrac{E\alpha\Delta T}{1-\nu} \\ 0 \end{Bmatrix} \tag{23}$$

for the plane-stress state.

These stress-strain relations largely suffice for the present discrete element formulations pertaining to shells. For the solid of revolution elements, the more general three-dimensional elastic orthotropic stress-strain relations which are used may be found in Reference 25.

SINGLE-LAYER MERIDIONALLY-CURVED ELEMENT OF REVOLUTION (REFERENCE 13)

Geometry

The geometry of a typical meridionally-curved, variable-thickness discrete element of revolution (termed the SOR element) is shown in Figure 5; let this be termed the pth discrete element which is bounded by nodes p and p+1. At nodes p and p+1, the geometry is

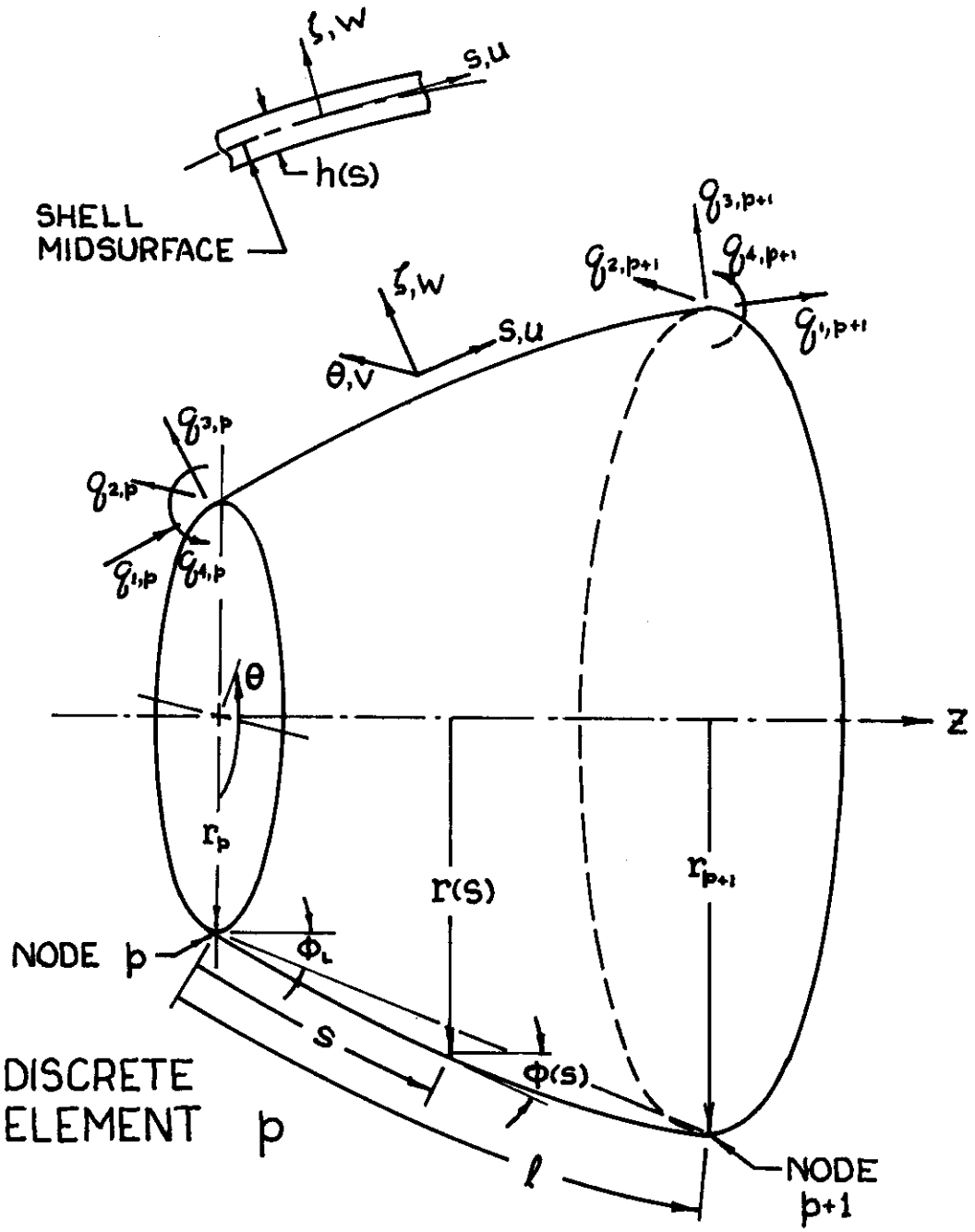

Figure 5. Geometry and Generalized Displacements for a Meridionally-Curved Single-Layer Shell Element of Revolution

characterized by radii r_p and r_{p+1}, respectively, and by meridional slopes ϕ_p and ϕ_{p+1}, respectively. It is assumed that the shell midsurface meridional slope may be described by

$$\phi(s) = a_0 + a_1 s + a_2 s^2 \tag{24}$$

where s represents the meridional distance measured from node p, and the constants a_0, a_1, and a_2 are to be determined by the following conditions:

$$\phi(s = s_p = 0) = \phi_p \tag{25}$$

$$\phi(s = s_{p+1}) = \phi_{p+1} \tag{26}$$

$$\int_0^{s_{p+1}} \sin(\phi - \phi_L)\, ds = 0 \tag{27}$$

where ϕ_L is defined by

$$\phi_L = \tan^{-1} \frac{r_{p+1} - r_p}{z_{p+1} - z_p} \tag{28}$$

If $(\phi - \phi_L)$ is small, Equation 27 may be replaced by

$$\int_0^{s_{p+1}} (\phi - \phi_L)\, ds = 0 \tag{29}$$

For convenience, let the meridional length s_{p+1} of the element be approximated by the length ℓ of a circular arc passing through nodes p and p+1 at the proper slopes; ℓ is given by

$$\ell = \frac{L(\phi_{p+1} - \phi_p}{2 \sin\left(\frac{\phi_{p+1} - \phi_p}{2}\right)} \tag{30}$$

where L is the chord length which is given by

$$L = \left[(r_{p+1} - r_p)^2 + (z_{p+1} - z_p)^2\right]^{1/2} \tag{31}$$

Setting $s_{p+1} = \ell$ and applying Equation 24 to Equations 25, 26 and 29,

$$a_0 = \phi_p \tag{32}$$

$$a_1 = \frac{6\phi_L - 4\phi_p - 2\phi_{p+1}}{\ell} \tag{33}$$

$$a_2 = \frac{3\phi_p + 3\phi_{p+1} - 6\phi_L}{\ell^2} \tag{34}$$

The midsurface radius r(s) may be expressed as

$$r(s) = r_p + \int_0^s \sin\phi\, ds \tag{35}$$

Also, for convenience, the shell thickness h(s) is assumed to vary linearly with s from node p to node p + 1:

$$h(s) = h_p - \frac{s}{\ell}(h_p - h_{p+1}) \tag{36}$$

STRAIN-DISPLACEMENT RELATIONS

The shell is assumed to be thin and to obey the Kirchhoff assumptions that straight-line normals to the midsurface before deformation (a) remain straight and normal to the midsurface and (b) retain their original lengths after deformation.

The engineering* components of the midsurface strains (subscript "o") and curvature changes are given by the following strain-displacement relations, for a thin shell of revolution with a curved meridian, as derived from the general theory of Novozhilov (Reference 34):

$$(\epsilon_s)_o = \frac{\partial u}{\partial s} - w\frac{\partial \phi}{\partial s} \tag{37}$$

$$(\epsilon_{s\theta})_o = \frac{1}{r}\left(r\frac{\partial v}{\partial s} - v\sin\phi + \frac{\partial u}{\partial \theta}\right). \tag{38}$$

$$(\epsilon_\theta)_o = \frac{1}{r}\left(\frac{\partial v}{\partial \theta} + u\sin\phi + w\cos\phi\right) \tag{39}$$

$$\kappa_s = -\left(\frac{\partial^2 w}{\partial s^2} + u\frac{\partial^2 \phi}{\partial s^2} + \frac{\partial u}{\partial s}\frac{\partial \phi}{\partial s}\right) \tag{40}$$

$$\kappa_{s\theta} = \frac{2}{r}\left[-\frac{\partial^2 w}{\partial s\,\partial \theta} + \frac{\sin\phi}{r}\frac{\partial w}{\partial \theta} + \cos\phi\frac{\partial v}{\partial s} - \frac{\sin\phi\cos\phi}{r}v - \frac{\partial \phi}{\partial s}\frac{\partial u}{\partial \theta}\right] \tag{41}$$

$$\kappa_\theta = -\frac{1}{r}\left[\frac{1}{r}\frac{\partial^2 w}{\partial \theta^2} - \frac{\cos\phi}{r}\frac{\partial v}{\partial \theta} + \left(\frac{\partial w}{\partial s} + u\frac{\partial \phi}{\partial s}\right)\sin\phi\right] \tag{42}$$

where u, v, and w are the shell midsurface displacements.

---

*Note that the present "engineering" definition of $(\epsilon_{s\theta})_o$ is conventional (Reference 32), but $\kappa_{s\theta}$ is not. However, these quantities are defined such that the shear stress $\sigma_{s\theta}$ at any distance ζ from the midsurface may be expressed as $\sigma_{s\theta} = G\left[(\epsilon_{s\theta})_o + \zeta\kappa_{s\theta}\right]$

It is convenient to represent the circumferential variation of the displacements at any meridional station s by Fourier series as:

$$u(s,\theta) = u^{(0)}(s) + \sum_{j=1}^{\infty} u^{(j)}(s)\cos j\theta + \sum_{j=1}^{\infty} \bar{u}^{(j)}(s)\sin j\theta$$

$$v(s,\theta) = v^{(0)}(s) + \sum_{j=1}^{\infty} v^{(j)}(s)\sin j\theta + \sum_{j=1}^{\infty} \bar{v}^{(j)}(s)\cos j\theta \qquad (43)$$

$$w(s,\theta) = w^{(0)}(s) + \sum_{j=1}^{\infty} w^{(j)}(s)\cos j\theta + \sum_{j=1}^{\infty} \bar{w}^{(j)}(s)\sin j\theta$$

The unbarred coefficients are referred to herein as the A-series and the barred (¯) coefficients as the B-series part of this representation. Equations 43 can be applied to Equations 37 through 42, and strain components associated with each harmonic j can be found for both the A-series and the B-series parts.

When a pole occurs, r = 0, and a singularity is encountered in using Equations 37, 38, 39, 40, 41, and 42 to develop the element stiffness matrix. However, Greenbaum (Reference 56) has shown that the proper strain-displacement relations at a pole depend upon the particular Fourier harmonic of displacement involved; these relations may be applied when required. For dome-ended shells of revolution, the A-series pole strain-displacement relations for any harmonic (j = 0, 1, 2, . . .) are:

$$(\epsilon_s^{(j)})_o = \frac{\partial u^{(j)}}{\partial s} - w^{(j)}\frac{\partial \phi}{\partial s} \qquad (44)$$

$$(\epsilon_{s\theta}^{(j)})_o = -j\frac{\partial u^{(j)}}{\partial s} \qquad (45)$$

$$(\epsilon_\theta^{(j)})_o = \frac{\partial u^{(j)}}{\partial s} - w^{(j)}\frac{\partial \phi}{\partial s} + j\frac{\partial v^{(j)}}{\partial s} \qquad (46)$$

$$\kappa_s^{(j)} = -\frac{\partial}{\partial s}\left(\frac{\partial w^{(j)}}{\partial s} + u^{(j)}\frac{\partial \phi}{\partial s}\right) \qquad (47)$$

$$\kappa_{s\theta}^{(j)} = +j\frac{\partial}{\partial s}\left(\frac{\partial w^{(j)}}{\partial s} + u^{(j)}\frac{\partial \phi}{\partial s}\right) \qquad (48)$$

$$\kappa_\theta^{(j)} = -\frac{\partial}{\partial s}\left(\frac{\partial w^{(j)}}{\partial s} + u^{(j)}\frac{\partial \phi}{\partial s}\right) + \frac{j^2}{2}\frac{\partial^2 w^{(j)}}{\partial s^2} - j\frac{\partial \phi}{\partial s}\frac{\partial v^{(j)}}{\partial s} \qquad (49)$$

It may be noted that* at r = 0

$$(a)\ \text{for } j=0: \quad u=v=\left(\frac{\partial w}{\partial s}+u\frac{\partial \phi}{\partial s}\right)=0 \tag{50}$$

$$(b)\ \text{for } j=1: \quad u+v=0 \quad \text{and} \quad w=0 \tag{51}$$

$$(c)\ \text{for } j\geq 2: \quad u=v=w=\frac{\partial w}{\partial s}=0 \tag{52}$$

Similarly for the B-series part, corresponding pole strain-displacement relations may be obtained from Equations 44 through 49 by replacing unbarred quantities by barred ($\bar{}$) quantities and j by (-j). Again $(\epsilon^{(j)}_{s\theta})_o$ and $\kappa^{(j)}_{s\theta}$ are defined in the sense of the footnote following Equation 37.

The engineering strains at any ζ-location in the shell may be expressed in terms of the midsurface strains and curvature changes by:

$$\epsilon^{(j)}_{s} = (\epsilon^{(j)}_{s})_o + \zeta \kappa^{(j)}_{s} \tag{53}$$

$$\epsilon^{(j)}_{s\theta} = (\epsilon^{(j)}_{s\theta})_o + \zeta \kappa^{(j)}_{s\theta} \tag{54}$$

$$\epsilon^{(j)}_{\theta} = (\epsilon^{(j)}_{\theta})_o + \zeta \kappa^{(j)}_{\theta} \tag{55}$$

Generalized Displacements and the Assumed Displacement Fields

The generalized displacements q of the discrete element are defined to be the midsurface meridional, circumferential, and normal (ζ-direction) displacements and the total meridional rotation at each end or node (p and p+1) of the discrete element (Figure 5):

At $s=0$	At $s=\ell$
$q_{1,p} = u(o)$	$q_{1,p+1} = u(\ell)$
$q_{2,p} = v(o)$	$q_{2,p+1} = v(\ell)$
$q_{3,p} = w(o)$	$q_{3,p+1} = w(\ell)$
$q_{4,p} = \left(\frac{\partial w}{\partial s}+u\frac{\partial \phi}{\partial s}\right)_{s=o}$	$q_{4,p+1} = \left(\frac{\partial w}{\partial s}+u\frac{\partial \phi}{\partial s}\right)_{s=\ell}$

(56)

*While Equations 50 through 52 are consistent with Greenbaum's pole strain-displacement relations, none of these is imposed in the SABOR 4 program of Reference 36 as a boundary condition.

Since one may express u, v, and w by Fourier series (see Equation 43), and since the q's may be expressed similarly:

$$\begin{aligned}
q_1 &= q_1^{(o)} + \sum_{j=1}^{8} q_1^{(j)} \cos j\theta + \sum_{j=1}^{8} \bar{q}_1^{(j)} \sin j\theta \\
q_2 &= q_2^{(o)} + \sum_{j=1}^{8} q_2^{(j)} \sin j\theta + \sum_{j=1}^{8} \bar{q}_2^{(j)} \cos j\theta \\
q_3 &= q_3^{(o)} + \sum_{j=1}^{8} q_3^{(j)} \cos j\theta + \sum_{j=1}^{8} \bar{q}_3^{(j)} \sin j\theta \\
q_4 &= q_4^{(o)} + \sum_{j=1}^{8} q_4^{(j)} \cos j\theta + \sum_{j=1}^{8} \bar{q}_4^{(j)} \sin j\theta
\end{aligned} \tag{57}$$

it follows that Equation 56 also holds for each harmonic component for both the A-series and the (barred) B-series.

The next step is to assume a reasonable meridional distribution of the midsurface (now denoted by subscript "o") displacements u_o, v_o, and w_o (for each Fourier series component):

$$\begin{aligned}
u_o^{(j)}(s) &= \alpha_1^{(j)} + \alpha_2^{(j)} s \\
v_o^{(j)}(s) &= \alpha_3^{(j)} + \alpha_4^{(j)} s \\
w_o^{(j)}(s) &= \alpha_5^{(j)} + \alpha_6^{(j)} s + \alpha_7^{(j)} s^2 + \alpha_8^{(j)} s^3
\end{aligned} \tag{58}$$

where $\alpha_1^{(j)}, \ldots, \alpha_8^{(j)}$ are constants to be determined. It should be noted that the displacement field contains all of the lower order terms from a complete set of functions. Since these displacements are shell-coordinate (s,θ,ζ) displacements, the assumed distribution does not contain the rigid-body contributions necessary for equilibrium of finite-sized elements; however, in the limit as the element size approaches zero, this requirement is fulfilled. As will be seen later, this "displacement field" deficiency has <u>not</u> resulted in inaccurate solutions of the many problems to which the present formulation has been applied.

By combining Equations 56, and 58, the $\alpha^{(j)}$'s may be expressed in terms of the generalized displacements $q^{(j)}$; in turn, $u_o^{(j)}(s)$, $v_o^{(j)}(s)$, and $w_o^{(j)}(s)$ may be expressed in terms of the $q^{(j)}$. Next, applying these expressions to the strain-displacement relations enables one to determine the strain throughout the discrete element in terms of the $q^{(j)}$. Finally, by employing appropriate stress-strain laws, one may compute the strain energy U by:

$$U = \frac{1}{2} \iiint \sigma^T \epsilon \, r \, d\theta \, ds \, d\zeta$$

$$= \frac{1}{2} q^{(o)T} k^{(o)} q^{(o)} + \sum_{j=1}^{\infty} \frac{1}{2} q^{(j)T} k^{(j)} q^{(j)} + \sum_{j=1}^{\infty} \frac{1}{2} \bar{q}^{(j)T} \bar{k}^{(j)} \bar{q}^{(j)} \qquad (59)$$

whereby one can identify and determine the individual Fourier harmonic stiffness matrices: zeroth harmonic $k^{(o)}$, A -series harmonics $k^{(j)}$ for $j = 1 \ldots \infty$, and B-series $\bar{k}^{(j)}$ for $j = 1 \ldots \infty$. Since axisymmetric geometric and material properties have been assumed, one finds that the strain energy decomposes into separate harmonic contributions. It follows, that the equations of equilibrium for this type of discrete element are completely uncoupled when isotropic or nonskew orthotropic material is involved. When skew orthotropic material is involved, harmonic coupling occurs but only between the A-series and the B-series component of a given harmonic j.

Alternate Formulation

An alternate formulation for a meridionally-curved shell discrete element of revolution in which rigid-body displacements are taken into account properly is given by Speare in Reference 25. The midsurface geometry and nomenclature used in that formulation are shown in Figure 6; also shown are the generalized nodal displacements and nodal loads referred to both local coordinates ψ, θ, x and global coordinates z, θ, r. The curved midsurface curve C_m is defined in the ψ, θ, x coordinate system by:

$$\psi = a_1 + a_2 \zeta + a_3 \zeta^2 + a_4 \zeta^3$$

$$x = a_5 + a_6 \zeta + a_7 \zeta^2 + a_8 \zeta^3 \qquad (60)$$

where ζ is the nondimensional meridional length of the midsurface line of the discrete element and the a_i may be expressed (Reference 25) in terms of the locations, slopes, arc length s_o, and chord length s_c of the element by (see Figure 6):

$$
\begin{aligned}
a_1 &= 0 \\
a_2 &= s_o \cos\phi_1 \\
a_3 &= 3s_c - 2s_o \cos\phi_1 - s_o \cos\phi_2 \\
a_4 &= -2s_c + s_o \cos\phi_1 - s_o \cos\phi_2 \\
a_5 &= 0 \\
a_6 &= s_o \sin\phi_1 \\
a_7 &= -2s_o \sin\phi_1 - s_o \sin\phi_2 \\
a_8 &= s_o \sin\phi_1 + s_o \sin\phi_2
\end{aligned}
\tag{61}
$$

Along the directions ψ, θ, and x, the midsurface displacements are $\tilde{u}$, $\tilde{v}$, and $\tilde{w}$, respectively. Generalized displacements $\tilde{q}$, corresponding to $\tilde{u}$, $\tilde{v}$, and $\tilde{w}$ are defined at each node; in addition, the meridional rotation which is given by $\frac{1}{s_o}\left[\cos\phi \frac{\partial \tilde{w}}{\partial \zeta} - \sin\phi \frac{\partial \tilde{u}}{\partial \zeta}\right]$ is defined as a fourth generalized displacement at each node. Hence, an assumed displacement field which satisfies the rigid-body requirements may be expressed, for the jAth harmonic for example, as:

$$
\begin{aligned}
\tilde{u}^{(j)} &= \beta_1^{(j)} + \beta_2^{(j)} \zeta \\
\tilde{v}^{(j)} &= \beta_3^{(j)} + \beta_4^{(j)} \zeta \\
\tilde{w}^{(j)} &= \beta_5^{(j)} + \beta_6^{(j)} \zeta + \beta_7^{(j)} \zeta^2 + \beta_8^{(j)} \zeta^3
\end{aligned}
\tag{62}
$$

HSOR ELEMENT (REFERENCE 16)

This discrete element has a meridionally-curved midsurface of revolution exactly like that of the SOR element; however, the following quantities may vary circumferentially as well as meridionally: the elastic modulus E, Poisson's ratio ν, thickness h, and shell material mass density ρ, where the material is assumed to be isotropic but not homogeneous, in general. In Reference 16, however, it is assumed for simplicity that $h \equiv h(\theta)$ and $\rho \equiv \rho(\theta)$ for each individual discrete element.

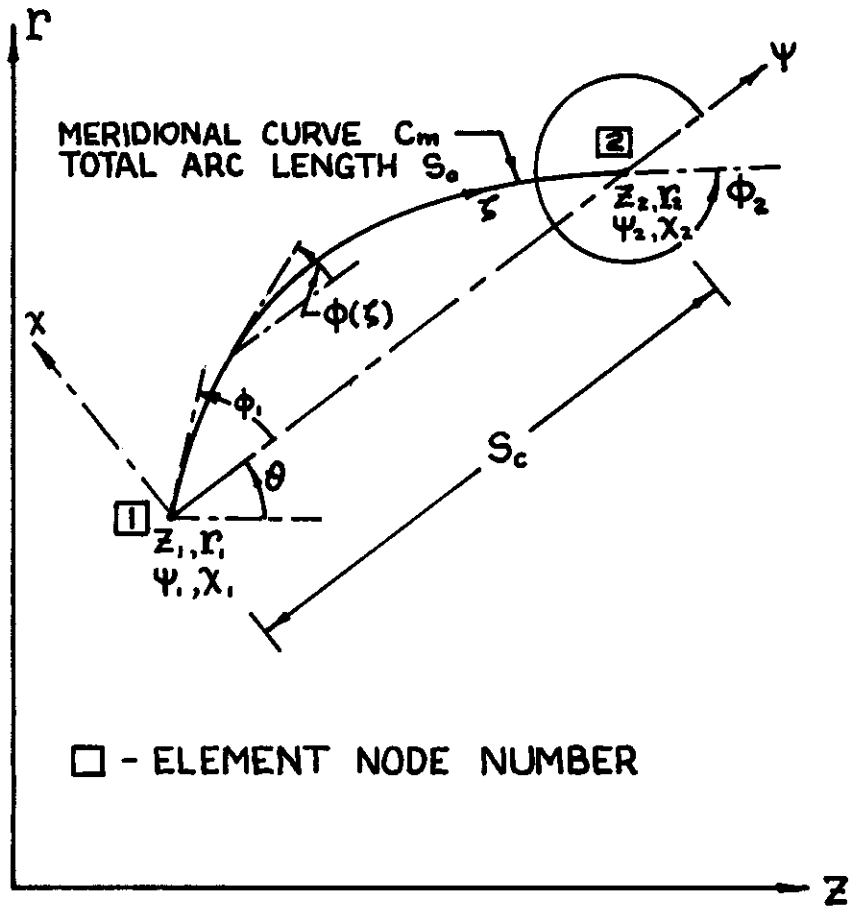

(a) Geometry

Figure 6. Geometry, Nomenclature, and Generalized Displacements for the Alternate Single-Layer Discrete Shell Element of Revolution

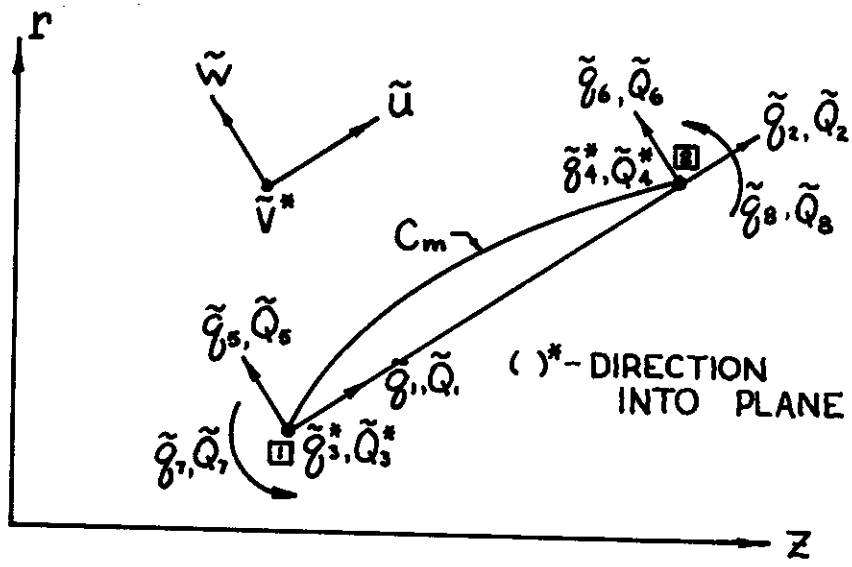

(b) Element Nodal Displacements and Nodal Forces

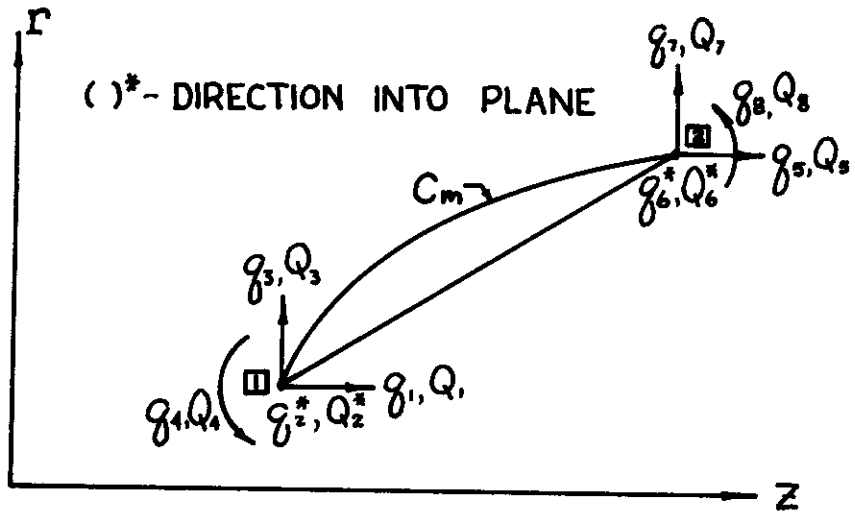

(c) Global Nodal Displacements and Nodal Forces

Figure 6 Concluded

The characterizing matrices for the HSOR discrete element may be determined in a fashion parallel to that described for the SOR element; the same assumed displacement fields, strain-displacement relations, etc., are employed. However, E and ν, or convenient combinations involving these quantities in the matrix which relates strain to stress are expressed in terms of Fourier series in θ. Thus, upon evaluating the strain energy U, it is found that extensive harmonic coupling exists; that is, the stiffness matrices are harmonically coupled. Therefore, in analyzing such structures, one must solve a (large) system of coupled equations rather than the (much smaller) harmonic-by-harmonic set which applies when true shells of revolution are involved.

BONDED DOUBLE-LAYER ELEMENT OF REVOLUTION (REFERENCE 19)

Figure 7 illustrates the geometry and displacement nomenclature for a bonded double-layer shell discrete element of revolution (termed BDL-SOR). As indicated in Figure 7, the bond layer is such that the midsurfaces of the two shell layers displace independently in the u and v directions but experience a common normal displacement w. Also, the total meridional rotation $\beta = \partial w/\partial s + u_{ob}(\partial\phi/\partial s)$ where u_{ob} is the meridional displacement at the midsurface of the bond layer; u_{ob} in turn is expressible in terms of u_u and u_ℓ, where subscripts u and ℓ denote the upper and the lower layer, respectively. The bond undergoes shearing but is assumed not to deform in the w-direction.

Six generalized displacements q at each end (s = 0 and s = ℓ_p) are used to characterize the behavior of each discrete element, as follows:

$$q_{1,p} = u_u \ (s=0)$$

$$q_{2,p} = v_u \ (s=0)$$

$$q_{3,p} = u_\ell \ (s=0)$$

$$q_{4,p} = v_\ell \ (s=0)$$

$$q_{5,p} = w \ (s=0)$$

$$q_{6,p} = \left(\frac{\partial w}{\partial s} + u_{ob}\frac{\partial\phi}{\partial s}\right)_{s=0}$$

$$
\begin{aligned}
q_{1,p+1} &= u_u \ (s=\ell_p) \\
q_{2,p+1} &= v_u \ (s=\ell_p) \\
q_{3,p+1} &= u_\ell \ (s=\ell_p) \\
q_{4,p+1} &= v_\ell \ (s=\ell_p) \\
q_{5,p+1} &= w \ (s=\ell_p) \\
q_{6,p+1} &= \left(\frac{\partial w}{\partial s} + u_{ob} \ \frac{\partial \phi}{\partial s}\right)_{s=\ell_p}
\end{aligned} \tag{63}
$$

where $u_{ob}(s,\theta)$ is given by

$$
u_{ob}(s,\theta) = K_u \ u_u(s,\theta) + K_\ell \ u_\ell(s,\theta) + \frac{1}{2} \frac{\partial \phi}{\partial s} \frac{h_u - h_\ell}{2} \frac{\partial w}{\partial s} \tag{64}
$$

In Equation 64 $h_u(s)$ and $h_\ell(s)$ are the thickness of the upper and the lower layer, respectively, and the quantities $K_u(s)$ and $K_\ell(s)$ are given by

$$
\begin{aligned}
K_u &= \frac{1}{2}\left[1 + \left(h_u + \frac{\eta}{2}\right) \frac{\partial \phi}{\partial s}\right] \\
K_\ell &= \frac{1}{2}\left[1 - \left(h_\ell + \frac{\eta}{2}\right) \frac{\partial \phi}{\partial s}\right]
\end{aligned} \tag{65}
$$

where η is the thickness of the bond layer. Hence, the total meridional rotation β is given by

$$
\beta(s) = K_u \ \frac{\partial \phi}{\partial s} \ u_u + K_\ell \ \frac{\partial \phi}{\partial s} \ u_\ell + K_w \ \frac{\partial w}{\partial s} \tag{66}
$$

where

$$
K_w(s) = 1 + \frac{1}{2} \ \frac{\partial \phi}{\partial s} \ \left(\frac{h_u - h_\ell}{2}\right) \tag{67}
$$

For this shell-of-revolution discrete element, all displacements (as well as strains, stresses, and applied loads) are considered to be represented by Fourier series. Hence, for the jth harmonic of the A-series, for example, an appropriate assumed displacement field is as follows:

$$
\begin{aligned}
u_u^{(j)}(s) &= \alpha_1^{(j)} + \alpha_2^{(j)} s \\
v_u^{(j)}(s) &= \alpha_3^{(j)} + \alpha_4^{(j)} s \\
u_\ell^{(j)}(s) &= \alpha_5^{(j)} + \alpha_6^{(j)} s \\
v_\ell^{(j)}(s) &= \alpha_7^{(j)} + \alpha_8^{(j)} s \\
w^{(j)}(s) &= \alpha_9^{(j)} + \alpha_{10}^{(j)} s + \alpha_{11}^{(j)} s^2 + \alpha_{12}^{(j)} s^3
\end{aligned} \tag{68}
$$

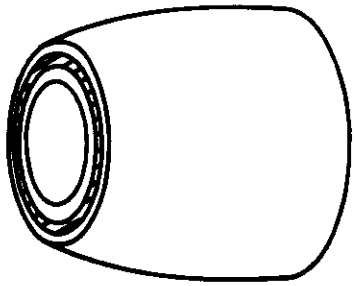

(a) Double-Layer Discrete Element

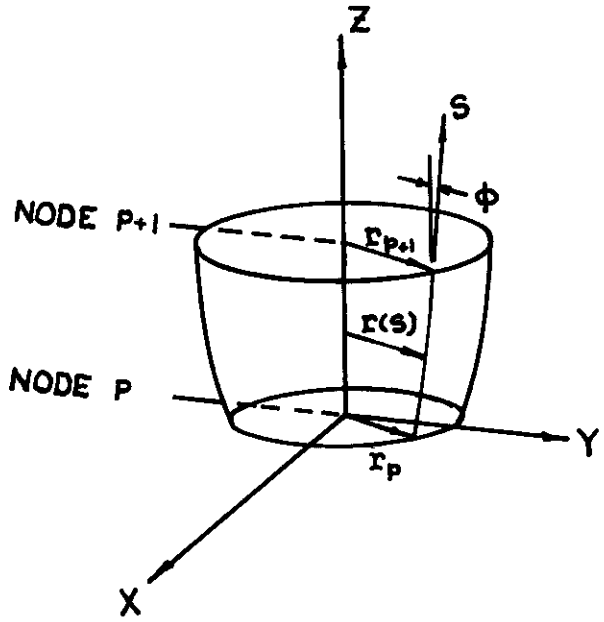

(b) Geometry

Figure 7. Geometry and Generalized Displacements for a Bonded Double-Layer Meridionally-Curved Shell Element of Revolution

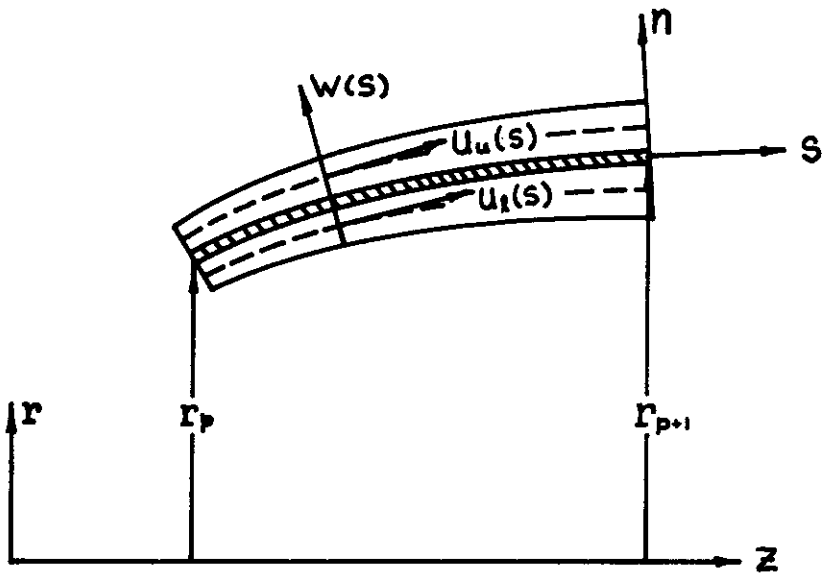

(c) In-Plane Displacements and Shell Coordinate

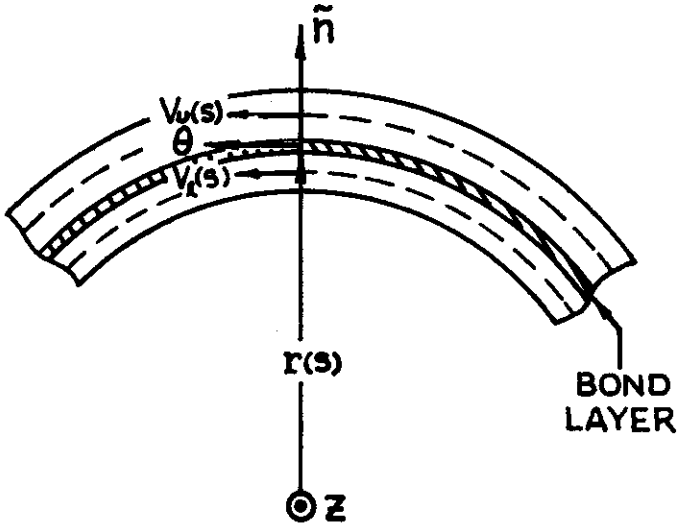

(d) Tangential Displacements and Coordinates

Figure 7 Continued

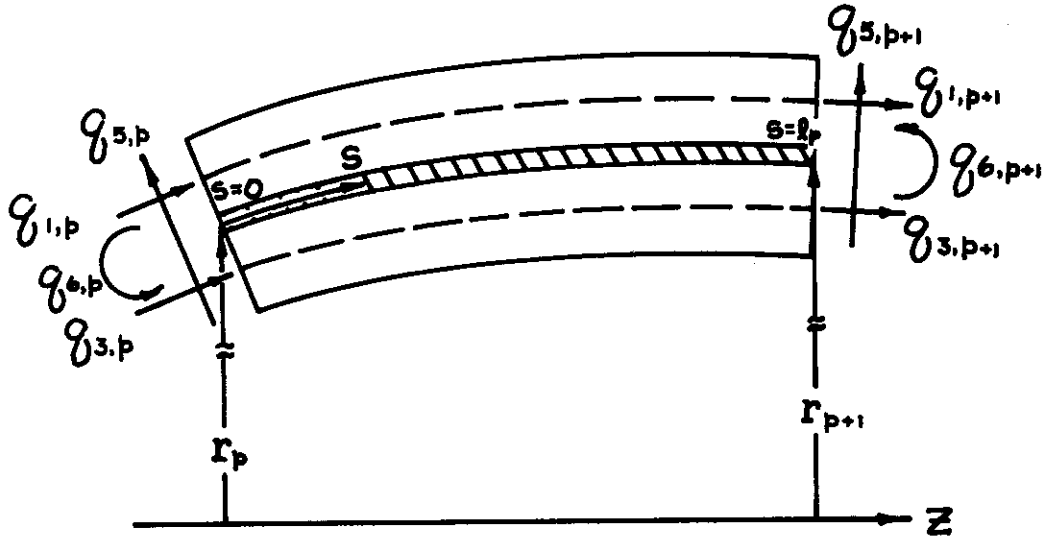

(e) In-Plane Nodal Generalized Displacements

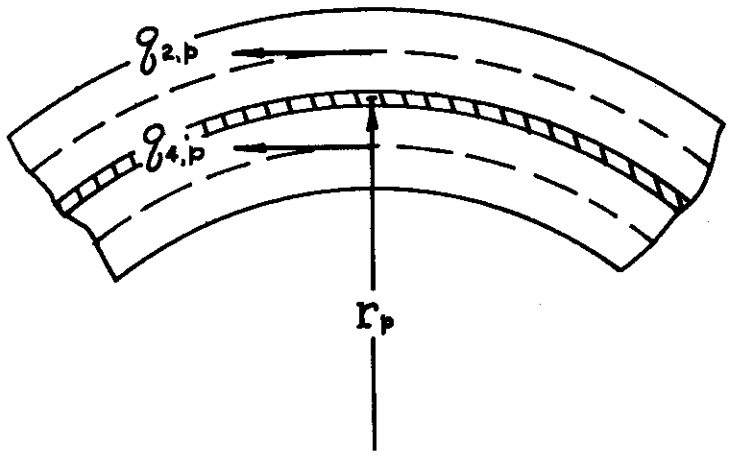

(f) Tangential Nodal Generalized Displacements

Figure 7 Concluded

where the $\alpha^{(j)}$'s, may be determined in terms of the jAth generalized displacement harmonics from Equation 63. Accordingly, this assumed displacement field for the shell layers of the discrete element is characterized completely by the 12 generalized displacements for each separate Fourier harmonic. Also, it should be noted that the assumed displacement field for the shell layers includes that for the bond layer since its u and v displacements are assumed to vary linearly through its thickness and to match those of the shell layer at each interface.

The shell is assumed to be thin and to obey in each layer (except the bond layer) the Kirchhoff assumptions that straight-line normals to the midsurface before the deformation (a) remain straight and normal to the layer midsurface and (b) retain their original lengths, after deformation.* With these assumptions and with appropriate strain-displacement relations (Equations 37 through 42) for the midsurface strains and curvature changes, one may then, with the aid of the assumed displacement field, determine the strain at any and all locations in the shell layers of the discrete element. Finally, as shown in Reference 18, the tensor components of the shear strains in the bond layer, $\epsilon^{(b)}_{s\zeta}$ and $\epsilon^{(b)}_{\theta\zeta}$, may be expressed as:

$$2\epsilon^{(b)}_{s\zeta} = \beta_1^* u_u + \beta_2^* u_\ell + \beta_3^* \frac{\partial w}{\partial s}$$
$$2\epsilon^{(b)}_{\theta\zeta} = \gamma_1^* v_u + \gamma_2^* v_\ell + \gamma_3^* \frac{\partial w}{\partial \theta} \qquad (69)$$

where

$$\gamma_1^* = \frac{1}{\eta} - \frac{h_u}{2\eta}\frac{\cos\phi}{r} - \frac{\cos\phi}{2r}$$
$$\gamma_2^* = -\frac{1}{\eta} - \frac{h_\ell}{2\eta}\frac{\cos\phi}{r} - \frac{\cos\phi}{2r}$$
$$\gamma_3^* = \left[\frac{h_u + h_\ell}{2\eta} + 1\right]\left[1 - \frac{h_u - h_\ell}{2}\frac{\cos\phi}{r}\right]\frac{1}{r} \qquad (70)$$
$$\beta_1^* = \frac{1}{\eta} + \frac{1}{2}\left[1 + \frac{h_u}{\eta}\right]\frac{\partial\phi}{\partial s}$$
$$\beta_2^* = -\frac{1}{\eta} + \frac{1}{2}\left[1 + \frac{h_\ell}{\eta}\right]\frac{\partial\phi}{\partial s}$$
$$\beta_3^* = \left[\frac{h_u + h_\ell}{2\eta} + 1\right]\left[1 + \frac{\partial\phi}{\partial s}\frac{h_u - h_\ell}{2}\right]$$

*While the shell-bond-shell combination is assumed to be thin, the thickness of the bond layer may be much greater than the facing thicknesses as in typical sandwich construction.

Treating the shell layer material as skew orthotropic and the bond layer as shear-supporting isotropic material, the appropriate stress-strain relations may be applied together with the above strain information to determine the strain energy for the complete bonded double-layer discrete element (BDL-SOR). It may be readily shown that the resulting stiffness matrices are coupled only between the A-series and the B-series of a given harmonic if the shell material is skew orthotropic, but are completely uncoupled if the shell material is either nonskew orthotropic or isotropic.

SOLID-OF-REVOLUTION ELEMENTS (REFERENCES 24 AND 25)

For analyzing the solid core regions of core-stiffened shells, solid elements of revolution (SOLOR) having triangular or quadrilateral cross sections, as depicted in Figure 8, have been developed. At each corner (node) of the so-called "core interior element" which has a triangular cross section (SOLOR-INT), three generalized displacements are chosen to characterize the behavior of this discrete element; these three displacements are $\tilde{u}$, $\tilde{v}$, and $\tilde{w}$ in the element coordinate directions ψ, θ, and x, respectively, as indicated in Figure 9a or u, v, and w in global coordinate directions x, θ, and r, respectively, as indicated in Figure 9b.

For those solid core regions which are in contact with a shell, the nodes of the solid element which bound the side which interfaces with the shell have ascribed to them a meridional-rotational degree of freedom in addition to the aforementioned three degrees of freedom at each node, in order to be compatible with the interfacing shell element; discrete elements of this character are termed "core interface" or compatible core elements. The generalized displacements and nodal loads of a compatible core element with a triangular cross section (termed SOLOR-CT) are indicated in Figures 9c and 9d, and those for a compatible core element of quadrilateral cross section (termed SOLOR-CQ) are indicated in Figure 10.

For all of these elements it is assumed that the core material is homogeneous and orthotropic with two of its principal axes lying in the r, z plane. With respect to the so-called "element coordinates" ψ, θ, x of Figures 8, 9, and 10, the stress-strain relation may be expressed as

$$\left\lfloor \tilde{\sigma}_{\psi\psi} \; \tilde{\sigma}_{xx} \; \tilde{\sigma}_{\theta\theta} \; \tilde{\sigma}_{\psi x} \; \tilde{\sigma}_{\psi\theta} \; \tilde{\sigma}_{x\theta} \right\rfloor^T = \left[\tilde{E} \right]_c \left\lfloor \tilde{\epsilon}_{\psi\psi} \; \tilde{\epsilon}_{xx} \; \tilde{\epsilon}_{\theta\theta} \; \tilde{\epsilon}_{\psi x} \; \tilde{\epsilon}_{\psi\theta} \; \tilde{\epsilon}_{x\theta} \right\rfloor^T \tag{71}$$

where the tilde (~) denotes that such quantities are referred to the element coordinates.

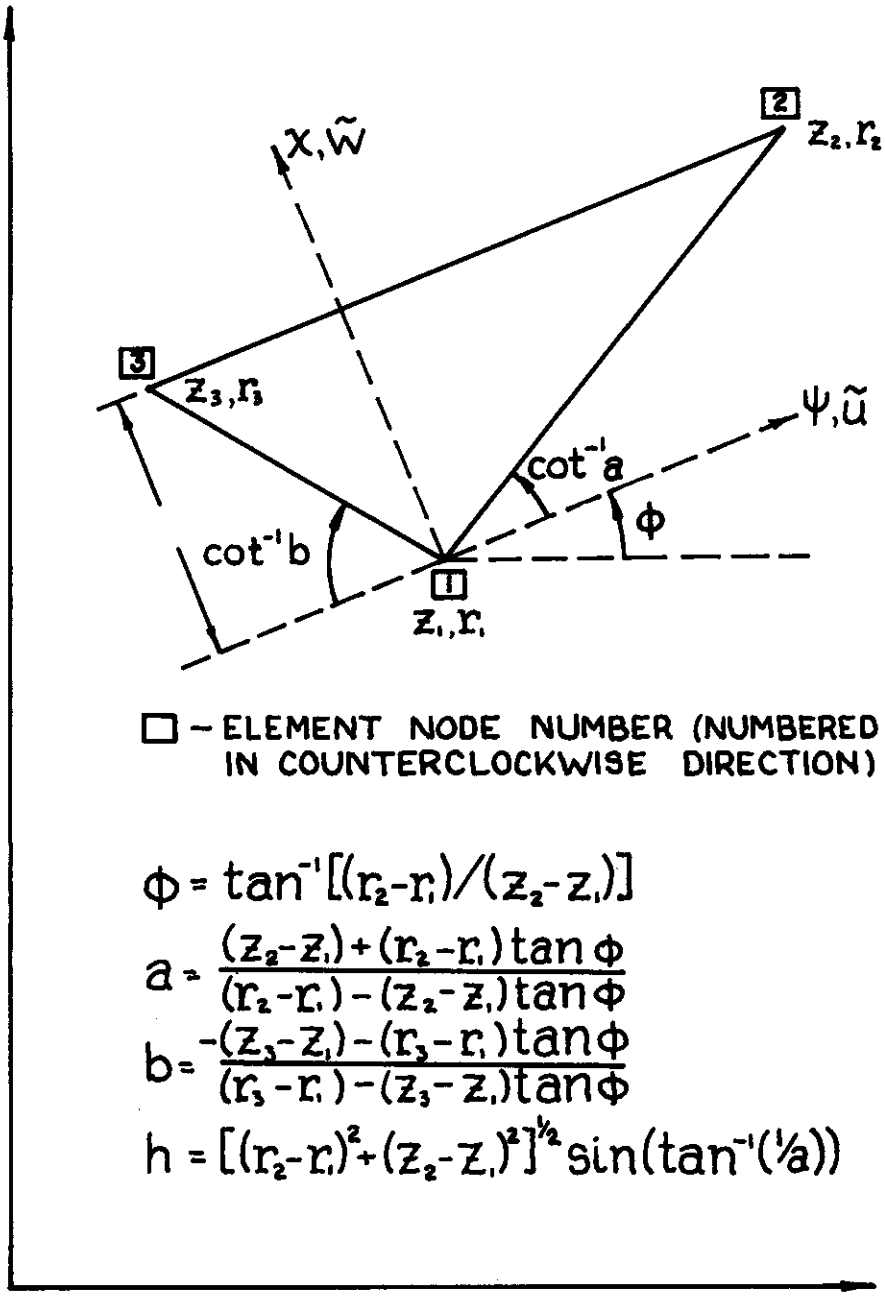

(a) Triangular Ring Element

Figure 8. Geometries of Solid of Revolution Elements

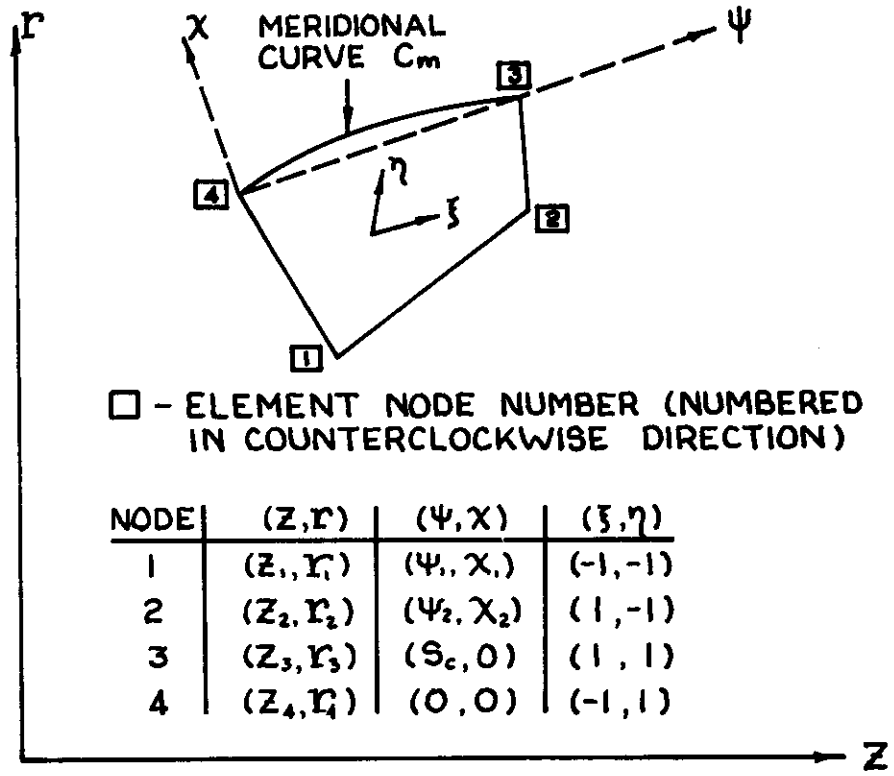

NODE	(z,r)	(ψ,χ)	(ξ,η)
1	(z_1, r_1)	(ψ_1, χ_1)	(-1,-1)
2	(z_2, r_2)	(ψ_2, χ_2)	(1,-1)
3	(z_3, r_3)	$(S_c, 0)$	(1, 1)
4	(z_4, r_4)	(0, 0)	(-1, 1)

(b) Quadrilateral Ring Element

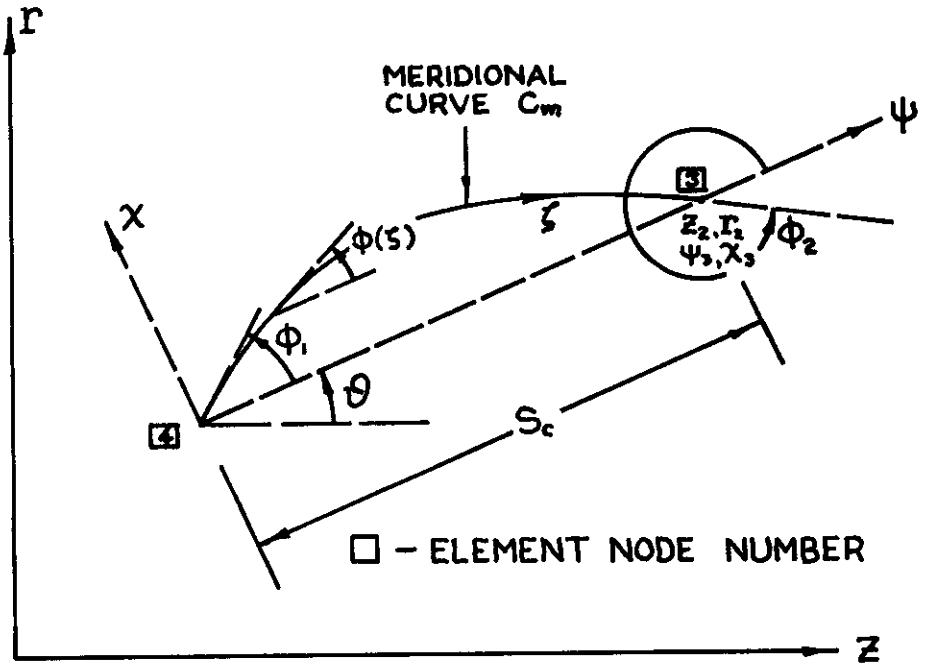

(c) Geometry of Curved Side

Figure 8 Concluded

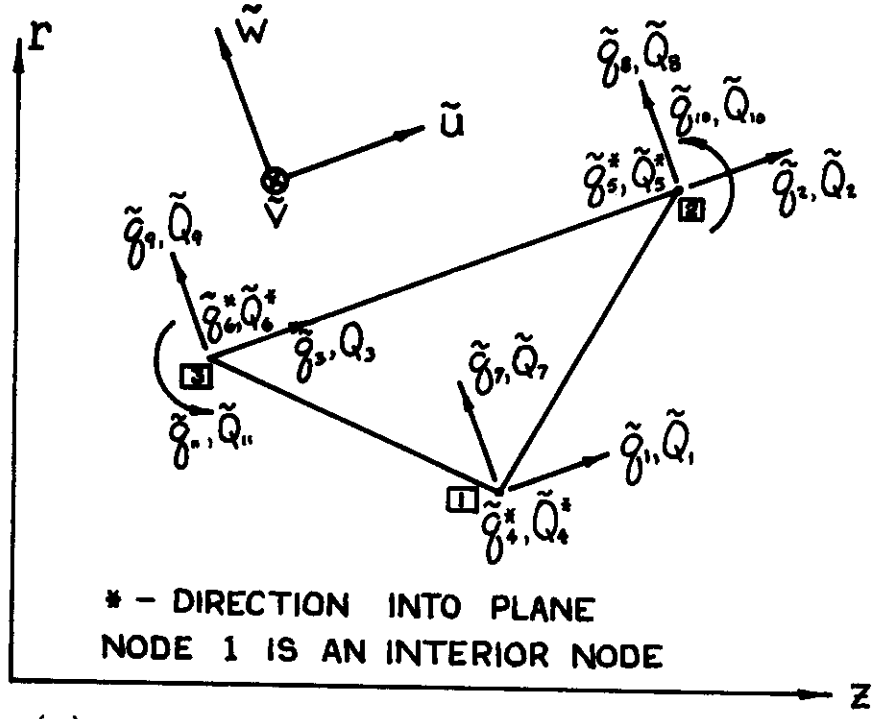

(a) Element Nodal Displacements and Forces for the Core Interface Element

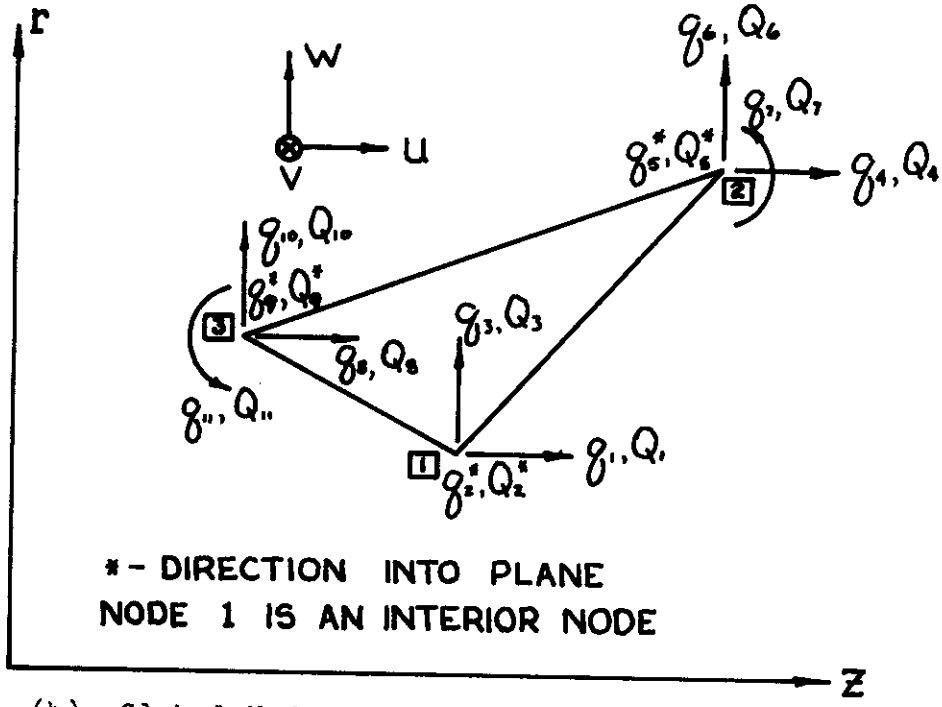

(b) Global Nodal Displacements and Forces for the Core Interface Element

Figure 9. Nodal Displacements and Nodal Loads for Triangular Solid Elements of Revolution

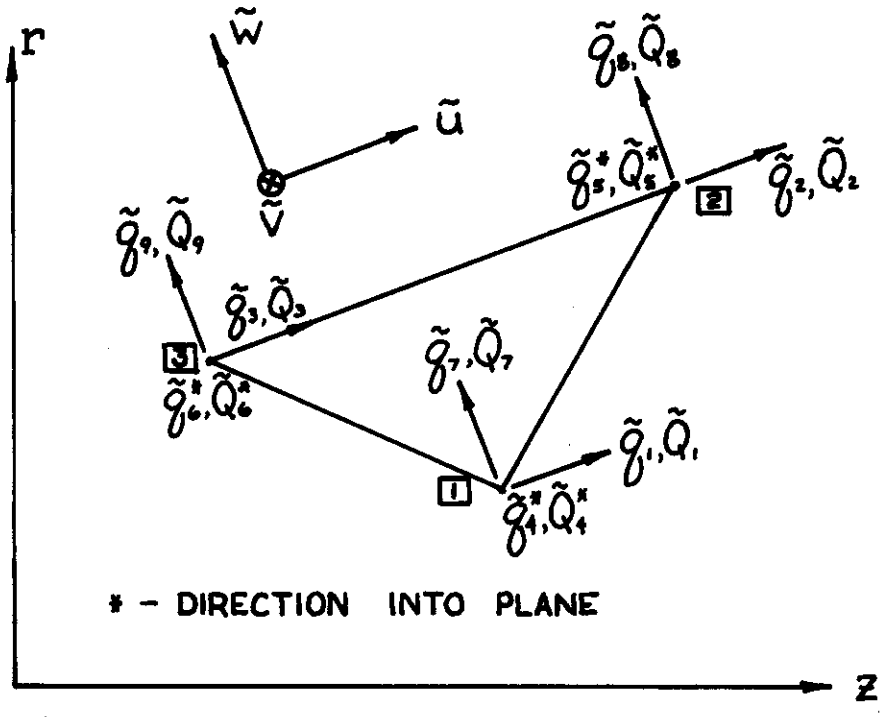

(c) Element Nodal Displacements and Forces for the Core Interior Element

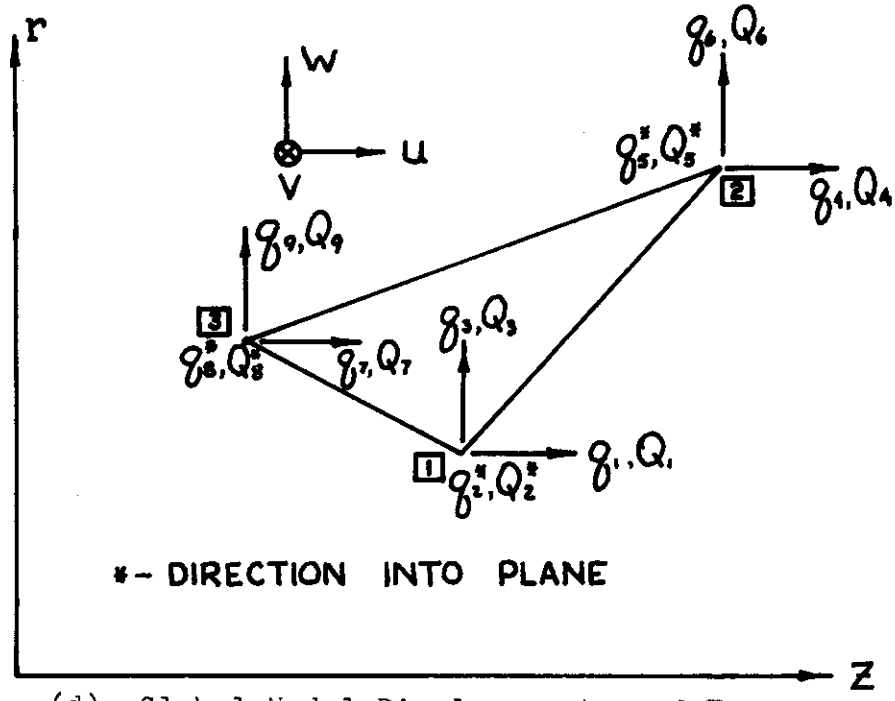

(d) Global Nodal Displacements and Forces for the Core Interior Element

Figure 9 Concluded

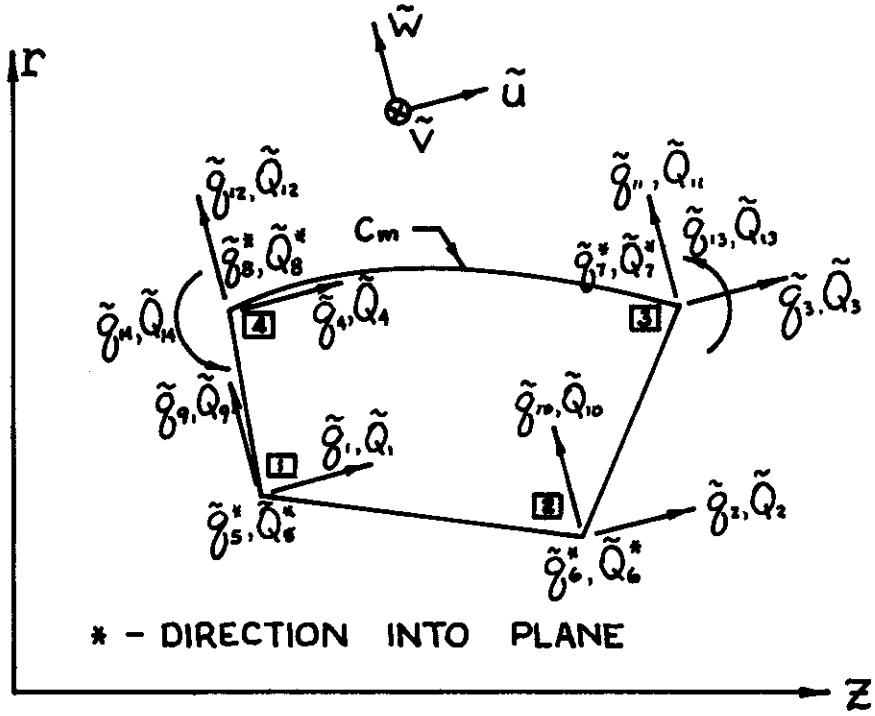

(a) Element Nodal Displacements and Nodal Forces

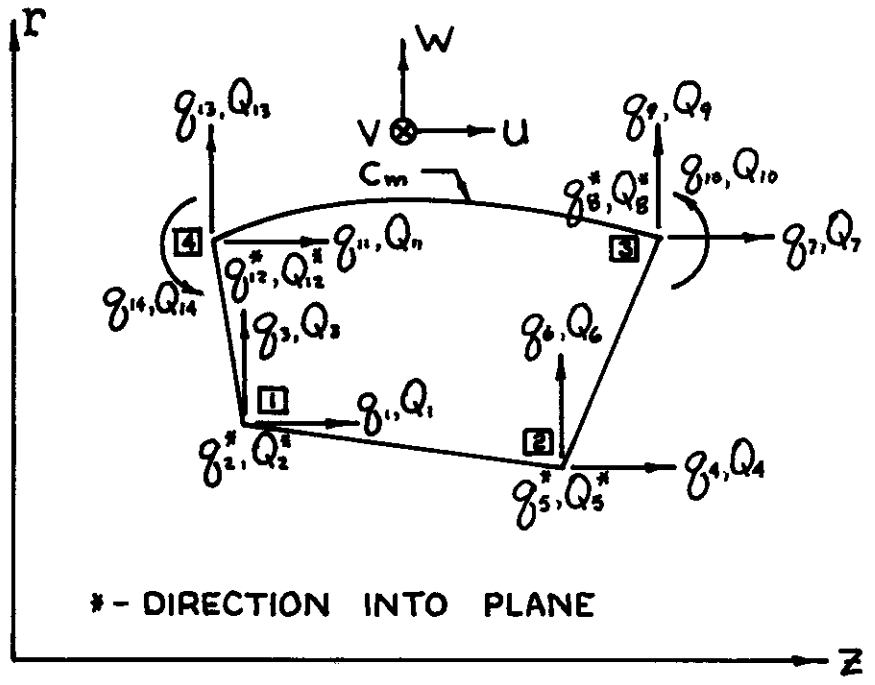

(b) Global Nodal Displacements and Nodal Forces

Figure 10. Nodal Displacements and Nodal Loads for the Quadrilateral Solid Element of Revolution (SOLOR-CQ)

For all of these elements the strain-displacement relations, in terms of the element coordinate system, are as follows (in engineering strain notation):

$$
\begin{aligned}
\tilde{\epsilon}_{\psi\psi} &= \frac{\partial \tilde{u}}{\partial \psi} \\
\tilde{\epsilon}_{xx} &= \frac{\partial \tilde{w}}{\partial x} \\
\tilde{\epsilon}_{\theta\theta} &= \frac{\tilde{u}}{r} \sin\phi + \frac{\tilde{w}}{r} \cos\phi + \frac{1}{r}\frac{\partial \tilde{v}}{\partial \theta} \\
\tilde{\epsilon}_{\psi x} &= \frac{\partial \tilde{u}}{\partial x} + \frac{\partial \tilde{w}}{\partial \psi} \\
\tilde{\epsilon}_{\psi\theta} &= \frac{\partial \tilde{v}}{\partial \psi} + \frac{1}{r}\frac{\partial \tilde{u}}{\partial \theta} - \frac{\tilde{v}}{r}\sin\phi \\
\tilde{\epsilon}_{x\theta} &= \frac{\partial \tilde{v}}{\partial x} + \frac{1}{r}\frac{\partial \tilde{w}}{\partial \theta} - \frac{\tilde{v}}{r}\cos\phi
\end{aligned}
\qquad (72)
$$

where $\tilde{u}$, $\tilde{v}$, and $\tilde{w}$ are the displacements along the element-coordinate directions ψ, θ, and x, respectively, as indicated in Figures 9 and 10.

The SOLOR-INT Element

For the interior core triangular solid element of revolution, the jAth harmonic of an appropriate assumed displacement field is:

$$
\begin{aligned}
\tilde{u}^{(j)} &= (\beta_1^{(j)} + \beta_2^{(j)}\psi + \beta_3^{(j)} x)\cos j\theta \\
\tilde{v}^{(j)} &= (\beta_4^{(j)} + \beta_5^{(j)}\psi + \beta_6^{(j)} x)\sin j\theta \\
\tilde{w}^{(j)} &= (\beta_7^{(j)} + \beta_8^{(j)}\psi + \beta_9^{(j)} x)\cos j\theta
\end{aligned}
\qquad (73)
$$

Similar expressions apply for the zeroth and for the B-series Fourier harmonic displacements. With respect to the element coordinates ψ, θ, x, one may define nine generalized displacements $\tilde{\mathbf{q}}^{(j)}$ for this element as the values of $\tilde{u}^{(j)}$, $\tilde{v}^{(j)}$, and $\tilde{w}^{(j)}$ at the three corners of the SOLOR-INT element; hence, the β's are replaced by their equivalents in terms of the $\tilde{q}^{(j)}$'s. Also, it is useful to define three generalized displacements $\mathbf{q}$ at each corner of the triangular cross section with respect to the global coordinate system z, θ, r. Quantities referred to the element coordinate system may be converted to refer to the global coordinate system by applying first or second order geometric transformations, as appropriate.

With this information one can express the strain energy in terms of the global generalized displacements $\mathbf{q}$ in order to determine the associated stiffness matrix for each harmonic. It should be noted that complete harmonic uncoupling of the stiffness matrix occurs since two of the principal planes of the orthotropic material were assumed to be in the r,z plane. For more general skew orthotropicity, coupling occurs but only between the A- and the B- series component of the same Fourier harmonic j.

The SOLAR-CT Element

For the interface (or compatible) triangular solid of revolution element, the meridional rotation, $\partial \tilde{w}/\partial \psi$ at each of the corners which bound the "interfacing side" is added as a degree of freedom. Therefore, an appropriate assumed displacement field may be obtained from Equation 73 by adding two terms to $\tilde{w}^{(j)}$ as follows:

$$\tilde{w}^{(j)} = \Big(\beta_7^{(j)} + \beta_8^{(j)} \psi + \beta_9^{(j)} x + \beta_{10}^{(j)} \left[ab\,\psi x^2 + (a-b)\psi^2 x - \psi^3 \right] + \beta_{11}^{(j)} \left[abx^3 + (a-b)\,\psi x^2 - \psi^2 x \right] \Big) \cos j\theta \tag{74}$$

The appropriate $\tilde{u}^{(j)}$ and $\tilde{v}^{(j)}$ for this element are the same as given by Equation 73.

The SOLOR-CQ Element (Reference 25)

As indicated in Figure 8b, this interfacing or compatible solid element of revolution has a quadrilateral cross section, one side of which is curved to match geometrically with a mating shell element. It is convenient to refer to the following coordinate systems in this discussion: (1) the global coordinates z, θ, r, (2) the element coordinates ψ, θ, x, and (3) the nondimensional curvilinear quadrilateral coordinates ξ, η in addition to θ. The coordinates ξ, η are defined in terms of the element coordinates ψ, x by:

$$\begin{aligned} \psi &= b_1 + b_2 \xi + b_3 \eta + b_4 \xi\eta + (\xi+1)(\xi-1)(\eta+1)(b_5 + b_6 \xi) \\ x &= b_7 + b_8 \xi + b_9 \eta + b_{10} \xi\eta + (\xi+1)(\xi-1)(\eta+1)(b_{11} + b_{12} \xi) \end{aligned} \tag{75}$$

where

$$
\begin{aligned}
b_1 &= \frac{1}{4}\left[\, 2C_1 + \psi_1 + \psi_2 \,\right] \\
b_2 &= \frac{1}{4}\left[\, 2C_1 - \psi_1 + \psi_2 \,\right] \\
b_3 &= \frac{1}{4}\left[\, 2C_1 - \psi_1 - \psi_2 \,\right] \\
b_4 &= \frac{1}{4}\left[\, 2C_1 + \psi_1 - \psi_2 \,\right] \\
b_5 &= \frac{1}{16}\left[\, 2a_3 + 3a_4 \,\right] \\
b_6 &= \frac{1}{16}\, a_4 \\
b_7 &= \frac{1}{4}\left[\, 2C_2 + x_1 + x_2 \,\right] \\
b_8 &= \frac{1}{4}\left[\, 2C_2 - x_1 + x_2 \,\right] \\
b_9 &= \frac{1}{4}\left[\, 2C_2 - x_1 - x_2 \,\right] \\
b_{10} &= \frac{1}{4}\left[\, 2C_2 + x_1 - x_2 \,\right] \\
b_{11} &= \frac{1}{16}\left[\, 2a_7 + 3a_8 \,\right] \\
b_{12} &= \frac{1}{16}\, a_8
\end{aligned}
\tag{76}
$$

and where

$$
\begin{aligned}
C_1 &= \frac{1}{2}\left[\, a_2 + a_3 + a_4 \,\right] \\
C_2 &= \frac{1}{2}\left[\, a_6 + a_7 + a_8 \,\right] \\
\psi_i &= (\, z_i - z_4 \,)\cos\theta + (\, r_i - r_4 \,)\sin\theta \\
x_i &= -(z_i - z_4)\sin\theta + (r_i - r_4)\cos\theta
\end{aligned}
\tag{77}
$$

The constants $a_1, \ldots a_8$ are given by Equation 61.

An appropriate jAth harmonic assumed displacement field $\tilde{u}$, $\tilde{v}$, and $\tilde{w}$ (see Figure 10) for the SOLOR-CQ element is given by

$$
\begin{aligned}
\tilde{u} &= (\, \beta_1 + \beta_2 \xi + \beta_3 \eta + \beta_4 \xi\eta \,)\cos j\theta \\
\tilde{v} &= (\, \beta_{11} + \beta_{12} \xi + \beta_{13} \eta + \beta_{14} \xi\eta \,)\sin j\theta \\
\tilde{w} &= \left[\, \beta_5 + \beta_6 \xi + \beta_7 \eta + \beta_8 \xi\eta + (\xi+1)(\xi-1)(\eta+1)(\beta_9\eta + \beta_{10}\xi) \right]\cos j\theta
\end{aligned}
\tag{78}
$$

and the meridional rotation γ along the shell-core interface can be defined as

$$\gamma = \frac{2}{s_o}\left(\frac{\partial \tilde{w}}{\partial \xi}\cos\phi - \frac{\partial \tilde{u}}{\partial \xi}\sin\phi\right)\Big|_{\eta=1} \tag{79}$$

It is seen that the $\tilde{u}$ and $\tilde{v}$ displacements along the curved side of the core element (i. e., along $\eta = 1$) are linear in ξ, and the $\tilde{w}$ displacement is cubic in ξ. These are in agreement with the interpolation functions given by Equation 62 for the "alternate" shell element of revolution; hence, displacement compatibility along the interelement boundary is satisfied.

Since $\tilde{u}$, $\tilde{v}$, and $\tilde{w}$ are expressed in terms of the dimensionless element coordinates ξ, η and θ, the strains are given by the following strain-displacement relations:

$$\begin{aligned}
\tilde{\epsilon}_{\psi\psi} &= \frac{\partial \tilde{u}}{\partial \xi}\frac{\partial \xi}{\partial \psi} + \frac{\partial \tilde{u}}{\partial \eta}\frac{\partial \eta}{\partial \psi} \\
\tilde{\epsilon}_{xx} &= \frac{\partial \tilde{w}}{\partial \xi}\frac{\partial \xi}{\partial x} + \frac{\partial \tilde{w}}{\partial \eta}\frac{\partial \eta}{\partial x} \\
\tilde{\epsilon}_{\theta\theta} &= \frac{\tilde{u}}{r}\sin\theta + \frac{\tilde{w}}{r}\cos\theta + \frac{1}{r}\frac{\partial \tilde{v}}{\partial \theta} \\
\tilde{\epsilon}_{\psi x} &= \frac{\partial \tilde{u}}{\partial \xi}\frac{\partial \xi}{\partial x} + \frac{\partial \tilde{u}}{\partial \eta}\frac{\partial \eta}{\partial x} + \frac{\partial \tilde{w}}{\partial \xi}\frac{\partial \xi}{\partial \psi} + \frac{\partial \tilde{w}}{\partial \eta}\frac{\partial \eta}{\partial \psi} \\
\tilde{\epsilon}_{\psi\theta} &= \frac{\partial \tilde{v}}{\partial \xi}\frac{\partial \xi}{\partial \psi} + \frac{\partial \tilde{v}}{\partial \eta}\frac{\partial \eta}{\partial \psi} + \frac{1}{r}\frac{\partial \tilde{u}}{\partial \theta} - \frac{\tilde{v}}{r}\sin\theta \\
\tilde{\epsilon}_{x\theta} &= \frac{1}{r}\frac{\partial \tilde{w}}{\partial \theta} + \frac{\partial \tilde{v}}{\partial \xi}\frac{\partial \xi}{\partial x} + \frac{\partial \tilde{v}}{\partial \eta}\frac{\partial \eta}{\partial x} - \frac{\tilde{v}}{r}\cos\theta
\end{aligned} \tag{80}$$

Quadrilateral Shell Element (Reference 37)

Figure 11 depicts the geometry, coordinate system, and displacements as well as the generalized displacements and associated generalized nodal loads which are employed to describe this quadrilateral shell element. This single-layer shell element is a portion of a shell of revolution, and its sides are lines of constant meridional location $\tilde{s}$ and of constant $\tilde{\theta}$ location, where $\tilde{s}$ and $\tilde{\theta}$ are dimensional meridional and circumferential coordinates, respectively. For convenience, dimensionless coordinates s and θ are employed and are defined such that:

$$\begin{aligned}
&\text{At } \tilde{s} = \tilde{s}_1 \;, \quad s = s_1 = -1.0 \\
&\text{At } \tilde{s} = \tilde{s}_2 \;, \quad s = s_2 = +1.0 \\
&\text{At } \tilde{\theta} = \tilde{\theta}_1 \;, \quad \theta = \theta_1 = -1.0 \\
&\text{At } \tilde{\theta} = \tilde{\theta}_2 \;, \quad \theta = \theta_2 = +1.0
\end{aligned} \tag{81}$$

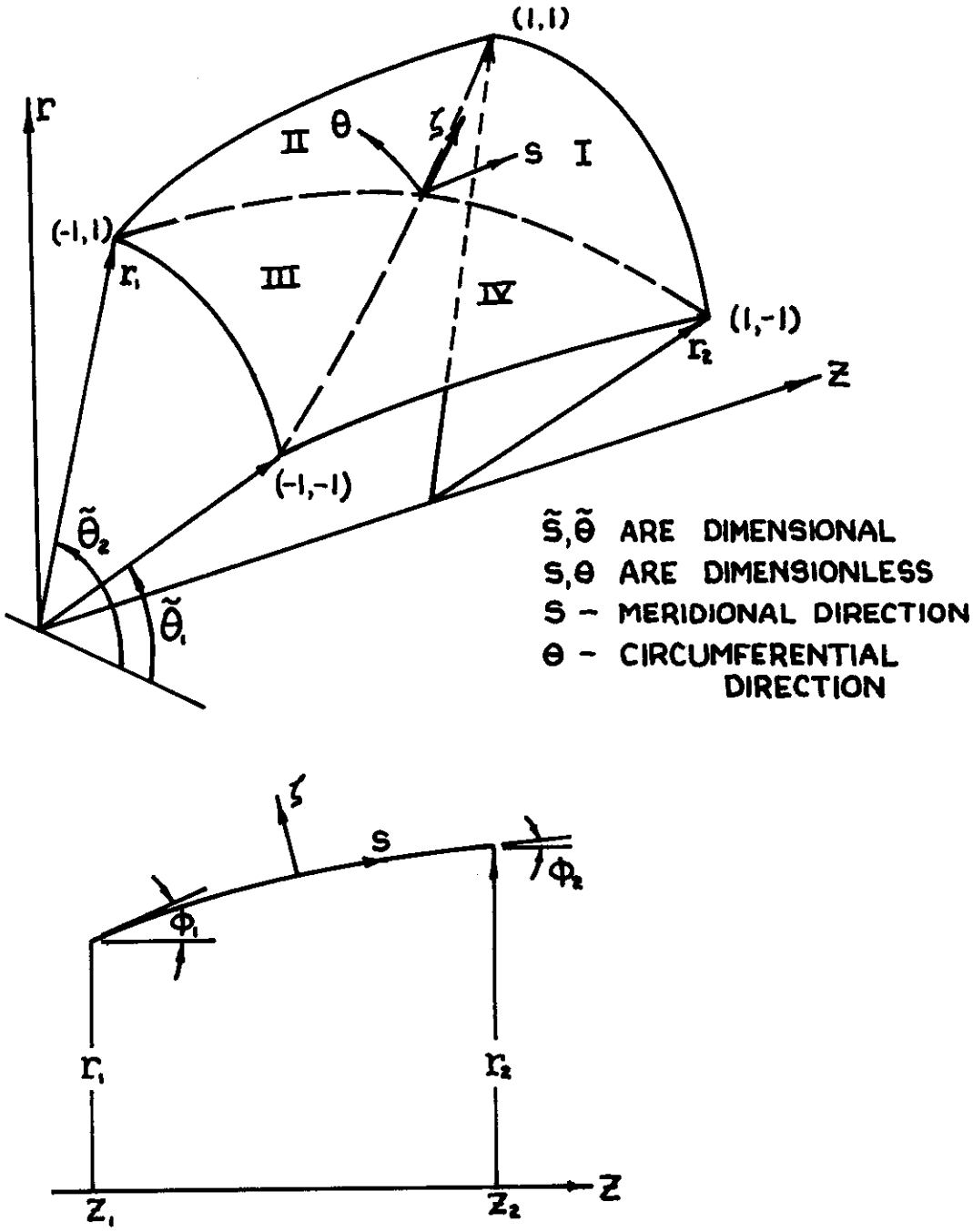

(a) Geometry

Figure 11. Geometry and Generalized Displacements for a Doubly-Curved Quadrilateral Shell Element

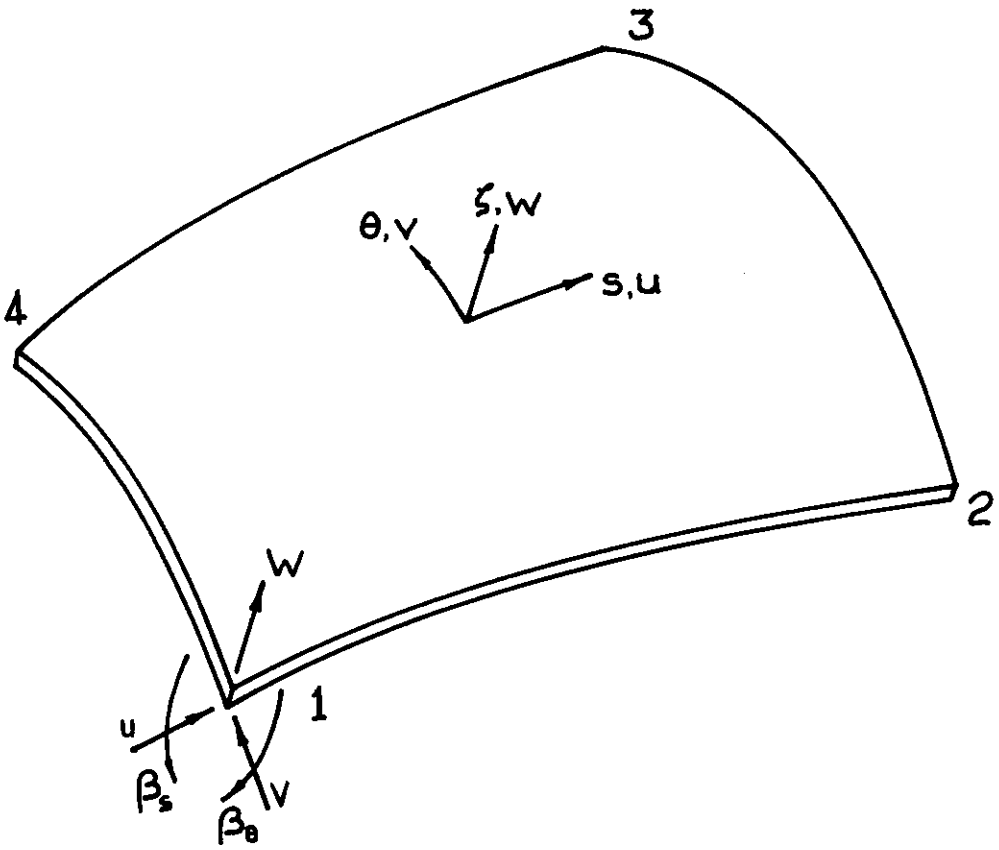

DISPLACEMENT AT EACH NODE (N)	GENERALIZED DISPLACEMENT AT EACH NODE (N)
u	$g_{N,1}$
v	$g_{N,2}$
w	$g_{N,3}$
$\beta_s \equiv \frac{\partial w}{\partial s} + u\frac{\partial \phi}{\partial s}$ = TOTAL MERIDIONAL ROTATION	$g_{N,4}$
$\beta_\theta \equiv \frac{1}{r}\left[\frac{\partial w}{\partial \theta} - v\cos\phi\right]$ = TOTAL CIRCUMFERENTIAL ROTATION	$g_{N,5}$

(b) Generalized Displacements

Figure 11 Concluded

The meridional slope $\phi(s)$ is represented by:

$$\phi(s) = a_0 + a_1 s + a_2 s^2 \tag{82}$$

where

$$\begin{aligned} a_0 &= \frac{1}{2}\phi_1 + \frac{7}{2}\phi_2 - 3\phi_p^* \\ a_1 &= \frac{1}{2}(\phi_2 - \phi_1) \\ a_2 &= -3(\phi_2 - \phi_p^*) \end{aligned} \tag{83}$$

and

$$\phi_p^* = \tan^{-1}\left[\frac{r_2 - r_1}{z_2 - z_1}\right]$$

The shell thickness $h(s, \theta)$ is represented by

$$h(s,\theta) = b_0 + b_1 s + b_2 \theta + b_3 s\theta \tag{84}$$

where

$$\begin{aligned} b_0 &= \frac{1}{4}\left[h(-1,-1) + h(1,-1) + h(1,1) + h(-1,1)\right] \\ b_1 &= \frac{1}{4}\left[-h(-1,-1) + h(1,-1) + h(1,1) - h(-1,1)\right] \\ b_2 &= \frac{1}{4}\left[-h(-1,-1) - h(1,-1) + h(1,1) + h(-1,1)\right] \\ b_3 &= \frac{1}{4}\left[h(-1,-1) - h(1,-1) + h(1,1) - h(-1,1)\right] \end{aligned} \tag{85}$$

Along the shell-coordinate directions s, θ, and ζ, the shell displacements are u, v, and w, respectively. The following 20-parameter assumed displacement field for the midsurface displacements u_0, v_0, and w_0 is used for the formulation which is called QUASH A:

$$\begin{aligned} u_0 &= \alpha_1 + \alpha_2 s + \alpha_3 \theta + \alpha_4 s\theta \\ v_0 &= \alpha_5 + \alpha_6 s + \alpha_7 \theta + \alpha_8 s\theta \\ w_0 &= \alpha_9 + \alpha_{10} s + \alpha_{11}\theta + \alpha_{12} s\theta + \alpha_{13} s^2 + \alpha_{14}\theta^2 \\ &\quad + \alpha_{15} s^3 + \alpha_{16}\theta^3 + \alpha_{17}\left[3s^3\theta + 3s\theta^3 - s^3\theta^3 - 5s\theta\right] \end{aligned} \tag{86}$$

$$+\alpha_{18}\begin{bmatrix}(s^2-2s+\theta^2)_{I}\\(2s\theta-2s)_{II}\\(-s^2-2s-\theta^2)_{III}\\(-2s\theta-2s)_{IV}\end{bmatrix}\quad+\alpha_{19}\begin{bmatrix}(2s\theta-2\theta)_{I}\\(\theta^2-2\theta+s^2)_{II}\\(-2s\theta-2\theta)_{III}\\(-\theta-2\theta-s^2)_{IV}\end{bmatrix}$$

$$+\alpha_{20}\begin{bmatrix}(s^3\theta^3-s^5\theta-3s\theta^3+3s^3\theta)_{I}\\(s\theta^5-s^3\theta^3-3s\theta^3+3s^3\theta)_{II}\\(s^3\theta^3-s^5\theta-3s\theta^3+3s^3\theta)_{III}\\(s\theta^5-s^3\theta^3-3s\theta^3+3s^3\theta)_{IV}\end{bmatrix} \tag{86}$$

where subscripts I, II, III, and IV refer to regions so numbered on Figure 11. Note that this assumed displacement field does not account properly for rigid body behavior; however, this deficiency does not affect the convergence of the solution.*

The generalized displacements **q** chosen to characterize this discrete element are the values of u, v, w, $\left[\partial w/\partial s + u(\partial\phi/\partial s)\right]$, and $1/r\left[\partial w/\partial\theta - v\cos\phi\right]$ at the four nodes (corners) of the element. Thus, $u_o(s,\theta)$, $v_o(s,\theta)$, and $w_o(s,\theta)$ as given by Equation 86 can be expressed in terms of these 20 generalized displacements.

Then, one may obtain the strains at any location in the shell element by employing the Kirchhoff displacement assumptions and the following general deep-shell-theory strain-displacement relations for the midsurface strains and curvature changes:

$$\begin{aligned}\epsilon_s &= \frac{1}{s^*}\frac{\partial u}{\partial s} - \frac{w}{s^*}\frac{\partial\phi}{\partial s}\\ \epsilon_\theta &= \frac{1}{r\theta^*}\frac{\partial v}{\partial\theta} + \frac{u}{r}\sin\phi + \frac{w}{r}\cos\phi\\ \epsilon_{s\theta} &= \frac{1}{s^*}\frac{\partial v}{\partial s} - \frac{v}{r}\sin\phi + \frac{1}{r\theta^*}\frac{\partial u}{\partial\theta}\ \text{(Eng. Def.)}\end{aligned} \tag{87}$$

*A more efficient (but lengthy) formulation called QUASH B in which rigid-body behavior is taken into account properly has been carried out and is being evaluated; this model, however, is an incompatible one and an improved formulation using the HYBRID III approach of Reference 31 is being developed.

$$\kappa_s = -\frac{1}{s^{*2}}\frac{\partial u}{\partial s}\frac{\partial \phi}{\partial s} - \frac{u}{s^{*2}}\frac{\partial^2 \phi}{\partial s^2} - \frac{1}{s^{*2}}\frac{\partial^2 w}{\partial s^2}$$

$$\kappa_A = \frac{\cos\phi}{r^2\theta^*}\frac{\partial v}{\partial \theta} - \frac{1}{r^2\theta^{*2}}\frac{\partial^2 w}{\partial \theta^2} - \frac{u\sin\phi}{rs^*}\frac{\partial \phi}{\partial s} - \frac{\sin\phi}{rs^*}\frac{\partial w}{\partial s} \qquad (87)$$

$$2\kappa_{s\theta} = -\frac{2}{rs^*\theta^*}\frac{\partial^2 w}{\partial s\,\partial \theta} + \frac{2\sin\phi}{r^2\theta^*}\frac{\partial w}{\partial \theta} + \frac{2\cos\phi}{rs^*}\frac{\partial v}{\partial s} - \frac{2v\sin\phi\cos\phi}{r^2} - \frac{2}{rs^*\theta^*}\frac{\partial \phi}{\partial s}\frac{\partial u}{\partial \theta}$$

where

$$s^* = \frac{\tilde{s}_2 - \tilde{s}_1}{2}$$

$$\theta^* = \frac{\tilde{\theta}_2 - \tilde{\theta}_1}{2} \qquad (88)$$

Finally, with the use of appropriate stress-strain relations such as Equation 19, for example, one may compute the strain energy in terms of the generalized displacements, thereby determining the desired stiffness matrix $[k]$ for the quadrilateral shell element (QUASH).

ILLUSTRATIVE RESULTS

In this subsection, illustrative results obtained by applying most of the previously discussed discrete elements to the analysis of statically loaded and/or heated structures are presented. In most cases, the present discrete element results are compared with independent analytical and/or numerical results.

Single-Layer Shells of Revolution

Shown in Figure 12 is a deep parabolic shell which has been analyzed. For the case of gravity loading (i. e., load harmonic jA = 1) and for the pinned support condition at C, the present discrete element predictions which are identified as case DP 5 are compared with the asymptotic solution of Reference 38 for the normal displacement w and the meridional stress resultant N_s in Figure 13.

SHELL GEOMETRY

Midplane : $r^2 = 4z$

(Focal Length = 1.0)

r_C = 6.0 in.

h = 0.01 in.

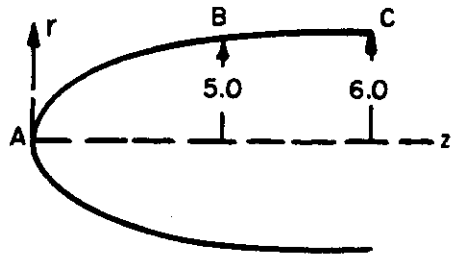

MATERIAL PROPERTIES

$E = 10^7$ psi $\qquad \nu$ = 1/3 for DP 5

ρ = 0.1 lb/in^3 $\qquad$ = 0.3 for DP 6 and DP 14

BOUNDARY CONDITIONS at $r = r_C$

(a) Pinned (P): $q_1 = q_3 = 0$

(b) Pinned - Sliding (PS) at $\alpha = -45°$

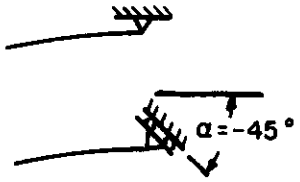

NONZERO LOADING

(1) Gravity (j = 1): $p^{(1)}_{1,p} = -\rho h \sin\phi_p$, $p^{(1)}_{3,p} = -\rho h \cos\phi_p$ } at node "p"

(2) Uniform Pressure: $p^{(o)}_3 = +1.0$ psi

Run I. D. No.	Discrete Element Type	No.	Breakdown AB	Breakdown BC	Loading	B. C.
DP 5	curved	50	30	20	Gravity	P
DP 6	"	50	30	20	$p^{(o)}_3$	PS
DP 14	"	95	*	*	$p^{(o)}_3$	PS

*35 uniform elements over $0 \le r \le 5.25$ and

60 uniform elements over $5.25 \le r \le 6.0$

Figure 12. Deep Parabolic-Shell-Problem Data

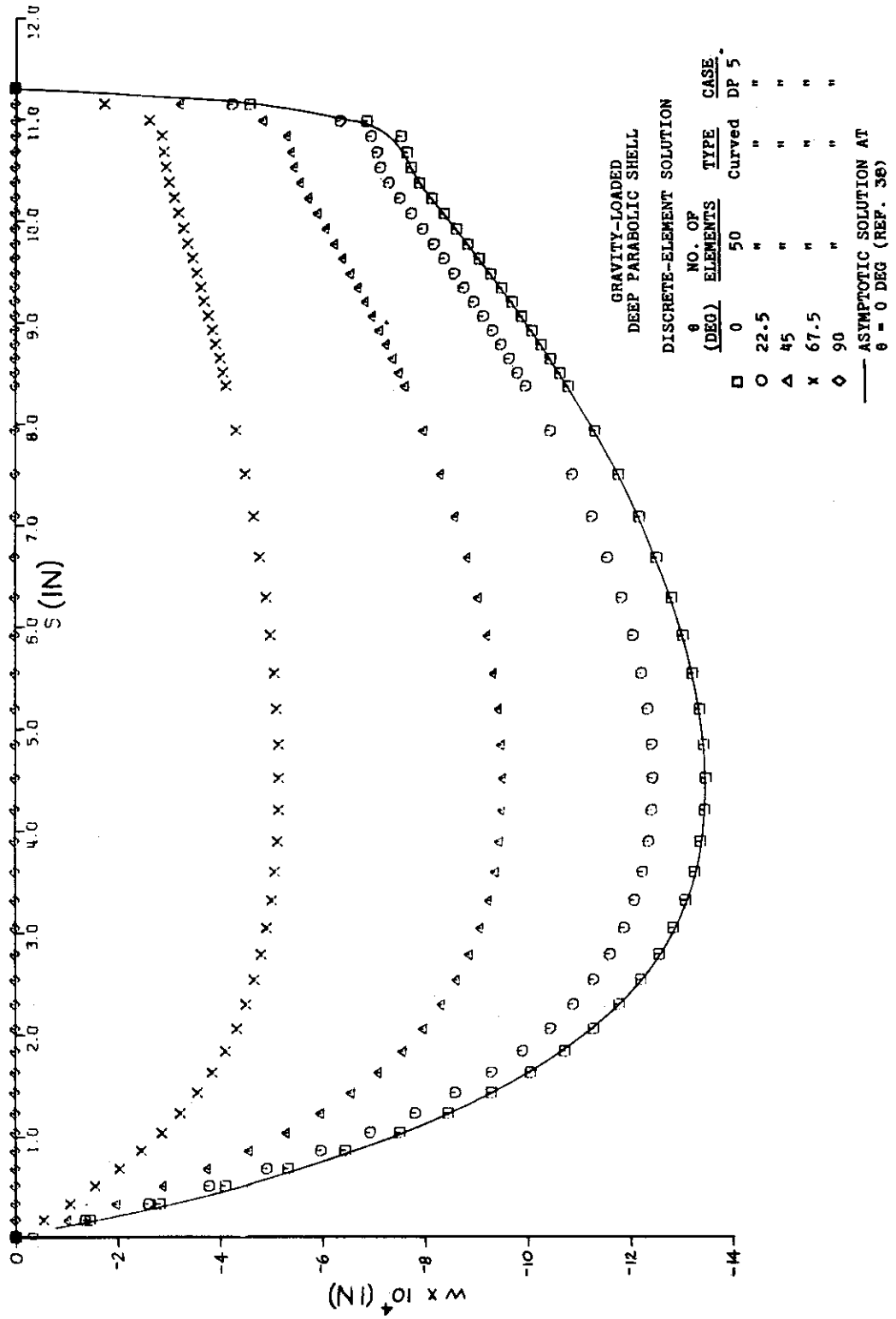

Figure 13. Comparison of Discrete-Element with Asymptotic Solution Results for a Pinned Gravity-Loaded (j = 1) Deep Parabolic Shell

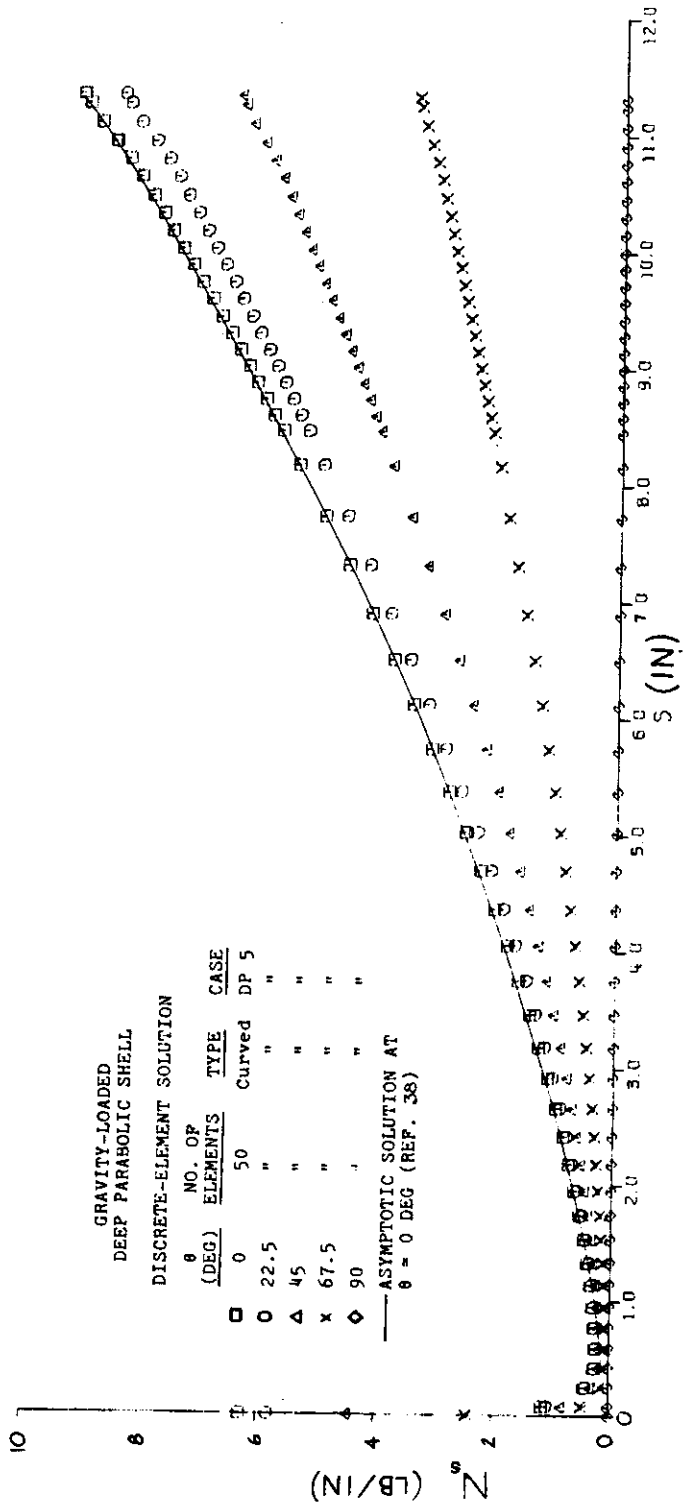

(b) N_s vs s

Figure 13 Concluded

For the case of uniform zeroth harmonic pressure loading $p_3^{(o)} = 1.0$ psi on the deep parabolic shell and the indicated pinned-sliding support condition, the present discrete-element results (identified as cases DP 6 and DP 14 for 50 and 95 discrete elements, respectively) are compared with results obtained (Reference 39) by the multisegment integration technique of Reference 40: in Figure 14a for w, and in Figure 14b for the meridional moment resultant M_s.

The variable thickness "cylindrical storage tank" problem solved by Bushnell and Hoff (Reference 41) is defined in Figure 15a. Compared with the predictions of Reference 41 are the present discrete element predictions for w in Figure 15b and for the outer surface meridional stress σ_s in Figure 15c. The discrete-element results shown include the following types of thickness variations over region AB: (1) linear, Case VTC 5, (2) parabolic, Case VTC 7, and (3) uniform, Case VTC 6.

The final example in this category involves the branched heated shell shown in Figure 16a. The discrete element predictions of Reference 13 are compared with those obtained independently (Reference 19): in Figure 16b for w and in Figure 16c for M_s.

The present predictions which include axisymmetric and asymmetric mechanical loading, thermal loading, various boundary conditions, variable thickness, and a branched shell demonstrate both the accuracy and the versatility of the method and program of References 13 and 36.

Bonded Double-Layer Shells of Revolution

A cantilevered, bonded, double-layer cylinder subjected to zeroth harmonic axial tension at the free end of its outer layer is depicted in Figure 17a. Shown also in Figure 17a are the present discrete-element predictions and the exact solution for the radial displacement w (Reference 18). Similar predictions for the bond shear stress resultant as a function of distance from the clamped end are shown in Figure 17b.

Cantilevered, bonded, double-layer cones of uniform and of varying thickness subjected to uniform external pressure as indicated in Figure 18 have been analyzed. The normal deflection w predicted by the discrete element method of Reference 19 are also shown in Figure 18, and a finite-difference solution for w (Reference 17) for the uniform thickness case is shown for comparison.

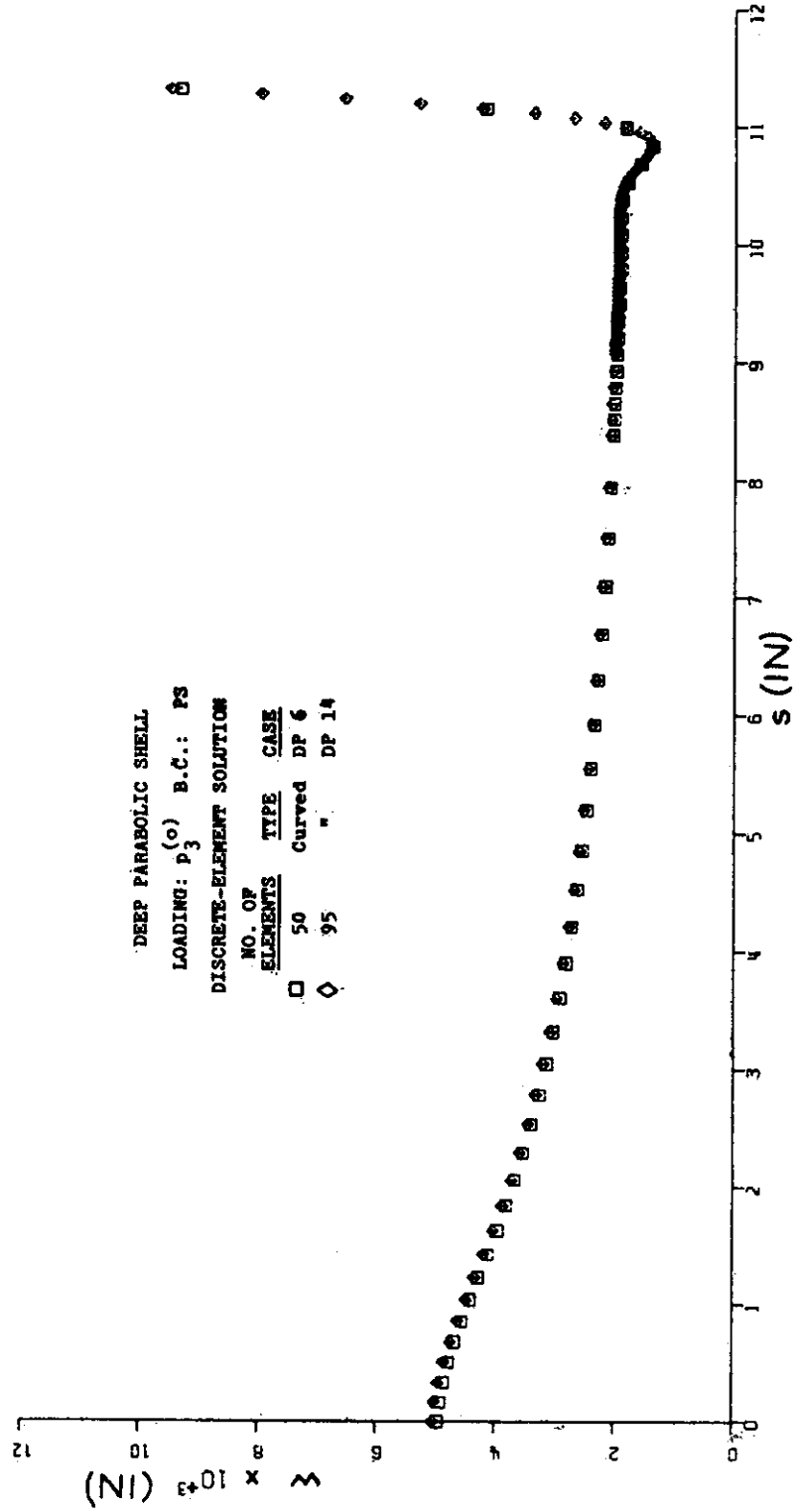

(a) W VS S

Figure 14. Comparison of Discrete-Element Solutions with a Multisegment Integration Solution for a Pressure-Loaded (j = 0) Deep Parabolic Shell with a Pinned-Sliding Boundary

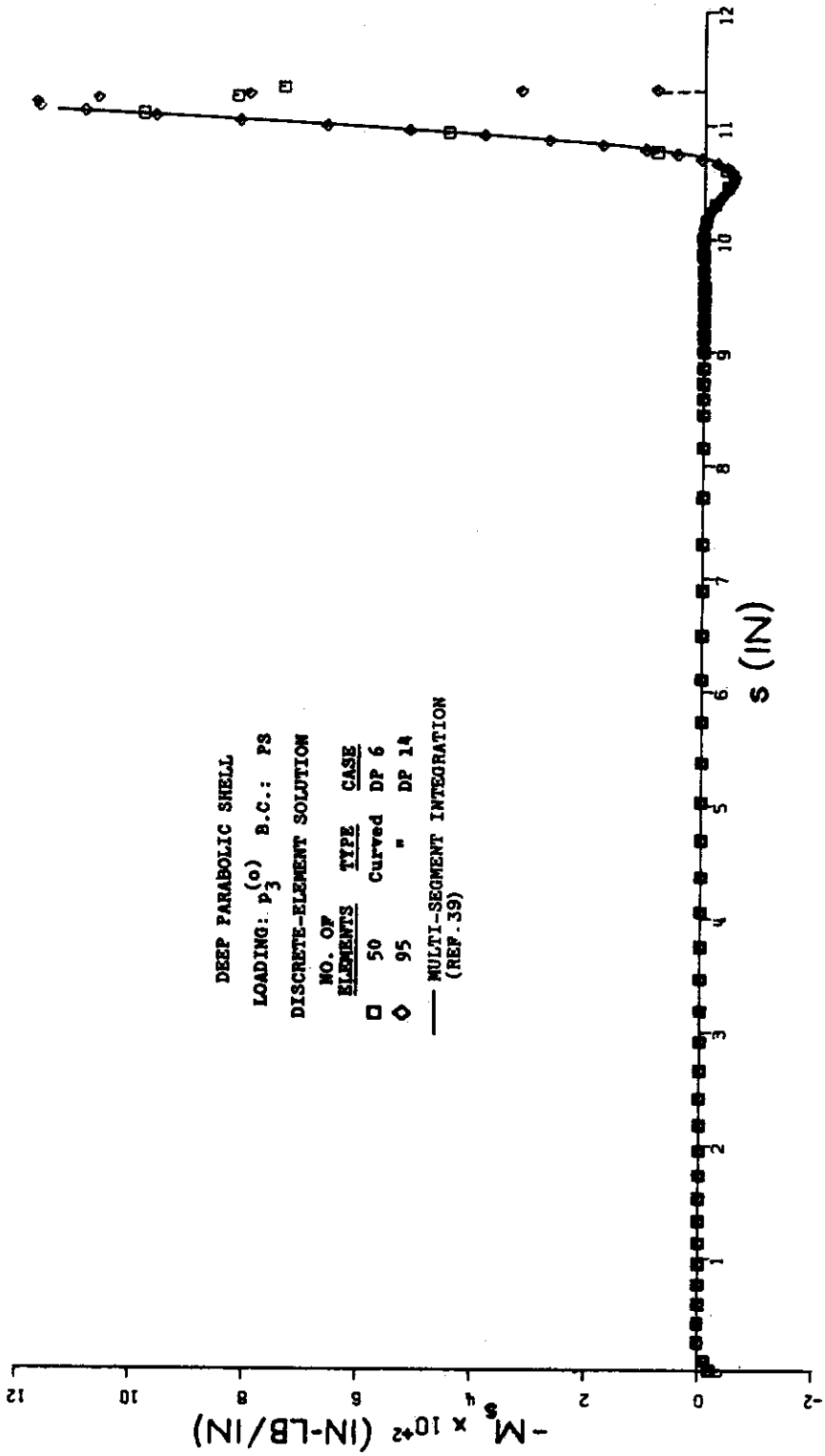

(b) M_s vs s

Figure 14 Continued

SHELL GEOMETRY

h_o = 0.1 in.

h_b = 0.3 in. and n = 10

or $h_b = h_o$ (see runs)

a = (see runs)

d = 20 in.

MATERIAL PROPERTIES

$E = 10^7$ psi

$\nu = 0.3$

BOUNDARY CONDITIONS

Clamped (C) at Base: Point A

NONZERO LOADING

$p_3(s,\theta) \equiv p_3^{(o)}(s) = \gamma(d-z)$

$\gamma = 0.1$

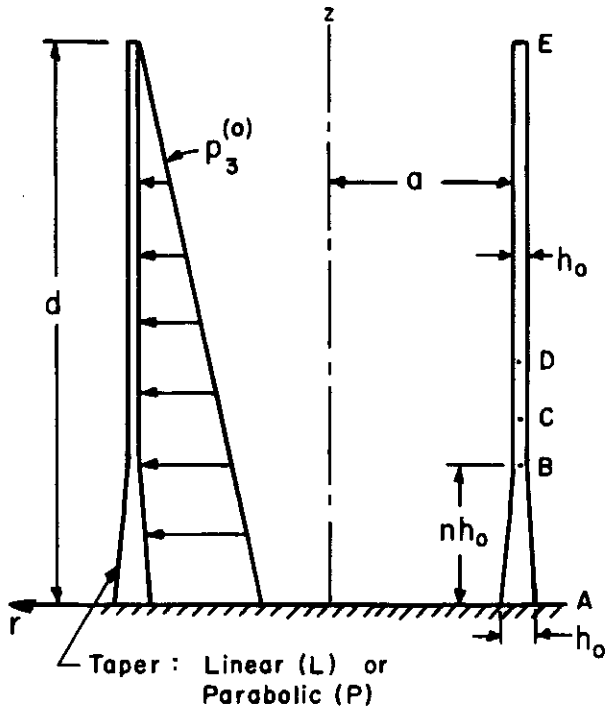

LOCATIONS

Point	z (in)
A	0
B	1
C	2
D	3
E	d

Run I.D. No.	Discrete Element Type	No.	Distribution	h_b (in.)	a (in.)	Loading	B.C.
VTC 5	cyl.	88	*	0.3 (L) +	10	$p_3^{(o)}$ (z)	C
VTC 6	"	"	*	0.1	10	"	"
VTC 7	"	"	*	0.3 (P) +	10	"	"

*60 uniform elements in $0 \le z \le 6$ in. and 28 uniform elements in $6 \le z \le 20$ in.

+ (L) and (P) denote, respectively, linear and parabolic thickness variation over region AB

(a) Problem Definition

Figure 15. Problem Definition and Solutions for a Variable-Thickness Cylindrical Storage Tank

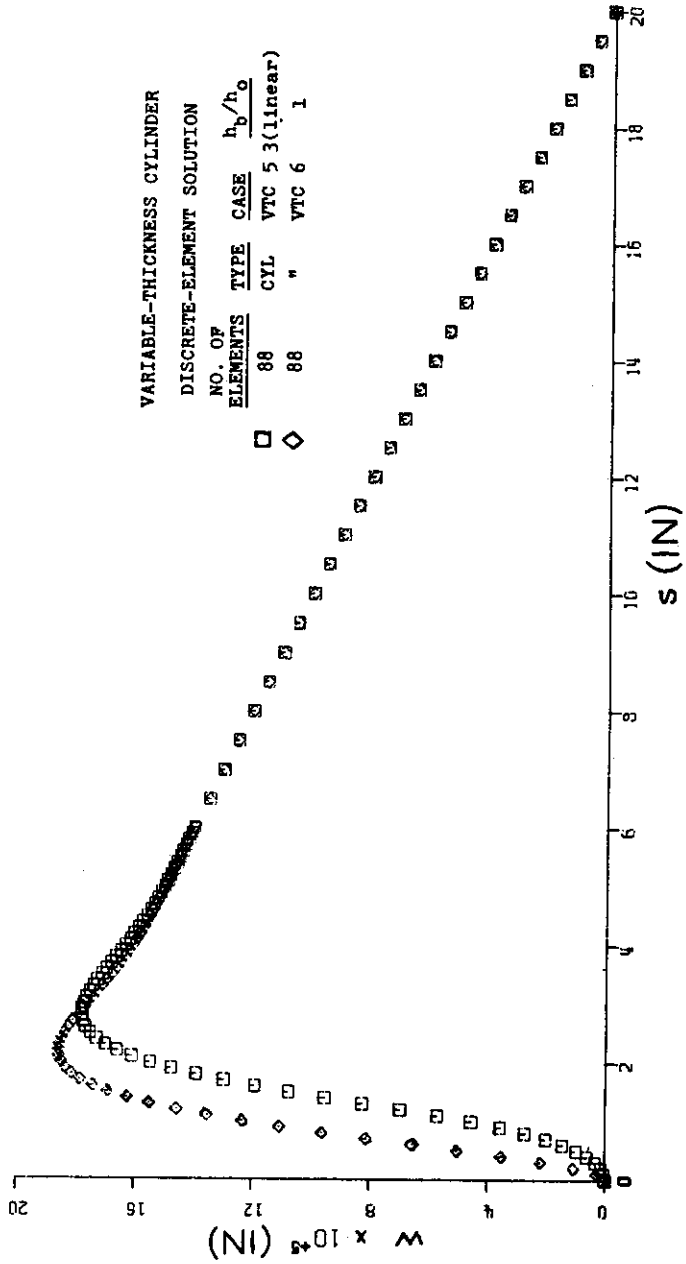

(b) W vs S

Figure 15 Continued

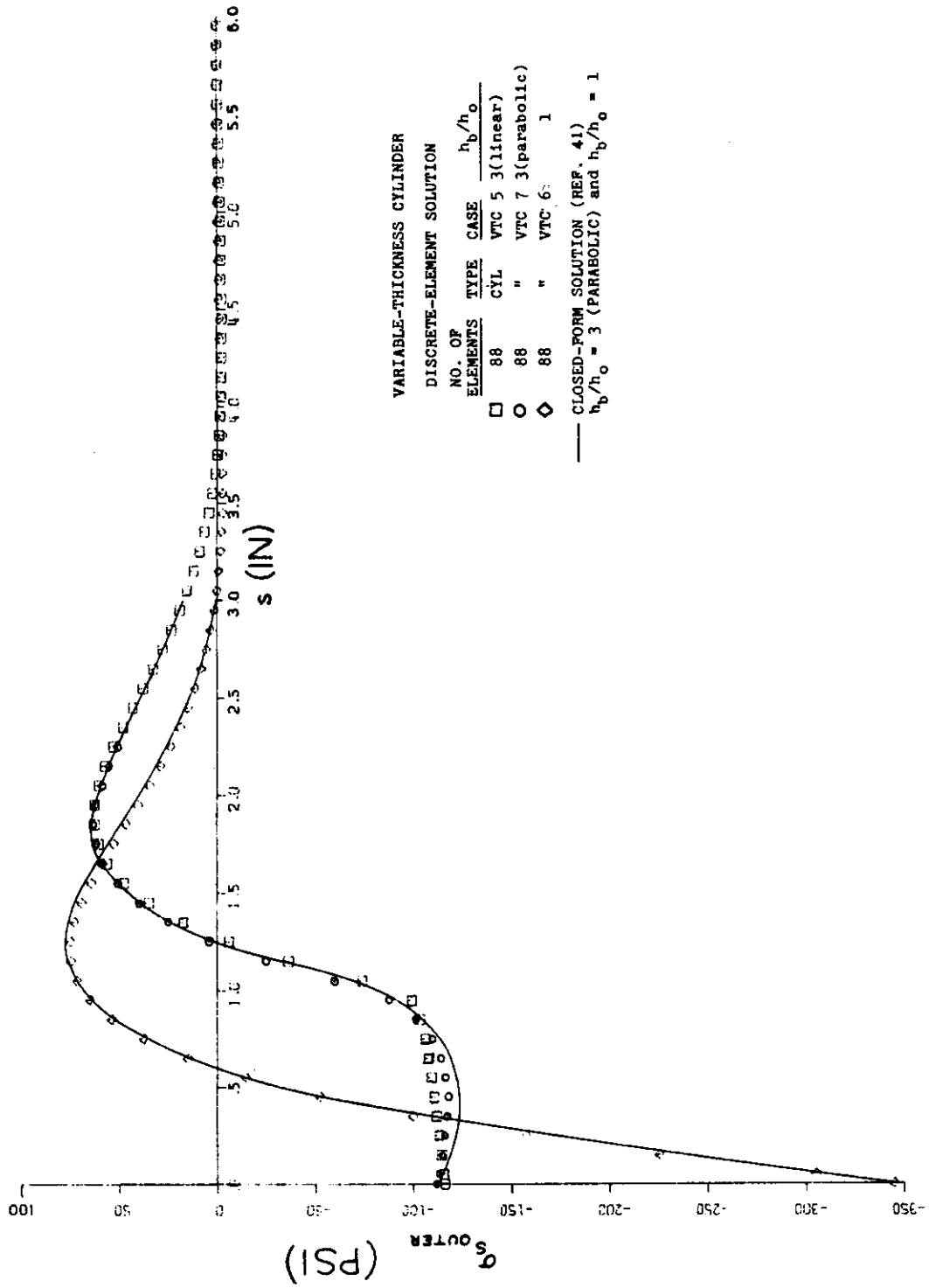

(c) Outer Surface σ_s vs s

Figure 15 Concluded

SHELL GEOMETRY

Main : R = 5.0 in.
h = 0.01 in.
L = 10.0 in.

Branch (Flat Plate) h_b

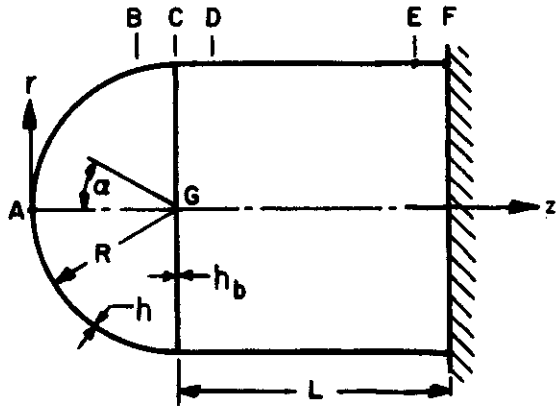

MATERIAL PROPERTIES

$E = 30 \times 10^6$ psi
$\nu = 0.3$
$\alpha = 13 \times 10^{-6}$ (in/in °F)

BOUNDARY CONDITIONS

Clamped (C)
at F : $q_1 = q_2 = q_3 = q_4 = 0$

NONZERO LOADING

(1) $p_3^{(0)} = -100$ psi

(2) $\Delta T^{(0)}(s, \zeta) = \Delta T^{(0)}(\zeta) = C_0 + C_1 \zeta$ } Main Shell

Where $C_0 = 10.5$, $C_1 = 210$

$\Delta T \equiv 0$ on Branch

LOCATIONS

	α	z (in.)
A	u	0
B	60°	-
C	90°	5
D	-	7.6179914
E	-	13.5
F	-	15.0
G	-	5.0

Run I. D. No.	Type	Discrete Element No.	Breakdown (Uniform) AB	BC	CD	DE	EF	GC	h_b (in.)	Loading	B.C.
HSCB-3	Curved	34	6	5	5	5	8	5	10^{-4}	$\Delta T^{(0)}$	C

(a) Problem Definition

Figure 16. Problem Definition and Discrete Element Solutions for a Thermally-Loaded (j = 0) Hemisphere-Cylinder Branched Shell

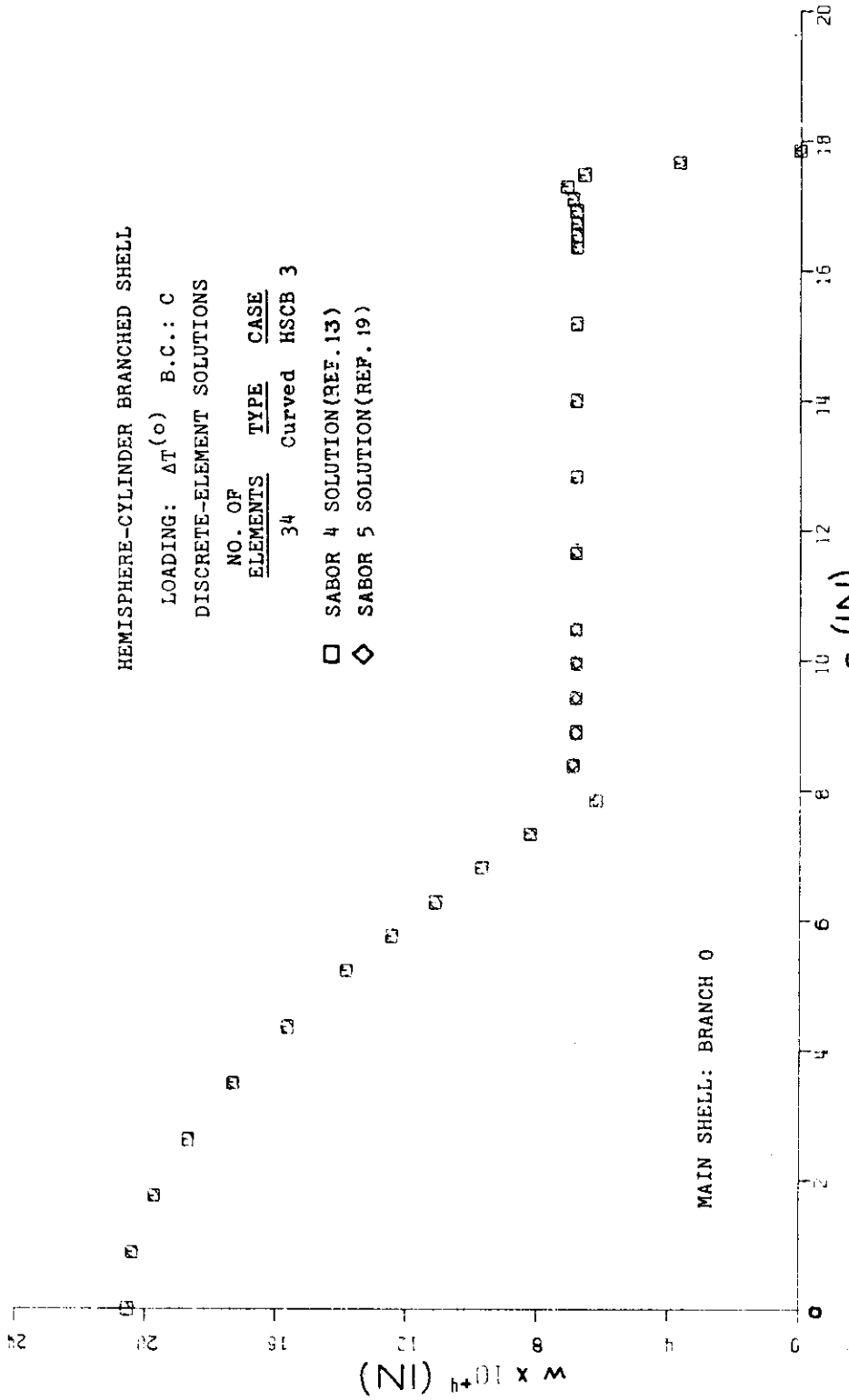

(b1) w vs s

Figure 16 Continued

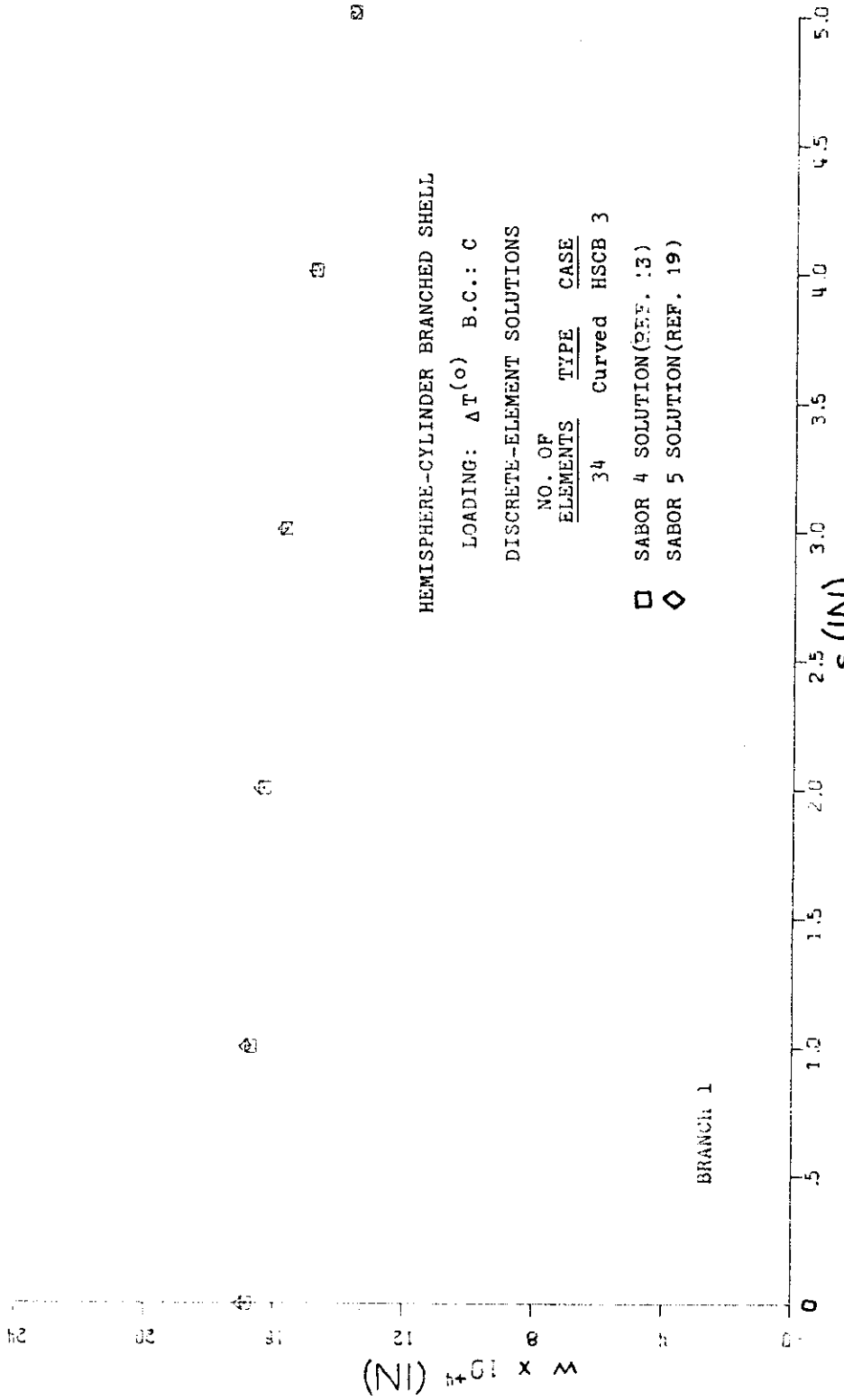

(b2) w vs s

Figure 16 Continued

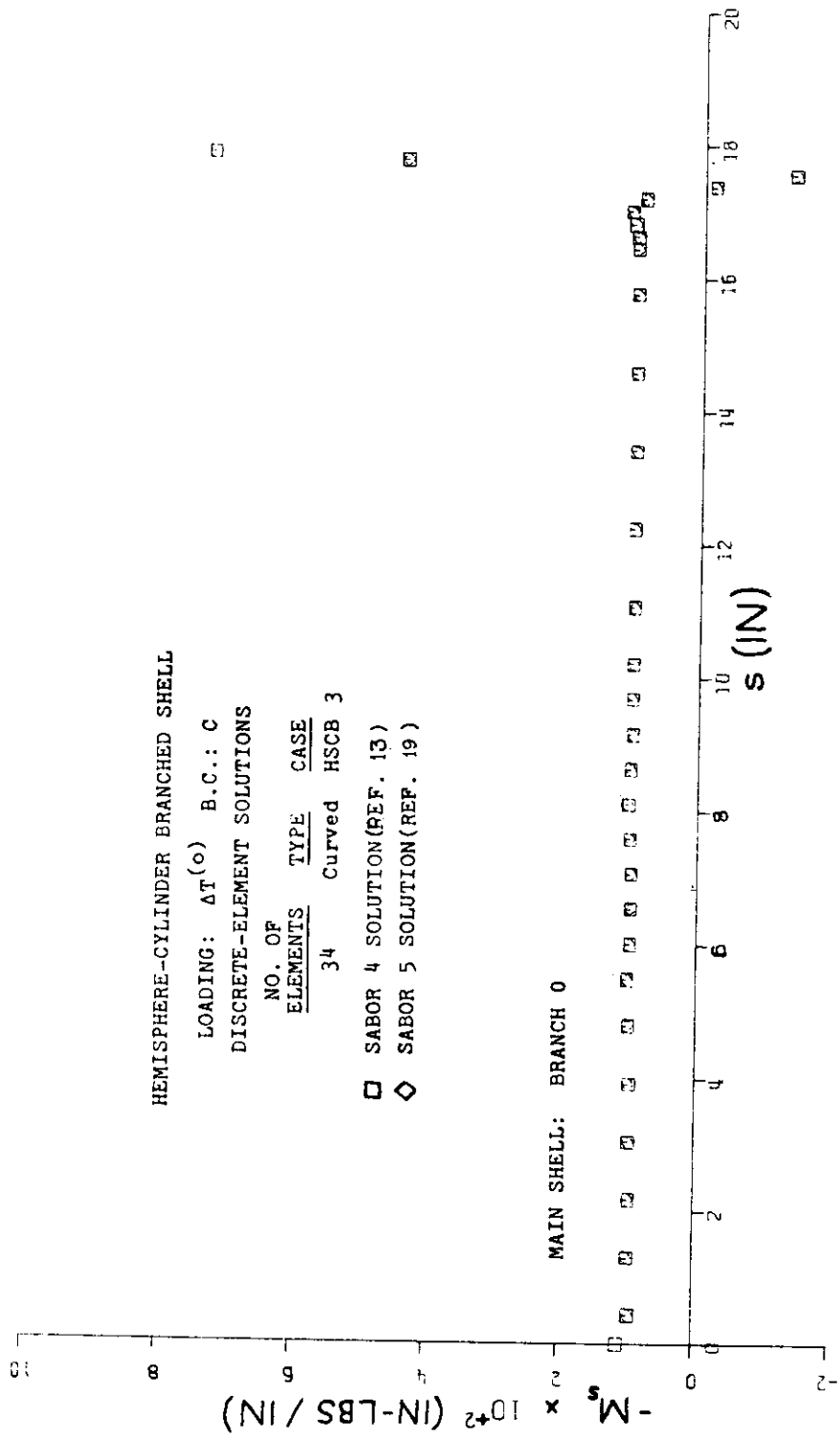

(c1) M_s vs s

Figure 16 Continued

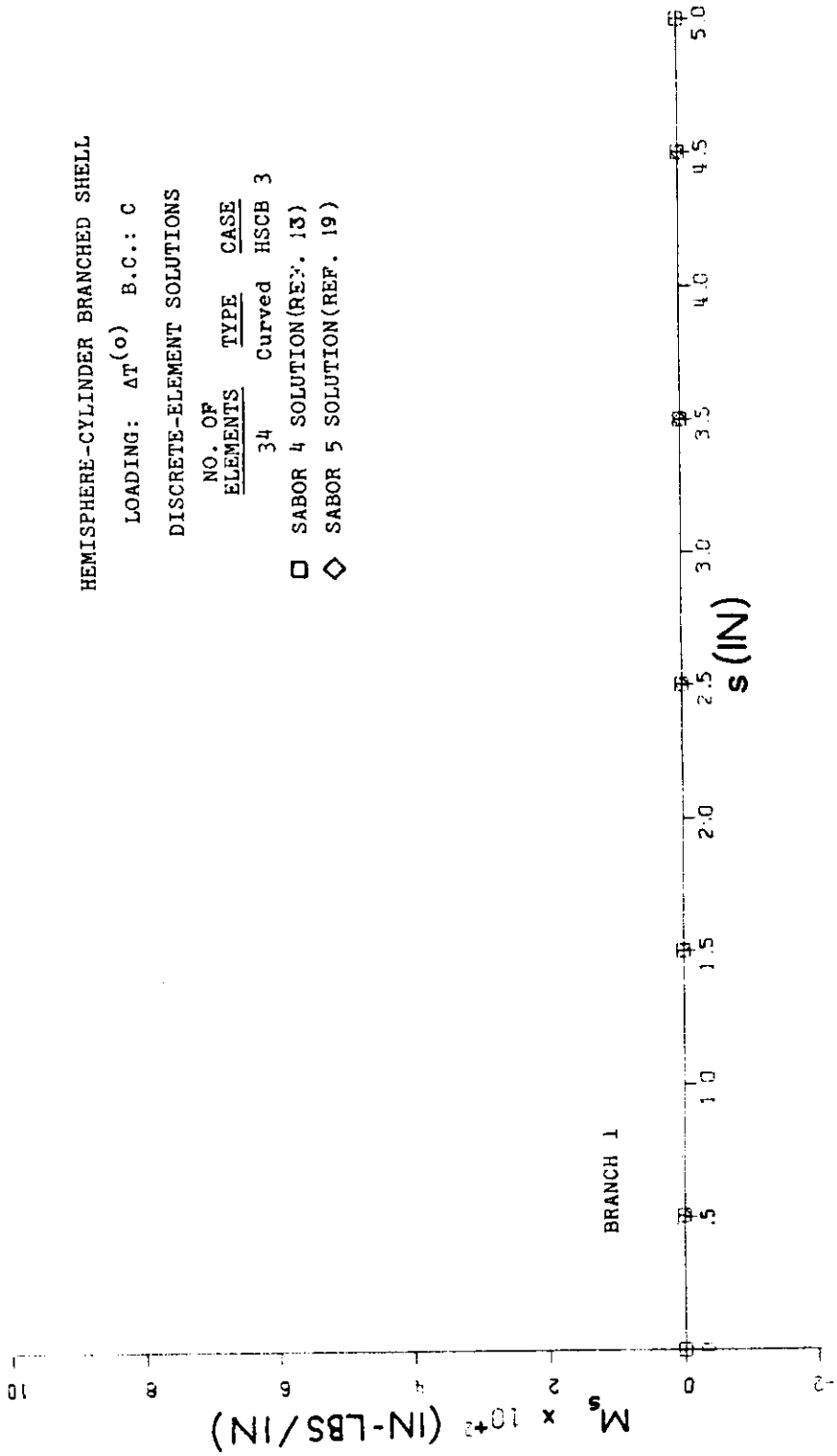

(c2) M_s vs s

Figure 16 Continued

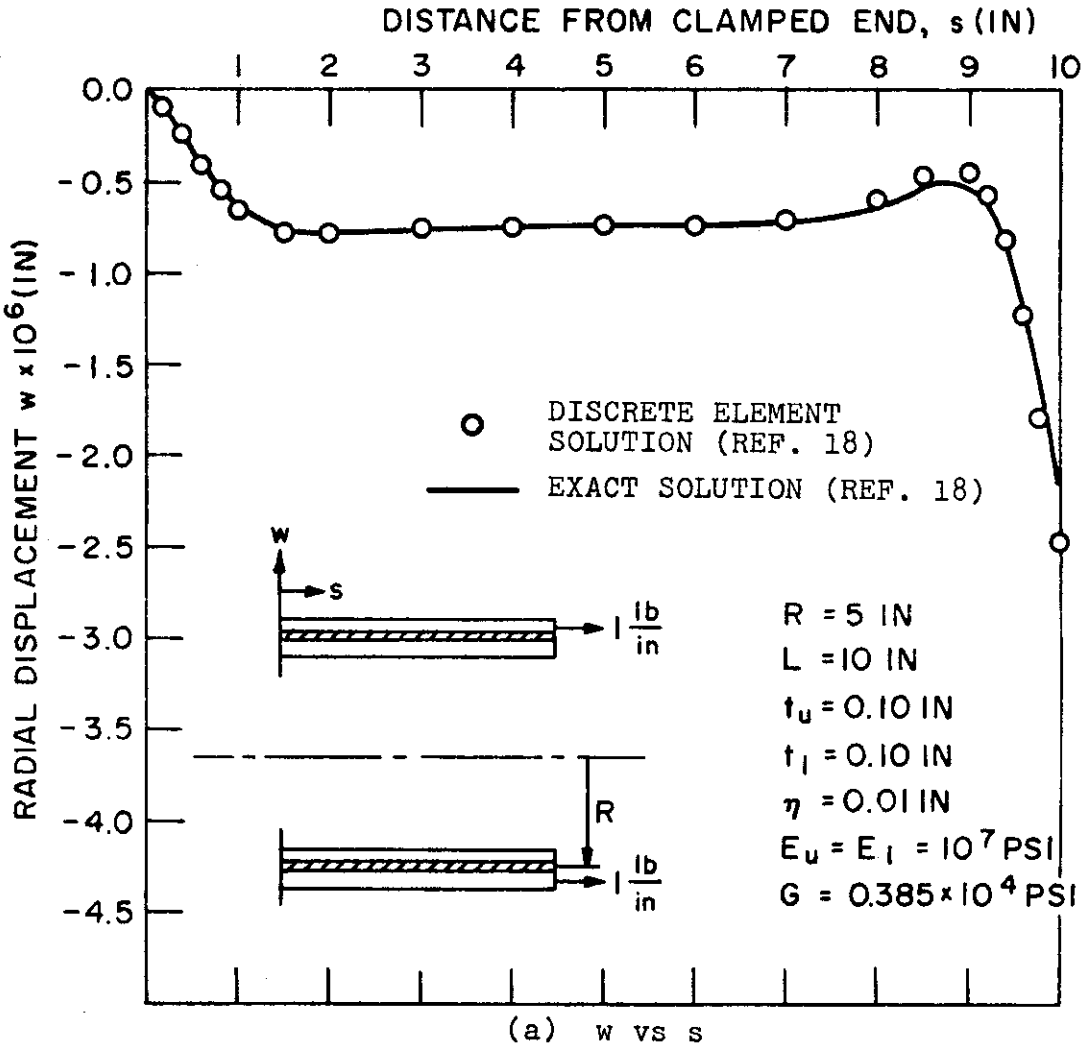

Figure 17. Shell Deflection and Bond Shear Stress Resultant Distribution for a Bonded Double-Layer Cantilevered Cylinder with a Uniform Axial Tension Applied in the Outer Layer at the Free End

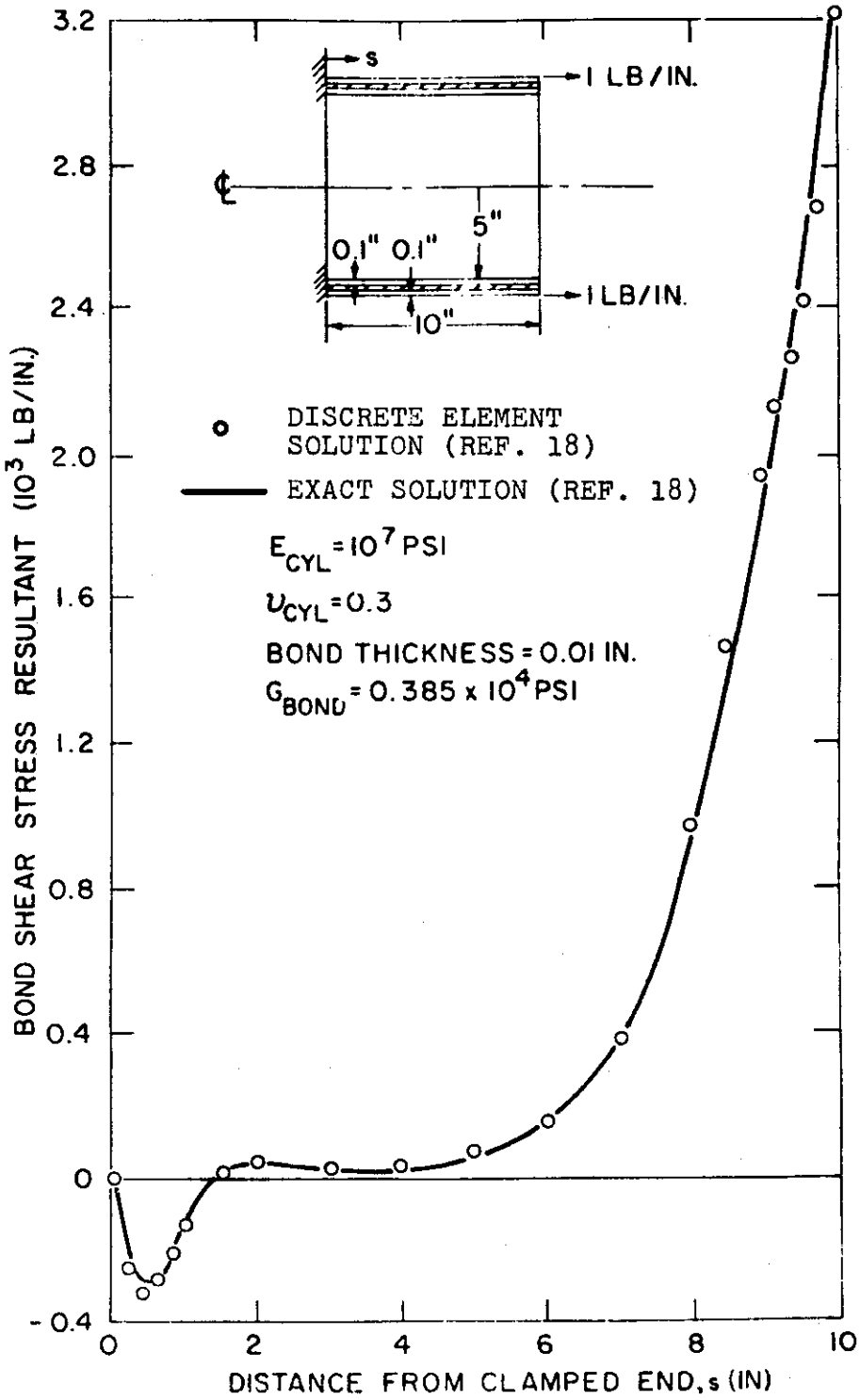

(b) Bond Shear Stress Resultant vs s

Figure 17 Concluded

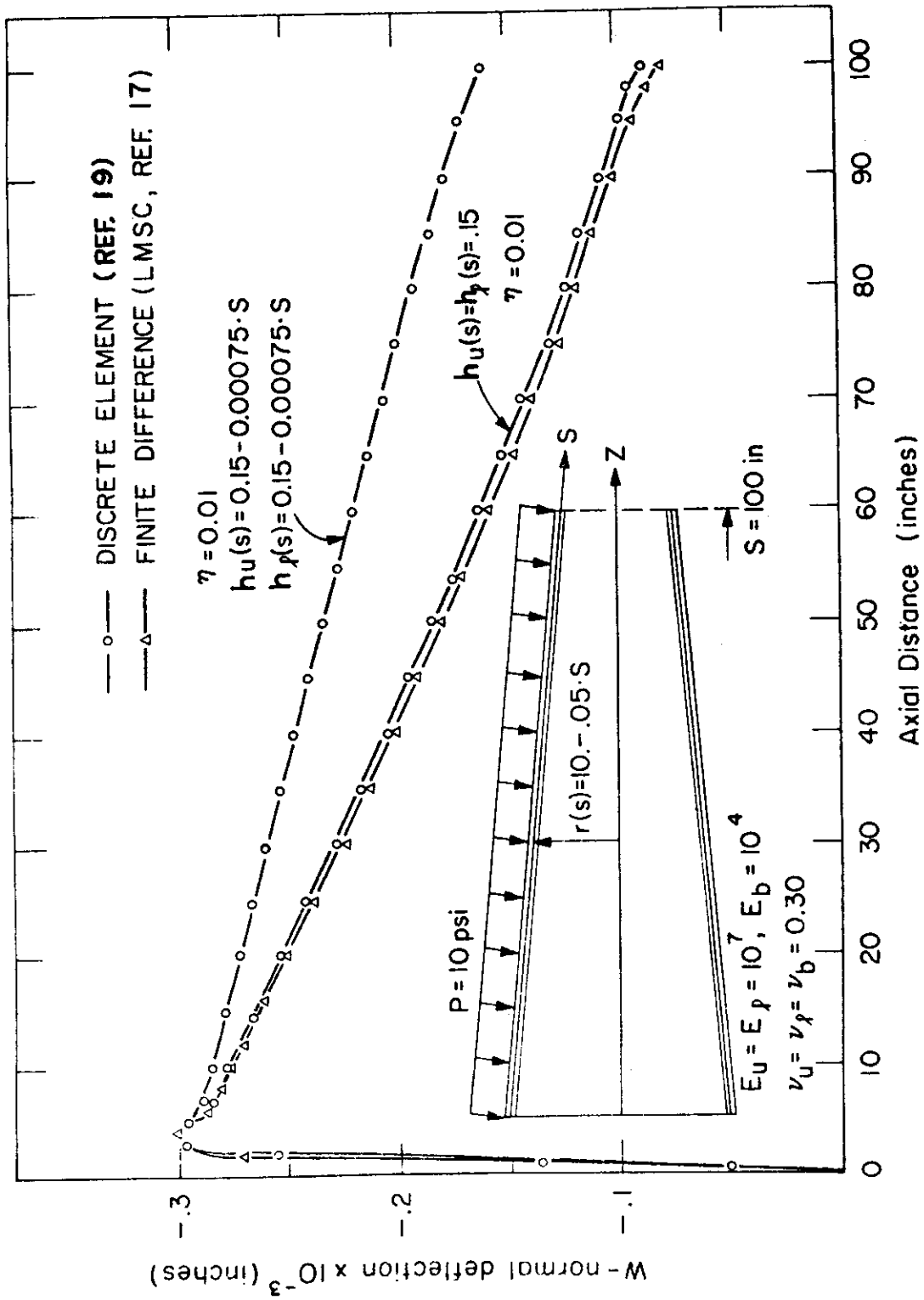

Figure 18. Comparison of the Normal Deflection from Finite-Element and Finite-Difference Solutions for Soft-Bonded Two-Layer End-Clamped Conical Shell Under External Hydrostatic Pressure (j = 0)

A Double-layer cylinder which is clamped at one end and is pinned-fixed at the midplane of both the upper layer and the lower layer at the other end is subjected to a zeroth harmonic meridional moment M_s of 1.0 lb/in. at its pinned-fixed end is shown in Figure 19a. The influence of various values of bond shear stiffness G_b on the radial displacements w of this shell is shown in Figure 19b. The dotted curve represents the w-deflection of a single-layer isotropic cylinder of h = 0.1 in., E = 10^7 psi, and ν = 0.3 (Case C4 of Figure 19a). It is seen that as the bond shear stiffness approaches the stiffness of the shell layers, the normal displacement w approaches that of the single-layer shell. The discrepancy observed when G_b is increased to equal G of the shell material is due to the additional degree of freedom provided by the bond layer, compared with the "equivalent" single-layer shell.

Specimen with Circumferentially-Varying Elastic Modulus

This asymmetric structure consists of an annular flat plate of uniform thickness (h = 0.05 in.), with an inner radius of 5 in. and an outer radius of 7 in. is subjected to a uniform lateral pressure load of 3 psi (i. e., $p_3^{(o)}$ = - 3 psi) as depicted in Figure 20a. The inner boundary is free and the outer boundary is clamped. It is postulated that the elastic modulus E of the plate is $E(s,\theta) \equiv E(\theta) = E_o + E_1 \cos$ where $E_o = 15 \times 10^6$ psi and $E_1 = 10 \times 10^6$ psi, and $\nu = 0.3333$ everywhere.

This structure has been analyzed by using HSOR elements (Reference 16) and by using triangular flat plate elements (References 42 and 43); the respective discrete element breakdowns are shown in Figures 20b and 20c.

Since this structure is asymmetric, the structural stiffness matrix is harmonically coupled. Hence, there will be various deformation harmonic contributions to the displacements although only zeroth harmonic loading is involved. Shown in Figure 20d are the lateral displacements w at the inner boundary as a function of θ. It is seen that one must include stiffness harmonic 0, 1A, 2A, 3A, and 4A to obtain a reasonably convergent solution for this case.

An independent discrete-element solution of this problem reported in Reference 42 was obtained by using the triangular flat-plate elements of Reference 43. By taking advantage of symmetry, 36-element and 144-element solutions were obtained. The w-displacement predicted at the inner boundary by the 144-element solution is compared in Figure 20e with the converged solution of Figure 20d. Good agreement is observed.

SHELL GEOMETRY

R = 5.0 in.

L = 2.50 in.

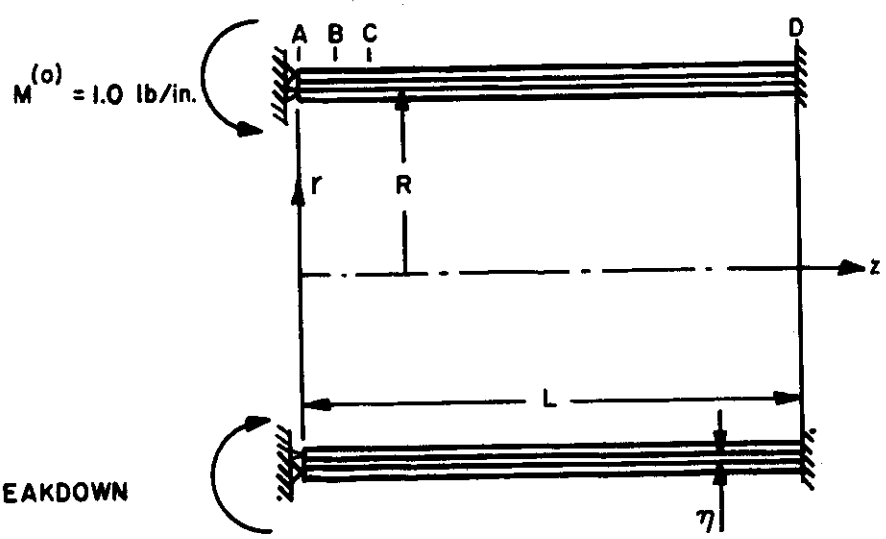

LOCATIONS

Point	z in.
A	0
B	0.25
C	0.50
D	2.50

DISCRETE ELEMENT BREAKDOWN

Region	No.
AB	15
BC	10
CD	40

CASE	h_u (in.)	h_ℓ (in.)	η (in.)	E_u (psi)	ν_u	E_ℓ (psi)	ν_ℓ	G_b (psi)
	0.0475	0.0475	0.0005	10^7	0.3	10^7	0.3	Varying
C4	0.10	0	0	10^7	0.3	0	0	0

(a) Problem Definition

Figure 19. Problem Definition and the Effects of Bond Shear Stiffness on the Deformations of an End-Moment-Loaded Bonded Double-Layer Cantilever Cylinder

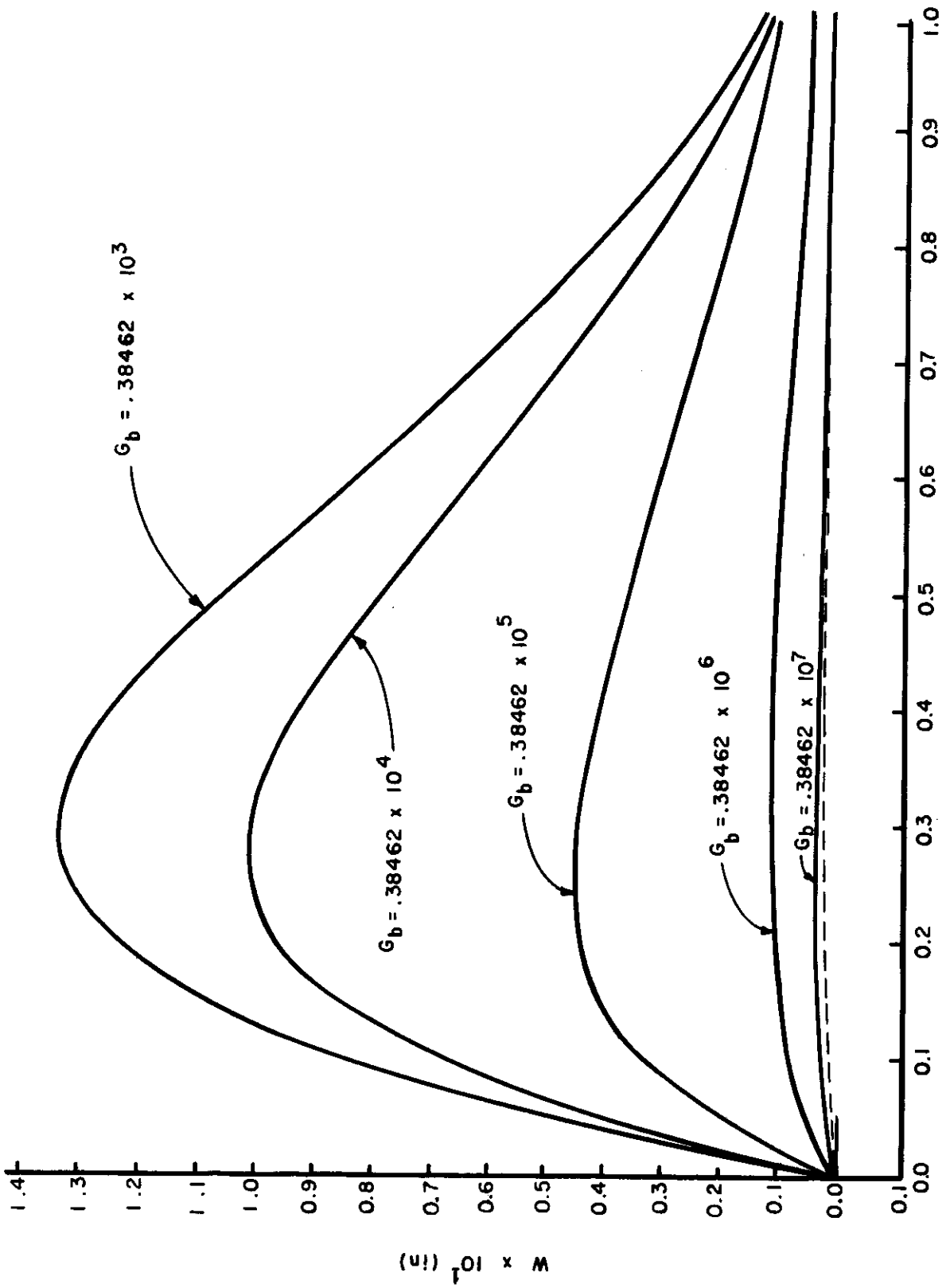

(b) Radial Deflection w vs s

Figure 19 Concluded

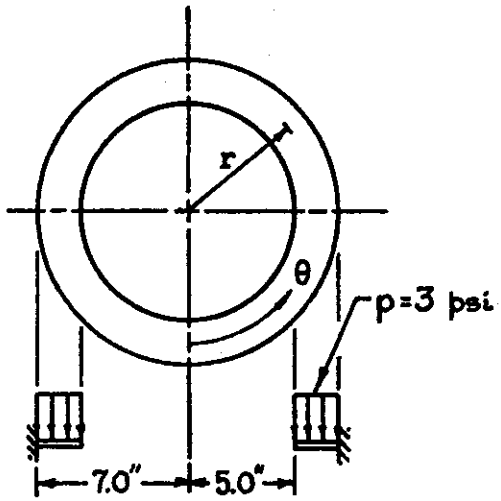

YOUNG'S MODULUS = $E = E_0 + E_1 \cos\theta$

$E_0 = 15 \times 10^6$ psi

$E_1 = 10 \times 10^6$ psi

THICKNESS = $h = 0.05$ in.

POISSON'S RATIO = $\nu = 0.333$

(a) Geometry and Structural Properties

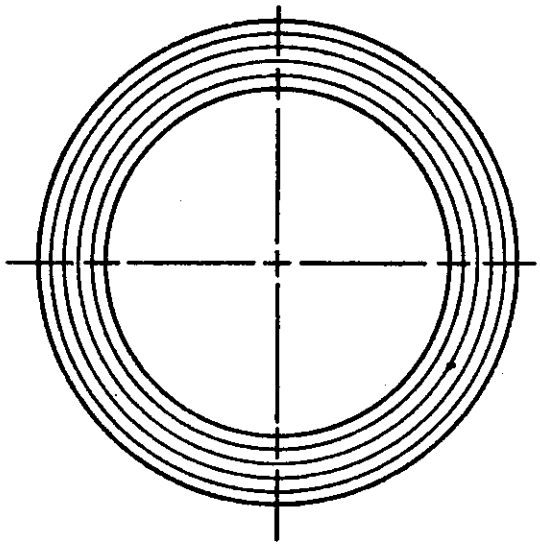

(b) Harmonic Shell of Revolution Element Breakdown (5 elements)

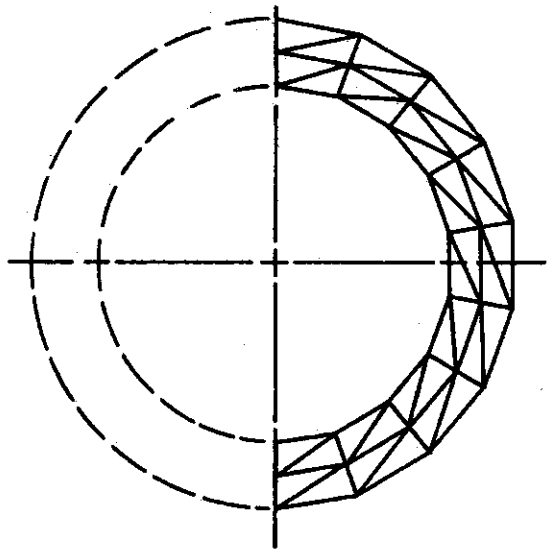

(c) Triangular Flat Plate Element Breakdown (36 elements)

Figure 20. Problem Definition and Discrete Element Deflection Solutions for a Laterally-Loaded Annular Flat Plate with a Circumferential Variation of its Elastic Modulus

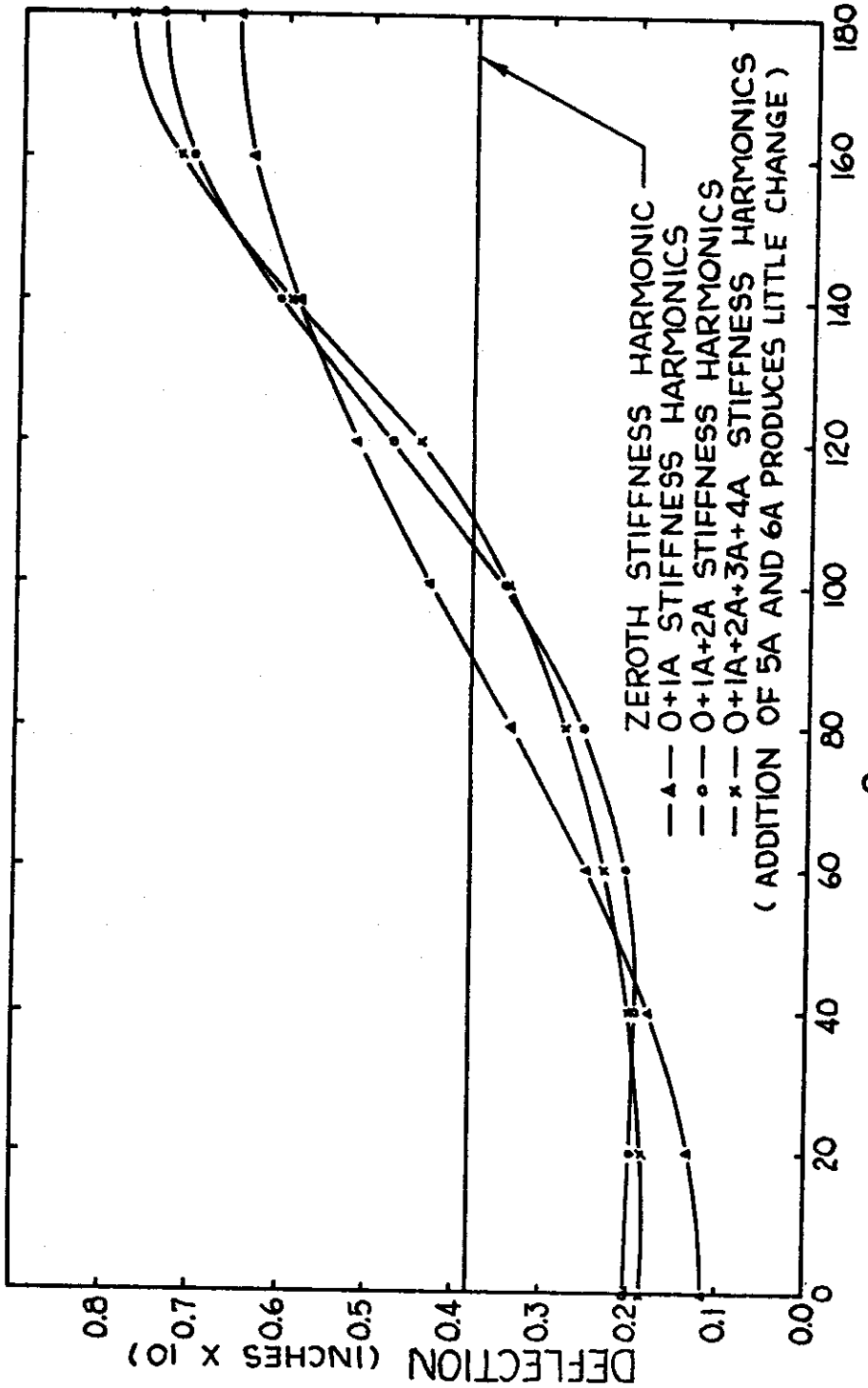

(d) w at Inner Edge vs θ by using HSOR Discrete Elements (Ref. 16)

Figure 20 Continued

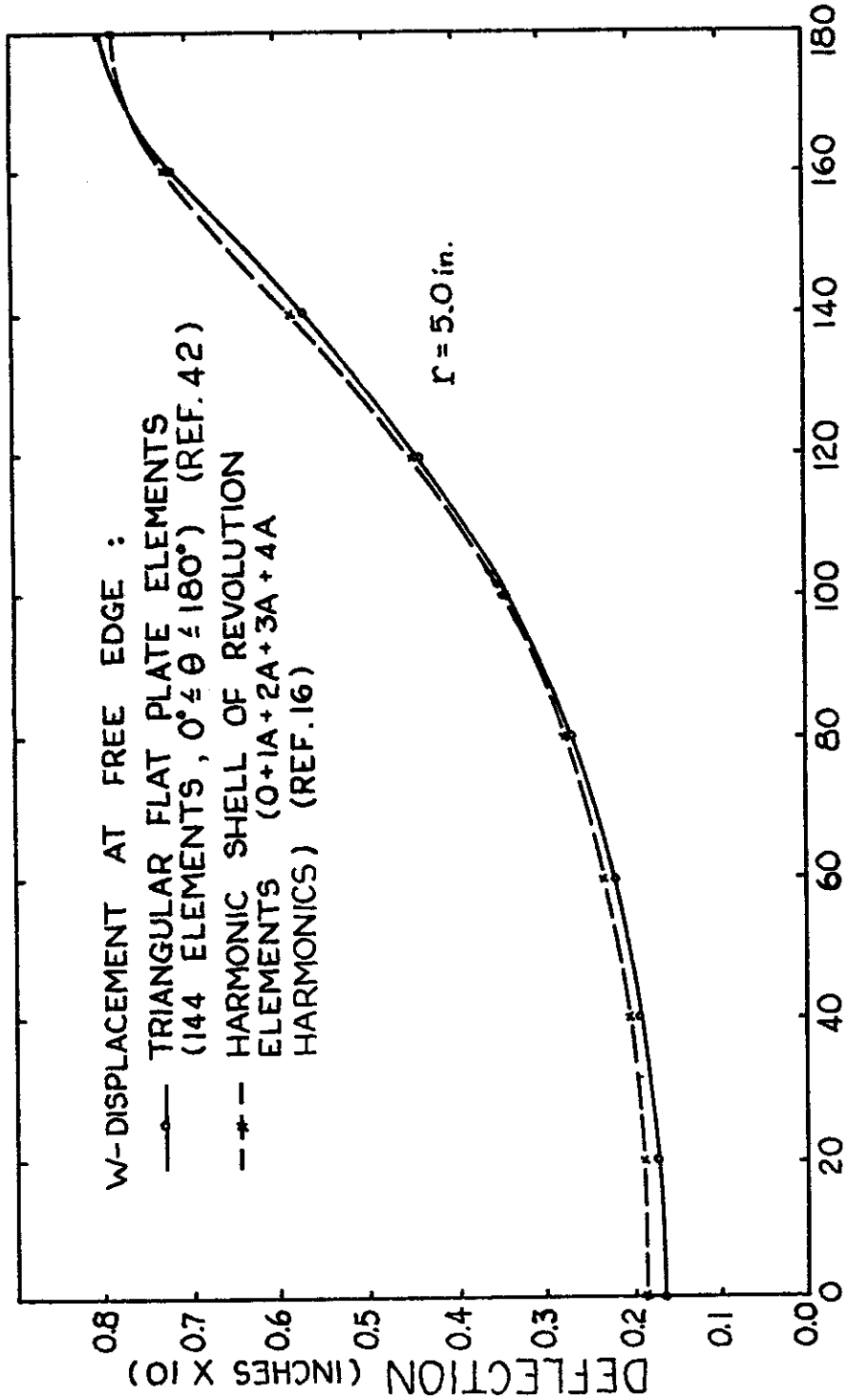

Figure 20 Concluded

In addition to the above case, a cantilevered cylinder with thickness $h(s,\theta) \equiv h(\theta) = h_o + h_1 \cos\theta$, and loaded at its free end by a zeroth harmonic radial ring load, but with all other properties being uniform, has been analyzed using HSOR elements (Reference 16). For this case it was found that stiffness harmonics 0, 1A, 2A, and 3A were needed to provide a converged solution.

Analysis of Core-Stiffened Shells and Solids of Revolution

Several examples of core-stiffened shells of revolution and solids of revolution subjected to axisymmetric and/or asymmetric loading have been analyzed (References 24 and 25), and some typical results are described in the following.

An infinitely long, core-stiffened cylindrical shell whose properties are defined in Figure 21 is subjected to a uniform external pressure of 100 psi (i. e., $p_3^{(o)} = -100$ psi); the pressure in the hollow interior whose radius r_o is 3.0 in. is zero. The discrete element breakdown indicated in Figure 21 was employed: this includes one shell element, one interface core element, and 23 interior core elements. The plane strain condition was imposed by restricting all nodal displacements in the z-direction to be zero. The predicted radial displacement and normal stress in the radial direction for the core material (Reference 25) are shown in Figure 21 as a function of the radial location, and are compared with the exact solution of Reference 24.

An infinitely long cylindrical shell which is filled completely with core-stiffening material and is subjected to second harmonic pressure loading: $p_3^{(2)} = +100 \cos 2\theta$ psi was analyzed. The discretized structure consists of one shell element, one core-interface element, and 29 core-interior elements, as indicated in Figure 22a. Again, the plane strain condition was invoked by requiring the axial displacements at all nodes to be zero. The discrete element and the exact predictions of Reference 25 for the radial and the circumferential displacement distributions are shown in Figure 22a; the associated radial, circumferential, and shearing stress distributions are given in Figure 22b.

Finally, an example of the improvement which one may realize by using an appropriate combination of compatible core-interface elements (SOLOR-CT), interior core elements (SOLOR-INT), and shell elements (SOR), rather than simply SOLOR-INT and SOR elements, is shown in Figure 23a; an infinitely-long foam-filled cylindrical shell is subjected to a zeroth harmonic ring load at station $z = 0$. One discretization (about $z = 0$) used is shown in

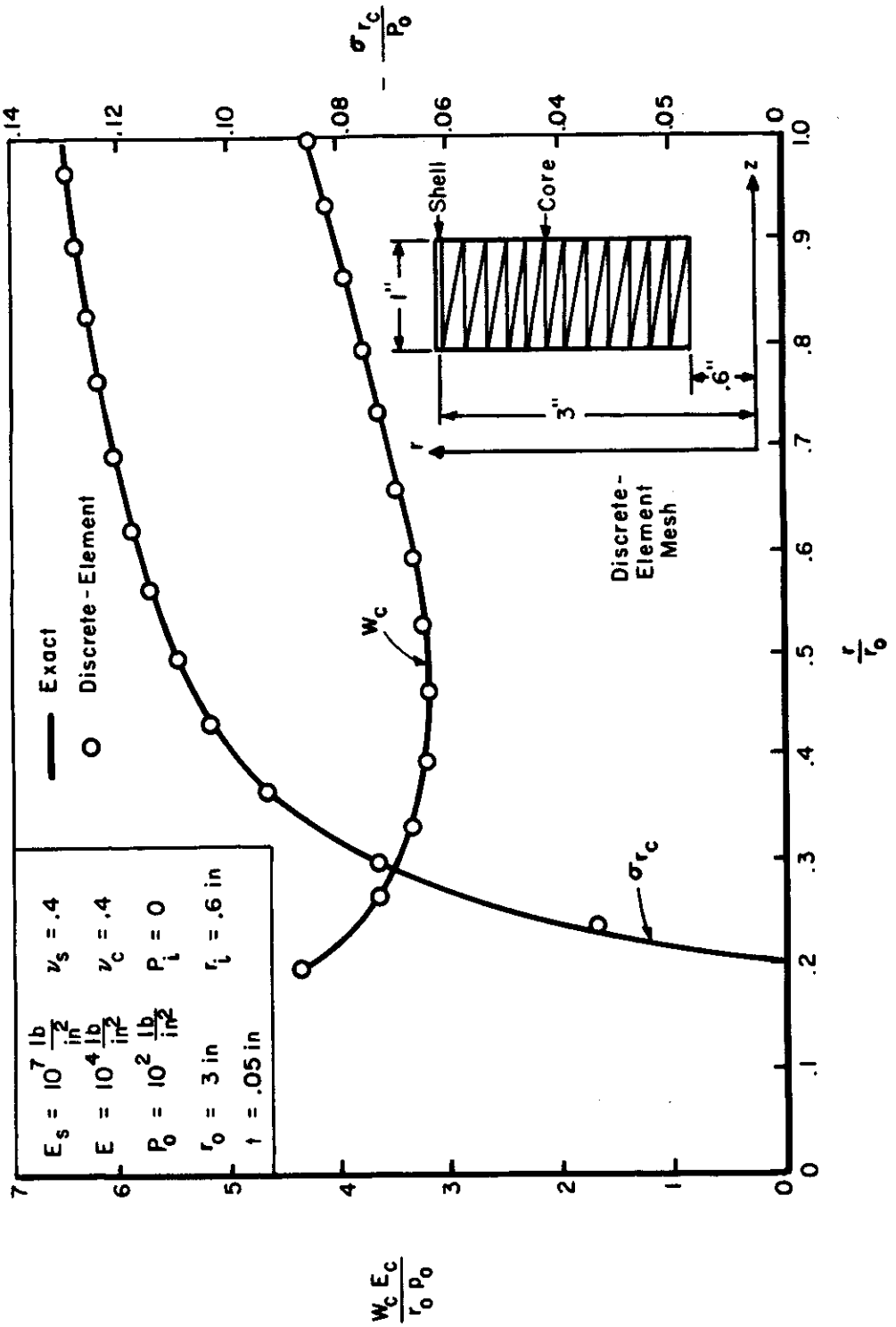

Figure 21. Radial Displacement and Stress in an Infinite Foam-Stiffened Circular Cylinder Under Uniform Pressure

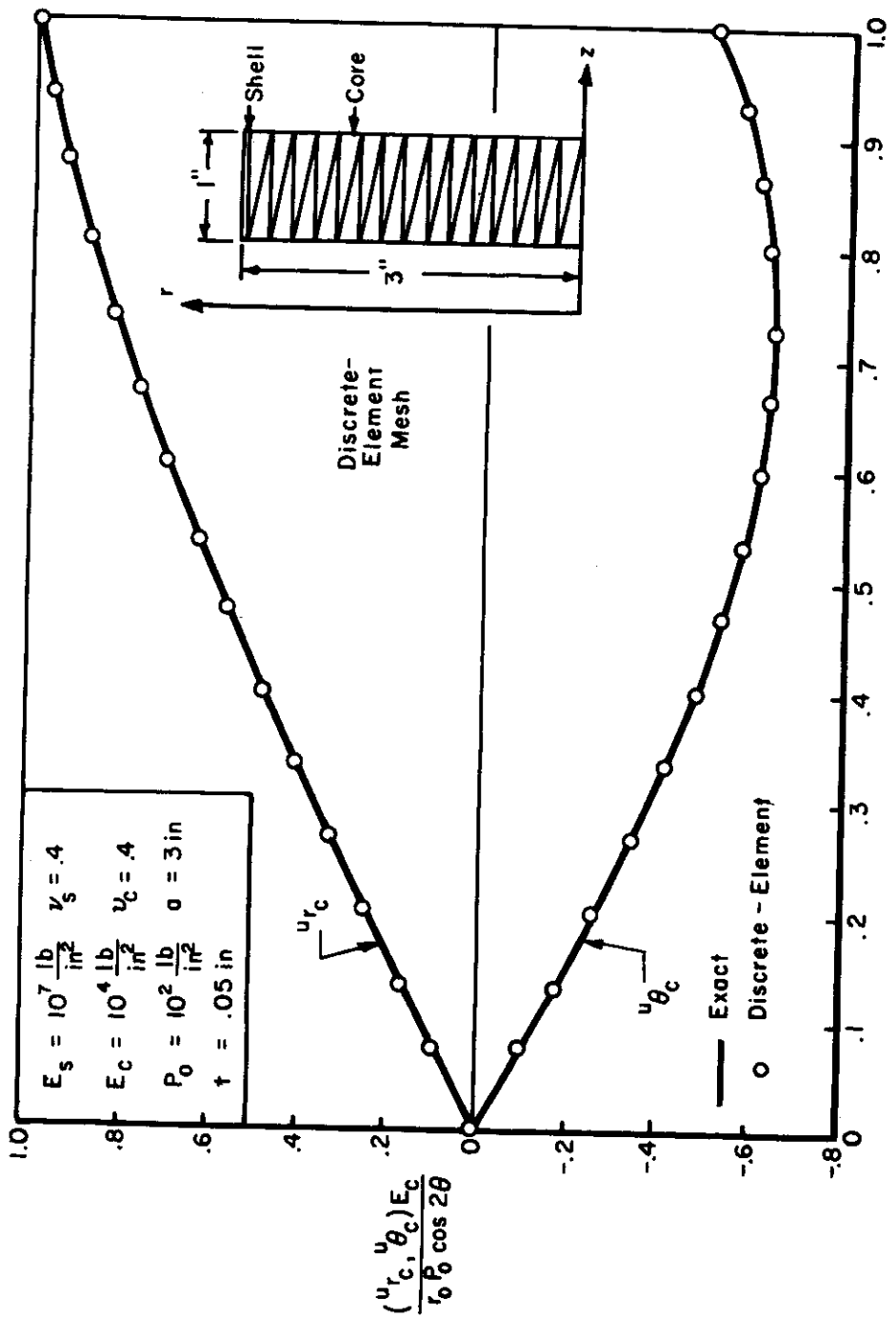

(a) Geometry, Discrete Elements, and Displacements

Figure 22. Infinite Foam-Filled Circular Cylinder Subjected to Uniform Second Harmonic Pressure Loading

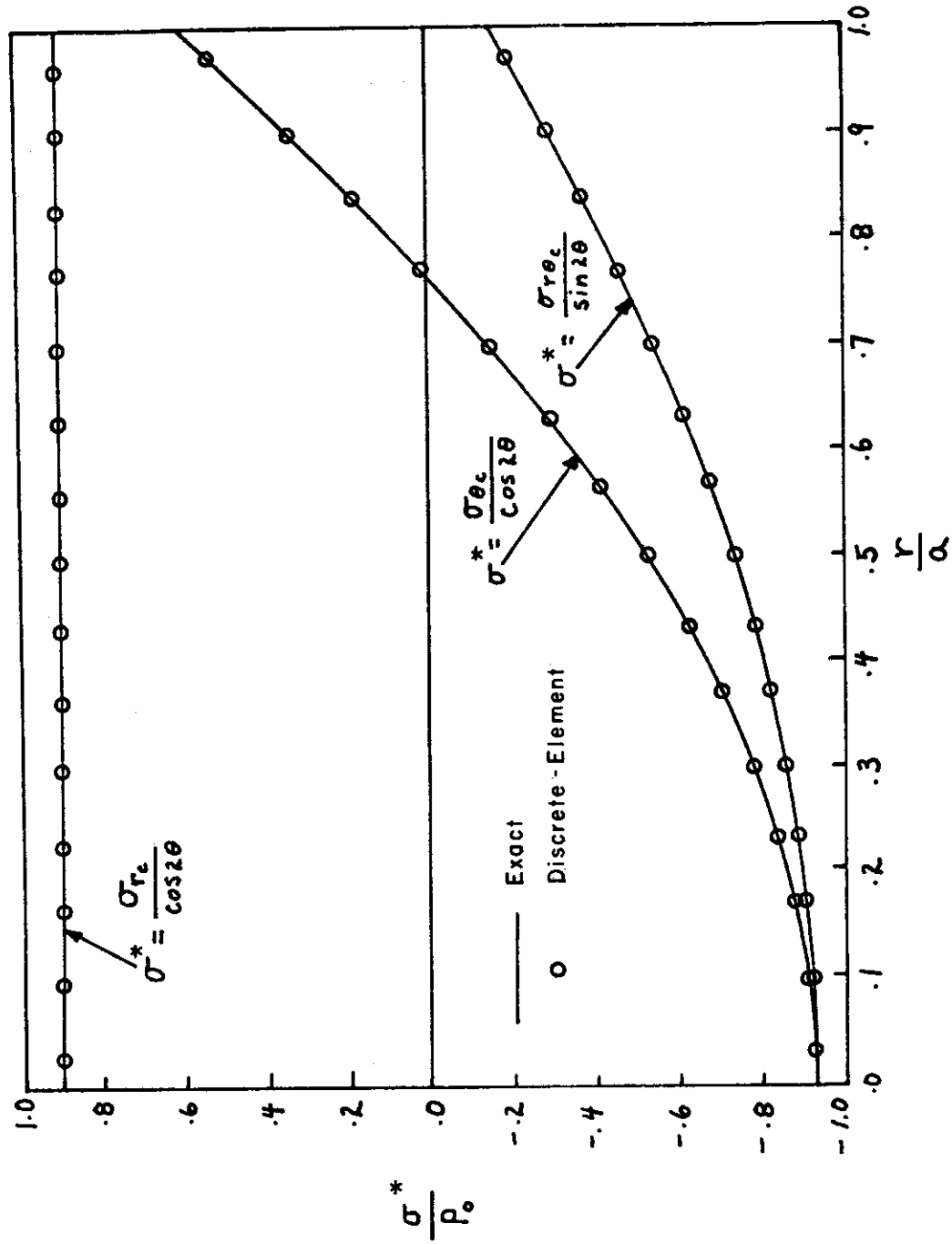

(b) Stresses

Figure 22 Concluded

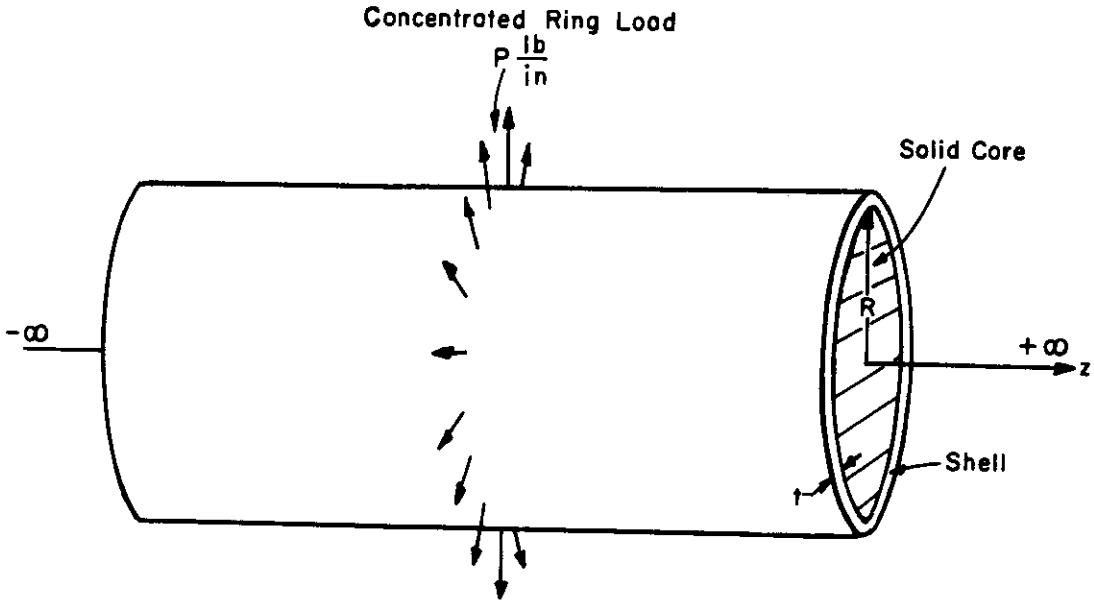

Young's Modulus of Shell E_s
Shear Modulus of Core G_c
Poisson's Ratio of Shell ν_s
Poisson's Ratio of Core ν_c

(a) Infinite Core-Stiffened Cylinder Subjected to Concentrated Ring Loading

Figure 23. Infinite Foam-Filled Cylinder Subjected to Zeroth Harmonic Ring Loading at z = 0

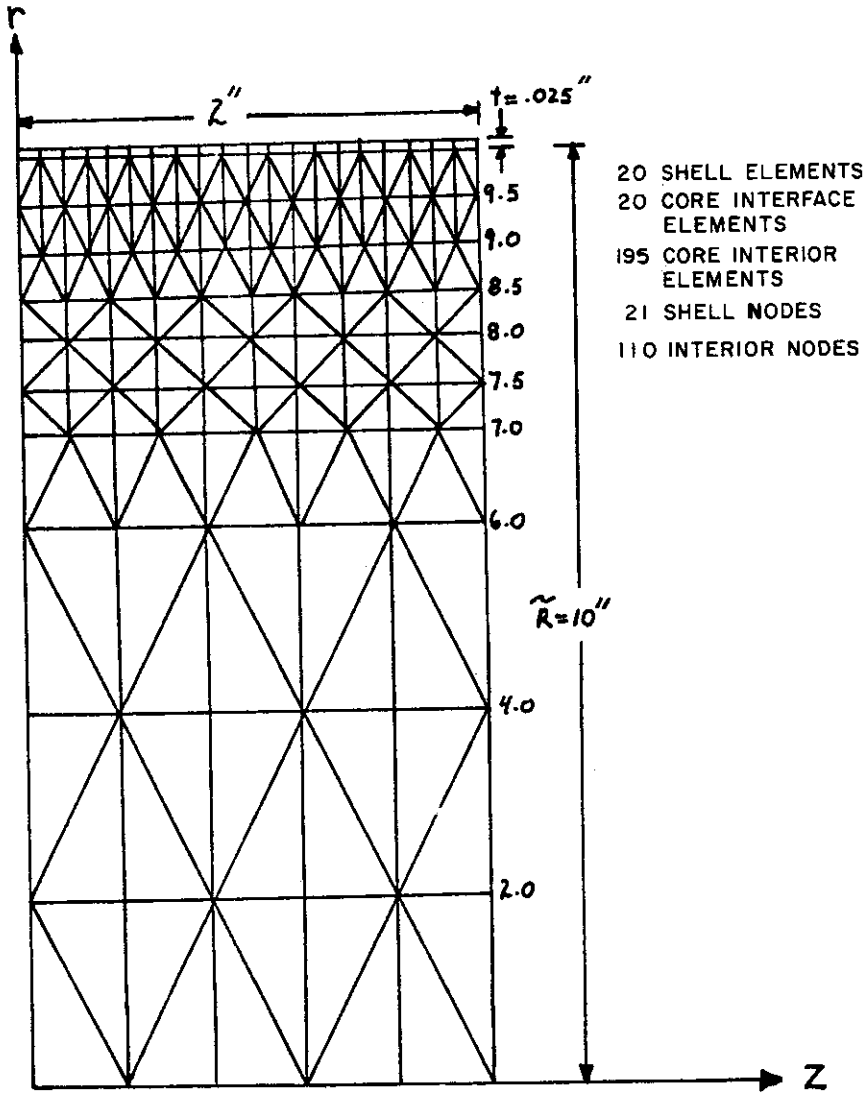

(b) Discrete-Element Mesh

Figure 23 Continued

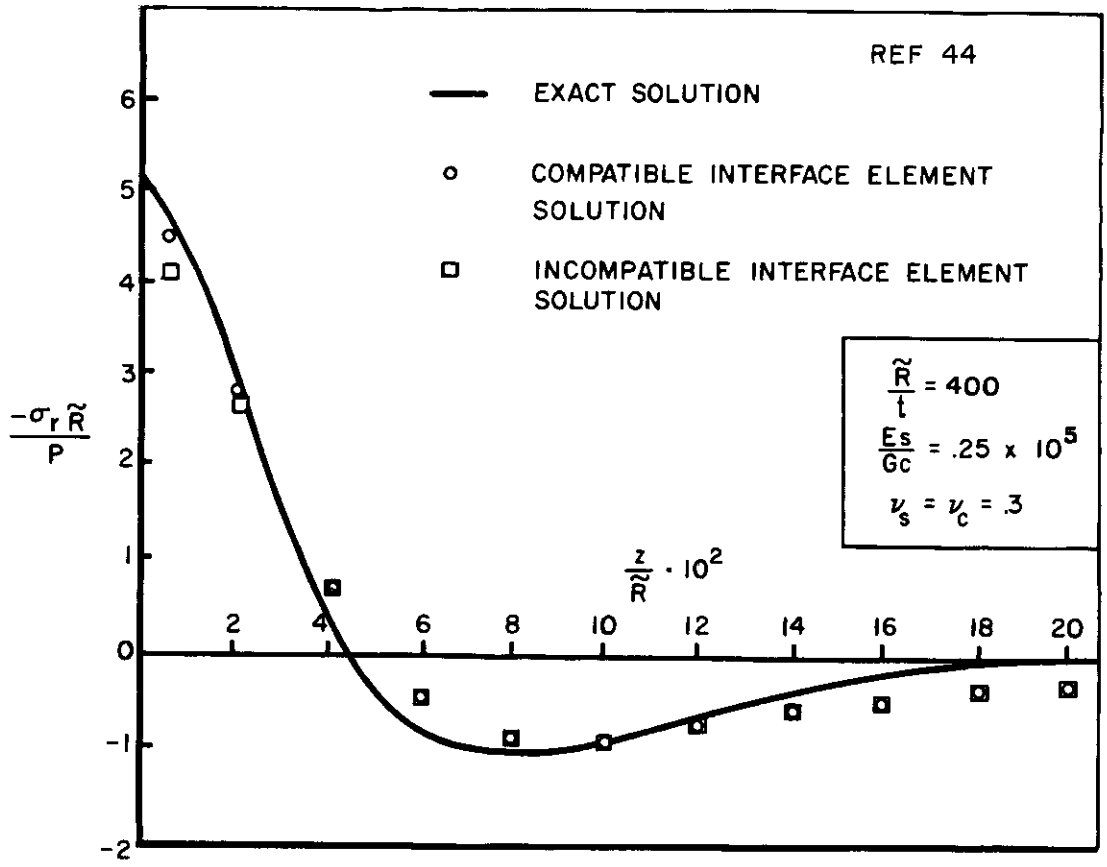

(c) Radial Stress Along Shell-Core Interface

Figure 23 Concluded

Figure 23b to consist of 20 shell elements, 20 core-interface elements, and 195 core-interior elements; in a second case, the same basic breakdown was used but all core elements were of the core interior type. Shown in Figure 23c are these two discrete element solutions and the exact solution of Yao(Reference 44) for the radial stress at the shell-core interface as a function of axial location z/R. It is seen that the "compatible interface element" solution is superior to the "incompatible interface element" solution.

SECTION IV

ELASTIC-PLASTIC ANALYSIS OF PLANE-STRESS PROBLEMS

Two general methods have been developed for the elastic-plastic analysis of continua. These are known as (1) the initial strain method and (2) the tangent modulus method. For the case of small deflections, the initial strain method results in a set of load-deflection equations of equilibrium in which the elastic stiffness matrix is employed throughout the elastic-plastic load-deflection range of interest, and plasticity effects are taken into account through the use of clearly-defined "effective plastic loading". The tangent modulus method, on the other hand, is based upon the linearity of the incremental laws of plasticity, and a piecewise linear solution procedure is involved; the loading is applied in increments and at each load level a new set of coefficients is determined for the equilibrium equations. References 28, and 45 through 53 provide representative documentation of the development of these approaches. References 51 and 52 discuss some studies of the relative merits of these two methods. In the present discussion, however, attention is restricted to the initial strain approach.

FORMULATION (REFERENCE 28)

A typical shell of revolution problem is depicted in Figure 24. For convenience, let it be assumed that the externally-applied loads have a given meridional and circumferential distribution; one seeks to determine the elastic-plastic small-deflection response of this structure as a function of a characteristic amplitude of the applied loading.

The scope of this discussion and the assumptions involved may be summarized concisely as follows:

1. Shell Geometry

    a. Thin Single Layer

    b. Meridionally Curved or Conical

    c. Variable Thickness

    d. Branched

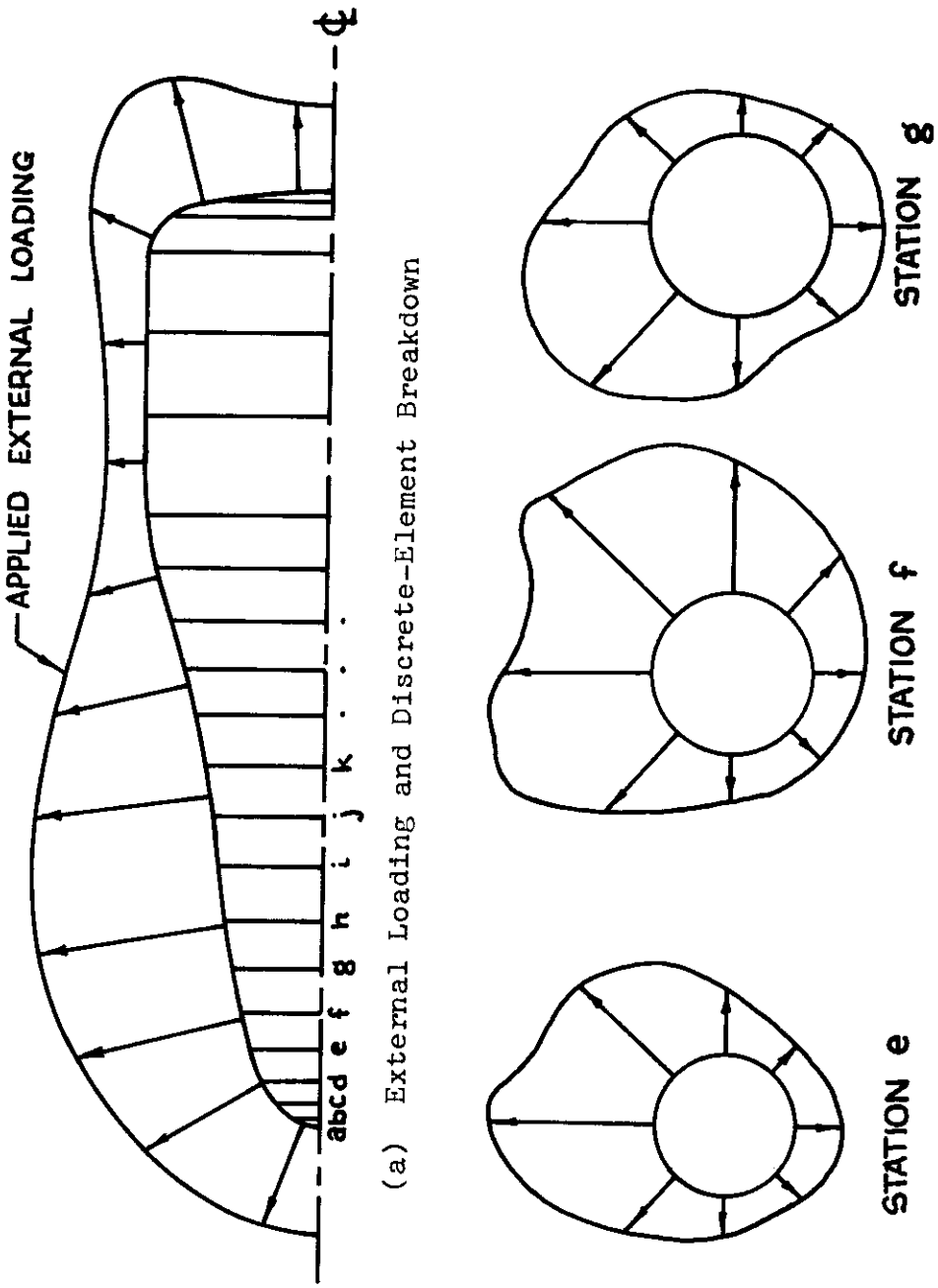

(a) External Loading and Discrete-Element Breakdown

(b) Example Circumferential Variations in Loading

Figure 24. Schematic of Typical Problem

2. Material Properties

   a. Elastic-Isotropic

   b. Plastic

   c. Strain Hardening

   d. Room Temperature

3. Loading is Mechanical (Axisymmetric and Asymmetric)

   a. Distributed

   b. Circumferential Line

   c. No body forces are included

4. Assumptions

   a. Displacements are small and obey the Kirchhoff assumption that normals to the undeformed midsurface are inextensible and remain normal to the deformed midsurface

   b. Shell is in a state of plane stress (σ_s, σ_θ , and $\sigma_{s\theta}$ are present)

In the interest of clarity of presentation, let it be assumed that the loaded structure to be analyzed consists of a (small) single discrete element of revolution. Further, the externally-applied loading has already been discretized into virtual-work-equivalent generalized nodal applied loads $\{\mathbf{Q}\}$. Although this elastic-plastic analysis will be described for a single discrete element, the proper analysis procedure for the complete structure consisting of n discrete elements should be clear from the earlier shell-of-revolution discussion of the treatment of the complete assembled discretized structure.

For the loaded single discrete element, one may apply the initial strain concept to the Principle of Stationary Total Potential Energy, where the plastic strains ϵ^p are treated as initial strains ϵ^o. For this problem, Equation 5 becomes

$$\pi_p = \int_V \hat{U}\, dV - \mathbf{q}^T \mathbf{Q} \tag{89}$$

where the first term represents the internal potential energy (strain energy) of the system and the second represents the potential energy of the applied discretized equivalent nodal loads. As noted earlier, in the initial strain approach the stresses depend only upon the elastic components, ϵ^e, of strain:

$$\sigma = \mathbf{E}\, \epsilon^e \tag{90}$$

where the $\mathbf{E}$ matrix is that which is appropriate for the type of material and stress state involved. Since the total strain ϵ consists of the sum of the elastic and the plastic component of strain, one may write

$$\epsilon = \epsilon^e + \epsilon^p \tag{91}$$

or

$$\epsilon^e = \epsilon - \epsilon^p \tag{92}$$

It follows that the strain energy density $\hat{U}$ may be expressed as

$$\hat{U} = \frac{1}{2} \sigma^T \epsilon^e \tag{93}$$

or

$$\hat{U} = \frac{1}{2} \left(\epsilon^T - \epsilon^{pT}\right) \mathbf{E} \left(\epsilon - \epsilon^p\right) \tag{94}$$

Hence, Equation 89 for the total potential energy of the system may be restated as follows by using Equation 94:

$$\pi_p = \int_0^{\ell} \int_{-h/2}^{h/2} \int_0^{2\pi} \frac{1}{2} \left(\epsilon^T - \epsilon^p\right) \mathbf{E} \left(\epsilon - \epsilon^p\right) r \, d\theta \, d\zeta \, ds - \mathbf{q}^T \mathbf{Q} \tag{95}$$

where the initial strains (herein represented by the plastic strains) are regarded as somehow being known; hence, in applying the PSTPE: $\delta\pi_p = 0$, only the displacements $\mathbf{q}$, not the plastic strains, are subject to variation.

The next step in this formulation process is to express the total strain ϵ at any and all locations in the discrete element in terms of the generalized nodal displacements $\mathbf{q}$ which are given by Equation 57. This may be done by introducing an appropriate assumed-displacement field for u, v, and w, by applying appropriate strain-displacement relations (Equations 37 through 42), and by applying the Kirchhoff deformation assumptions. Also, Fourier decomposition of the generalized displacements, as represented in Equation 58, (as well as all strains and all loads) may be carried out. Hence, the Fourier components of the total strain may be expressed as:

$$\begin{aligned} \epsilon^{(o)} &= \mathbf{A}^{(o)}(\zeta, s)\, \mathbf{q}^{(o)} \\ \epsilon^{(j)} &= \mathbf{A}^{(j)}(\zeta, s)\, \mathbf{q}^{(j)} \\ \bar{\epsilon}^{(j)} &= \bar{\mathbf{A}}^{(j)}(\zeta, s)\, \bar{\mathbf{q}}^{(j)} \end{aligned} \tag{96}$$

By applying Equation 96 to Equation 95 and evaluating the θ-integration from 0 to 2π, complete harmonic uncoupling results. Next, form $\delta\pi_p$ and set $\delta\pi_p = 0$ in accordance with the PSTPE. Since the $\delta q^{(o)} \ldots \delta q^{(j)} \ldots \delta \bar{q}^{(j)}$ are independent and arbitray, the terms which multiply each must be equal to zero. The result is the following set of load-deflection static equilibrium equations:

$$\begin{aligned} k^{(o)}\, q^{(o)} &= Q^{(o)} + Q_p^{(o)} \\ k^{(j)}\, q^{(j)} &= Q^{(j)} + Q_p^{(j)} \quad \text{for } j = 1, 2, \cdots \infty : \text{A-series} \\ \bar{k}^{(j)}\, \bar{q}^{(j)} &= \bar{Q}^{(j)} + \bar{Q}_p^{(j)} \quad \text{for } j = 1, 2, \cdots \infty : \text{B-series} \end{aligned} \tag{97}$$

Note that since these equations are linear, they may be written in <u>incremental</u> form:

$$\begin{aligned} k^{(o)}\, \Delta q^{(o)} &= \Delta Q^{(o)} + \Delta Q_p^{(o)} \\ k^{(j)}\, \Delta q^{(j)} &= \Delta Q^{(j)} + \Delta Q_p^{(j)} \\ \bar{k}^{(j)}\, \Delta \bar{q}^{(j)} &= \Delta \bar{Q}^{(j)} + \Delta \bar{Q}_p^{(j)} \end{aligned} \tag{98}$$

These are the basic equations which are employed in calculating the load-deflection behavior of this structure. The k's are the usual harmonic stiffness matrices for the discrete element:

$$k^{(o)} = 2\pi \int_0^{\ell} \int_{-h/2}^{h/2} A^{(o)T}\, E\, A^{(o)}\, r(s)\, d\zeta\, ds$$

$$k^{(j)} = \pi \int_0^{\ell} \int_{-h/2}^{h/2} A^{(j)T}\, E\, A^{(j)}\, r(s)\, d\zeta\, ds \tag{99}$$

$$\bar{k}^{(j)} = \pi \int_0^{\ell} \int_{-h/2}^{h/2} \bar{A}^{(j)T}\, E\, \bar{A}^{(j)}\, r(s)\, d\zeta\, ds$$

The $\Delta \mathbf{Q}$'s are increments of the externally-applied loads, and the $\Delta \mathbf{Q}_p$'s may be regarded as the additional equivalent loads which produce the part of $\Delta \mathbf{q}$ brought about by the $\Delta \boldsymbol{\epsilon}^p$. Explicitly, these ΔQ_p terms are:

$$\Delta \mathbf{Q}_p^{(o)} = 2\pi \int_0^{\ell} \int_{-h/2}^{h/2} \mathbf{A}^{(o)T} \; \mathbf{E} \; \Delta \boldsymbol{\epsilon}^{p(o)} \; r(s) \; d\zeta \; ds$$

$$\Delta \mathbf{Q}_p^{(j)} = \pi \int_0^{\ell} \int_{-h/2}^{h/2} \mathbf{A}^{(j)T} \; \mathbf{E} \; \Delta \boldsymbol{\epsilon}^{p(j)} \; r(s) \; d\zeta \; ds \qquad (100)$$

$$\Delta \bar{\mathbf{Q}}_p^{(j)} = \pi \int_0^{\ell} \int_{-h/2}^{h/2} \bar{\mathbf{A}}^{(j)T} \; \mathbf{E} \; \Delta \bar{\boldsymbol{\epsilon}}^{p(j)} \; r(s) \; d\zeta \; ds$$

These "incremental plastic loads" can be cast into a more convenient form by recognizing that the matrix $\mathbf{A}^{(j)}(\zeta,s)$ which relates the <u>total</u> strain at any location in the discrete element to the nodal displacement $\mathbf{q}^{(j)}$ may be written as the product of two matrices: $\mathbf{A}_\zeta$ which is a function of ζ and is harmonic independent, and $\mathbf{A}_s^{(j)}$ which does not involve ζ but depends upon s and the Fourier harmonic j. Hence,

$$\boldsymbol{\epsilon}^{(j)} = \mathbf{A}^{(j)}(\zeta, s) \; \mathbf{q}^{(j)}$$

$$= \underset{3\times 6}{\mathbf{A}_\zeta} \; \underset{6\times 8}{\mathbf{A}_s^{(j)}} \; \underset{8\times 1}{\mathbf{q}^{(j)}} \qquad (101)$$

Hence, for example,

$$\Delta \mathbf{Q}_p^{(j)} = \pi \int_0^{\ell} \int_{-h/2}^{h/2} \mathbf{A}_s^{(j)T} \; \mathbf{A}_\zeta^T \; \mathbf{E} \; \Delta \boldsymbol{\epsilon}^{p(j)} \; r(s) \; d\zeta \; ds \qquad (102)$$

Now, at some reference or control station (or stations) as depicted, for example, in Figure 25, form the following subquantity of Equation 102 by integrating wrt ζ from -h/2 to + h/2:

$$\underset{6\times 1}{\Delta \mathbf{N}_{p_c}^{(j)}} = \int_{-h/2}^{h/2} \underset{6\times 3}{\mathbf{A}_\zeta^T} \; \underset{3\times 3}{\mathbf{E}} \; \underset{3\times 1}{\Delta \boldsymbol{\epsilon}^{p(j)}} \; d\zeta \qquad (103)$$

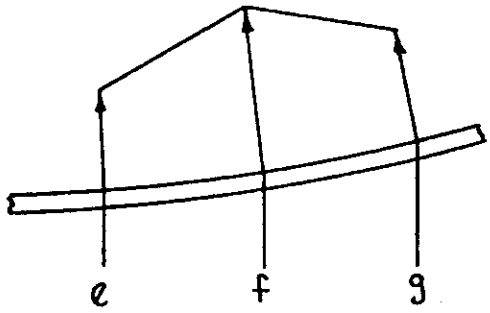

(a) Example Meridional Variations in Loading

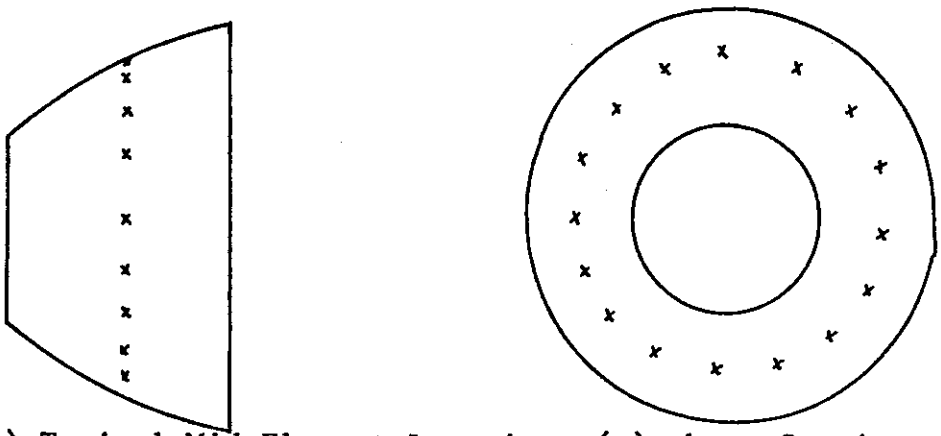

(b) Typical Mid-Element Locations (x) where Strains and Plastic Stress Resultants are Computed

Figure 25. Meridional Loading Variation and Representative Plastic Stress Resultant Computation Points

To simplify the analysis somewhat, assume that $\Delta \mathbf{N}_p^{(j)}(s)$ varies with the s-location in the discrete element such that

$$\underset{6\times 1}{\Delta \mathbf{N}_p^{(j)}(s)} = \underset{6\times 6}{\mathbf{G}^{(j)}(s)} \quad \underset{6\times 1}{\Delta \mathbf{N}_{p_c}^{(j)}} \tag{104}$$

Similarly, let

$$\Delta \mathbf{N}_p^{(o)}(s) = \mathbf{G}^{(o)}(s) \quad \Delta \mathbf{N}_{p_c}^{(o)} \tag{105}$$

$$\Delta \bar{\mathbf{N}}_p^{(j)}(s) = \bar{\mathbf{G}}^{(j)}(s) \quad \Delta \bar{\mathbf{N}}_{p_c}^{(j)} \tag{106}$$

where these G(s) matrices are appropriately-selected distribution matrices. For example, if $\Delta \mathbf{N}_p$ were assumed to be invariant with s, the $\mathbf{G}$ matrices would become the unit diagonal matrix. Various assumptions for G(s) may be made, and consistent control stations selected.

Applying Equation 104 to Equation 102, $\Delta \mathbf{Q}_p^{(j)}$ may be rewritten as

$$\Delta \mathbf{Q}_p^{(j)} = \left(\pi \int_o^{\ell} \mathbf{A}_s^{(j)^T} \mathbf{G}^{(j)}(s)\ r(s)\ ds \right) \Delta \mathbf{N}_{p_c}^{(j)} \equiv \mathbf{p}^{(j)}\ \Delta \mathbf{N}_{p_c}^{(j)} \tag{107}$$

Similarly one may write

$$\Delta \mathbf{Q}_p^{(o)} = \mathbf{p}^{(o)} \quad \Delta \mathbf{N}_{p_c}^{(o)} \tag{108}$$

$$\Delta \bar{\mathbf{Q}}_p^{(j)} = \bar{\mathbf{p}}^{(j)} \quad \Delta \bar{\mathbf{N}}_{p_c}^{(j)} \tag{109}$$

Clearly, for use in Equation 98, one can find $\Delta \mathbf{Q}_p^{(o)}$, $\Delta \mathbf{Q}_p^{(j)}$, and $\Delta \bar{\mathbf{Q}}_p^{(j)}$ immediately if one knows $\Delta \mathbf{N}_{p_c}^{(o)}$, $\Delta \mathbf{N}_{p_c}^{(j)}$, and $\Delta \bar{\mathbf{N}}_{p_c}^{(j)}$. These quantities, in turn, can be computed by evaluating

$$\Delta \mathbf{N}_{p_c} = \int_{-h/2}^{h/2} \mathbf{A}_\zeta^T\ \mathbf{E}\ \Delta \epsilon^p\ d\zeta \tag{110}$$

at many θ-locations of the control station(s), and by harmonically analyzing the results at each of these axial control stations. However, one notes from Equation 110 that the incremental plastic strain $\Delta \epsilon_c^p(\zeta, \theta)$ must be known to permit this evaluation. A means by which the $\Delta \epsilon_c^p(\zeta, \theta)$ may be determined is described in the following two subsections which deal with plasticity and the solution process.

Equations 98, 107, and 108 may be regarded as the principal (initial) set of "formulation equations" which is required for solving the posed problem. Further considerations and equations are needed, however.

PLASTICITY CONSIDERATIONS

Of the numerous ways of accounting for elastic-plastic behavior, strain hardening, unloading, reversed loading, reloading, etc., one of the most convenient schemes involves the use of a mechanical sublayer model (References 54 to 57). This model has been employed extensively in finite-difference elastic-plastic dynamic response studies (References 58 and 59).

With this model the material is represented as consisting of equally-strained sublayers (or subareas) of elastic, perfectly plastic material, with each sublayer having the same elastic modulus as the basic material being represented but each having appropriately different yield limits. For illustration, the stress-strain properties of a strain hardening material as depicted in Figure 26 is approximated in a piecewise linear manner by the coordinates, $(0,0)$, (σ_1, ϵ_1), (σ_2, ϵ_2), (σ_3, ϵ_3), and (σ_4, ϵ_4). This representation in turn is described by a 4-sublayer model whose perfectly-plastic yield limits are $\sigma_{01} = E\epsilon_1$, $\sigma_{02} = E\epsilon_2$, $\sigma_{03} = E\epsilon_3$, and $\sigma_{04} = E\epsilon_4$. It is seen that the stress-strain behavior of the ith sublayer is given by:

$$\sigma_{SB_i} = \begin{cases} E\epsilon & \text{for } \epsilon \leq \epsilon_i \\ \sigma_{o_i} & \text{for } \epsilon > \epsilon_i \end{cases} \tag{111}$$

At any given value of strain, the stress σ on the piecewise-linear representation of the actual stress-strain curve is given in terms of the M sublayer stresses σ_{SB_i} by

$$\sigma = \sum_{i=1}^{M} \sigma_{SB_i} A_{o_i} \tag{112}$$

where the A_{0i} are appropriately-chosen weighting factors. These weighting factors may be found by writing Equation 81 for each line-segment junction and solving the resulting set of equations.

Illustrative strain and stress distributions through the thickness h of the shell are shown in Figure 27. For the numerical evaluation of stress resultants, for example, it may be convenient to employ the idealized N-layer representation shown in the bottom sketch of

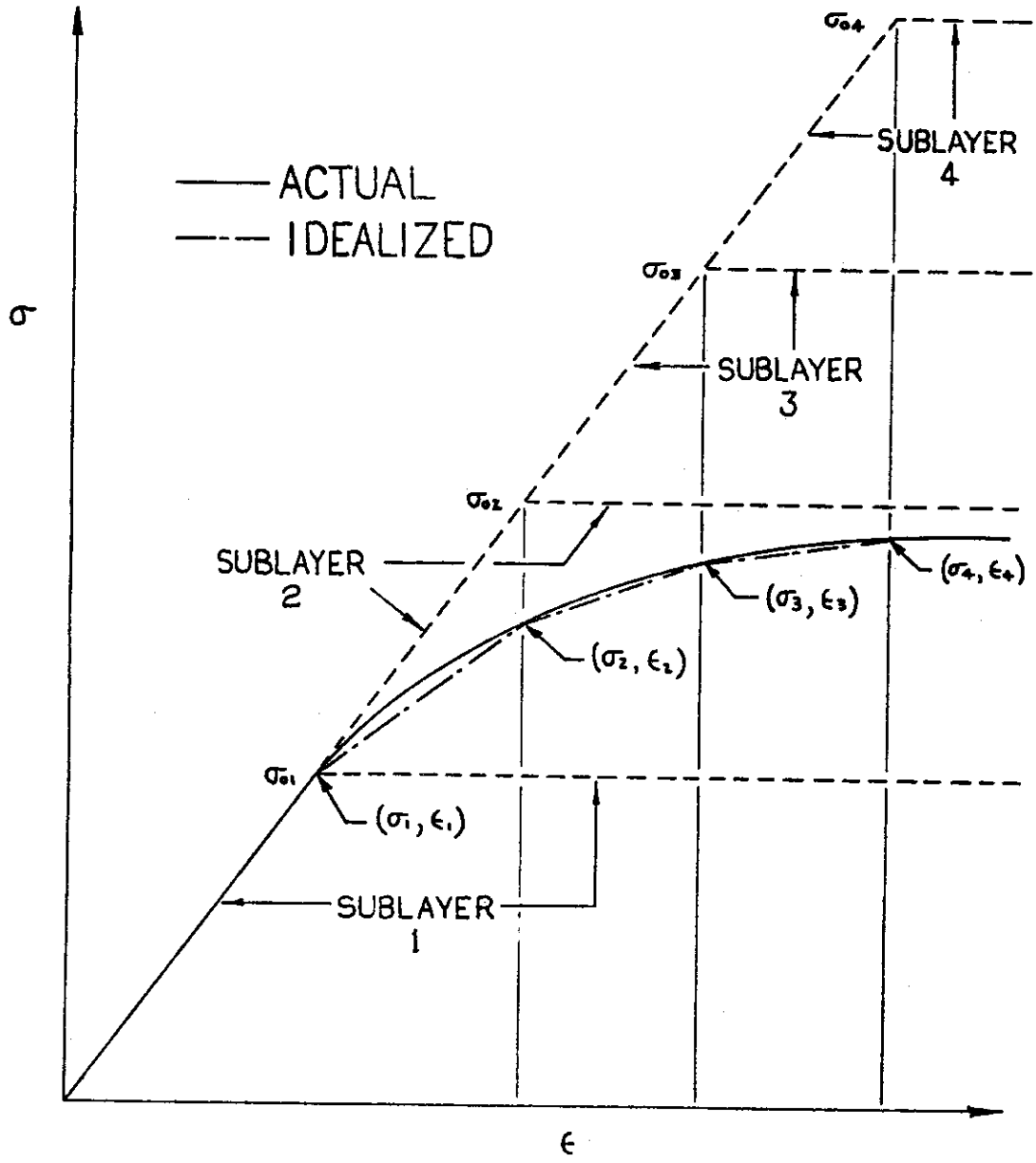

Figure 26. Idealization of Stress-Strain Characteristics

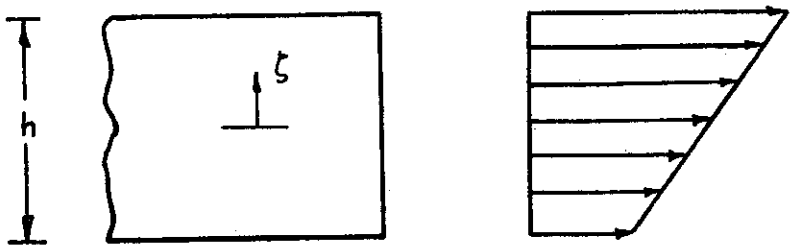

STRAIN DISTRIBUTION

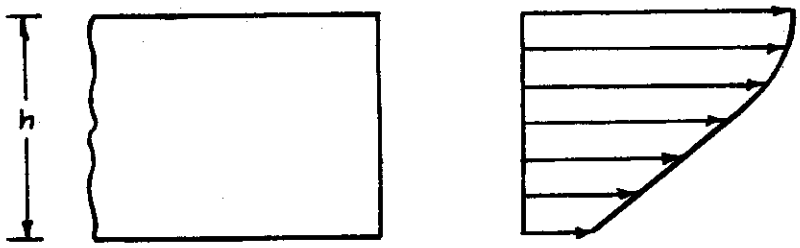

ACTUAL STRESS DISTRIBUTION

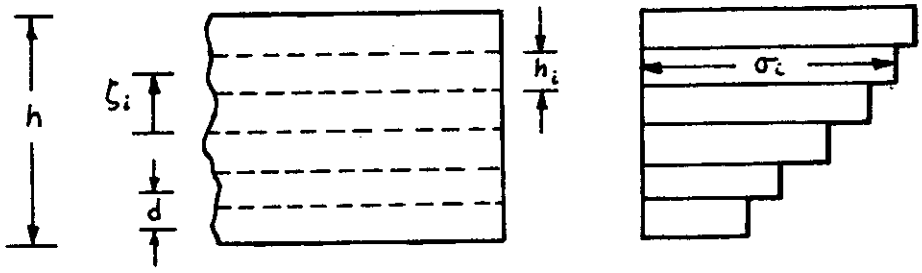

THICKNESS MODEL AND IDEALIZED STRESS DISTRIBUTION

Figure 27. Stress and Strain Distribution Across Shell Thickness

Figure 27; the stress of each of these layers in turn can be described by the use of M sublayers. Thus, in terms of the sublayer stresses, the stress resultants become

$$N_s = \sum_{i=1}^{N} \sum_{j=1}^{M} \sigma_{s_{ij}} t_j \; ; \qquad M_s = \sum_{i=1}^{N} \zeta_i \sum_{j=1}^{M} \sigma_{s_{ij}} t_j \tag{113}$$

where $\sigma_{s_{ij}}$ is the normal stress in the meridional direction s for the jth sublayer of the ith layer and t_j is the thickness of the jth sublayer, where the t_j's have been normalized such that for any layer i of the N layers

$$h_i = \sum_{j=1}^{M} t_j$$

The other stress resultants are given by similar expressions in terms of the sublayer stresses. The sublayer strains of any given layer are equal to the strains of that layer.

A similar double-summation evaluation may be employed for the ζ-integration required to form $\Delta \mathbf{N}_{p_c}$ of Equation 110.

Suppose that load increments $\Delta \mathbf{Q}$ have been applied successively and that at load increment i the complete state of stress $\boldsymbol{\sigma}_i$ (and strain) is known. Then, let $\Delta \mathbf{Q}_{i+1}$ be applied and let it be assumed that the correct incremental strain $\Delta \boldsymbol{\epsilon}_{i+1}$ has been found. One seeks for each sublayer to determine the resulting stress state $\boldsymbol{\sigma}_{i+1}$ and the incremental plastic strain $\Delta \boldsymbol{\epsilon}^p_{i+1}$.

To accomplish this the Mises-Hencky yield condition for plane stress:

$$\Phi = \sigma_s^2 + \sigma_\theta^2 - \sigma_s \sigma_\theta + 3\sigma_{s\theta}^2 - \sigma_o^2 = 0 \tag{115}$$

is employed, where σ_o is the yield stress of that sublayer for uni-axial loading conditions. This condition establishes a stress boundary such that all permissible stress states lie on or within the envelope $\Phi = 0$. If the path between two successive stress states lies completely within the envelope, only elastic strains occur. If all or a portion of that stress path lies on the boundary, plastic strains are possible. The direction of the plastic strain vector is

established by the plastic flow rule in accordance with the theory of the plastic potential (Reference 60); this direction is normal to the yield surface and consequently the plastic strains do not work. This flow rule can be expressed by:

$$d\epsilon_s^p = d\lambda \frac{\partial \Phi}{\partial \sigma_s} = d\lambda (2\sigma_s - \sigma_\theta)$$

$$d\epsilon_{s\theta}^p = d\lambda \frac{\partial \Phi}{\partial \sigma_{s\theta}} = d\lambda (6\sigma_{s\theta}) \tag{116}$$

$$d\epsilon_\theta^p = d\lambda \frac{\partial \Phi}{\partial \sigma_\theta} = d\lambda (2\sigma_\theta - \sigma_s)$$

In incremental form, Equation 116 may be written as

$$\Delta\epsilon_s^p = \lambda (2\sigma_s - \sigma_\theta)$$

$$\Delta\epsilon_{s\theta}^p = \lambda (6\sigma_{s\theta}) \tag{117}$$

$$\Delta\epsilon_\theta^p = \lambda (2\sigma_\theta - \sigma_s)$$

where λ is a non-negative constant of proportionality which is to be found by satisfying the yield condition itself. In matrix form the flow rule may be written as:

$$\begin{Bmatrix} \Delta\epsilon_s^p \\ \Delta\epsilon_{s\theta}^p \\ \Delta\epsilon_\theta^p \end{Bmatrix} = \lambda \begin{bmatrix} 2 & 0 & -1 \\ 0 & 6 & 0 \\ -1 & 0 & 2 \end{bmatrix} \begin{Bmatrix} \sigma_s \\ \sigma_{s\theta} \\ \sigma_\theta \end{Bmatrix} \tag{118}$$

or

$$\Delta\boldsymbol{\epsilon}^p = \lambda \mathbf{H}_1 \boldsymbol{\sigma} \tag{119}$$

Also, the yield condition can be expressed by

$$\Phi = \boldsymbol{\sigma}^T \begin{bmatrix} 1 & 0 & -\frac{1}{2} \\ 0 & 3 & 0 \\ -\frac{1}{2} & 0 & 1 \end{bmatrix} \boldsymbol{\sigma} - \sigma_o^2 = 0 \tag{120}$$

or

$$\Phi = \sigma^T H_2 \sigma - \sigma_0^2 = 0 \tag{121}$$

The assumed-to-be-known total incremental strain $\Delta\epsilon_{i+1}$ can be written in terms of its elastic and plastic components as:

$$\Delta\epsilon_{i+1} = \Delta\epsilon^e_{i+1} + \Delta\epsilon^p_{i+1} \tag{122}$$

Since the stress increment $\Delta\sigma_{i+1}$ depends only upon the elastic strain increment, it can be expressed as

$$\Delta\sigma_{i+1} = E_0 \Delta\epsilon^e_{i+1} \tag{123}$$

or

$$\Delta\sigma_{i+1} = E_0 \left(\Delta\epsilon_{i+1} - \Delta\epsilon^p_{i+1} \right) \tag{124}$$

Note that whereas $\Delta\epsilon_{i+1}$ is known, its elastic and plastic components are not known; these are to be determined.

For an initial inquiry, let a trial stress increment (superscript τ) be defined by

$$\Delta\sigma^\tau_{i+1} = E_0 \Delta\epsilon_{i+1} \tag{125}$$

Then the total trial stress is given by

$$\sigma^\tau_{i+1} = \sigma_i + \Delta\sigma^\tau_{i+1} \tag{126}$$

Using this trial total stress, one may compute a trial value of Φ, say Φ^τ_{i+1}, by

$$\Phi^\tau_{i+1} = \sigma^{\tau T}_{i+1} H_2 \sigma^\tau_{i+1} - \sigma_0^2 \tag{127}$$

Now if $\Phi^\tau_{i+1} < 0$, the stress state lies inside the yield boundary and only elastic behavior is present. However, if $\Phi^\tau_{i+1} \geq 0$ plasticity occurs and the increments of elastic strain and plastic strain must be determined; in this case the correct stress state σ_{i+1} is one such that the yield condition:

$$\Phi_{i+1} = \sigma_{i+1} H_2 \sigma_{i+1} - \sigma_0^2 = 0 \tag{121}$$

must be satisfied. Furthermore, one can express this correct state of stress by

$$\begin{aligned}\sigma_{i+1} &= \sigma_i + \Delta\sigma_{i+1} \\ &= \sigma_i + E_o \left(\Delta\epsilon_{i+1} - \Delta\epsilon^p_{i+1}\right) \\ &= \sigma_i + E_o \Delta\epsilon_{i+1} - E_o \Delta\epsilon^p_{i+1} \\ &= \sigma^\tau_{i+1} - E_o \Delta\epsilon^p_{i+1}\end{aligned} \tag{128}$$

But since Equation 119 determines only the direction of the plastic strain increment, one can, to a good approximation, write:

$$\Delta\epsilon^p_{i+1} = \lambda H_1 \sigma^\tau_{i+1} \tag{129}$$

Thus, Equation 128 becomes

$$\sigma_{i+1} = \left[I - \lambda E_o H_1\right] \sigma^\tau_{i+1} \tag{130}$$

Applying Equation 130 to the yield condition, Equation 121, and carrying out the indicated multiplication results in the following quadratic equation for λ:

$$A\lambda^2 + B\lambda + C = 0 \tag{131}$$

where

$$A = \sigma^{\tau T}_{i+1} H_1 E_o H_2 E_o H_1 \sigma^\tau_{i+1} \tag{132}$$

$$B = -2\sigma^{\tau T}_{i+1} H_1 E_o H_2 \sigma^\tau_{i+1} \tag{133}$$

$$C = \sigma^{\tau T}_{i+1} H_2 \sigma^\tau_{i+1} - \sigma_o^2 \equiv \Phi^\tau_{i+1} \tag{134}$$

It can be shown that the desired root is that given by

$$\lambda = \frac{-B - \sqrt{B^2 - 4AC}}{2A} \tag{135}$$

Using Equation 135, one can compute the desired stress state from Equation 130 and the plastic strain increment $\Delta\epsilon^p_{i+1}$ from Equation 129.

The above process is carried out for all layers and sublayers at many θ-locations (NPT of these locations) of each axial control station of the structure.

TYPICAL SOLUTION PROCEDURE

At this point, consider the typical problem as depicted by Figure 24. The assembled discretized structure is now to be used. The externally-applied loading has been harmonically analyzed and converted to equivalent generalized nodal harmonic loads $Q^{(o)}$, $Q^{(j)}$, and $\overline{Q}^{(j)}$; these have been appropriately summed for the assembled discretized structure to form $F^{(o)}$, $F^{(j)}$, etc. The static loading is to be applied in increments. One seeks the structural deformations after each increment of applied loading.

Solution Process

1. For the first (suitably small) increment of applied loading, one solves the following load-deflection equilibrium equations for the complete assembled discretized structure:

$$K^{(j)} \Delta q^{(j)} = \Delta F^{(j)} \tag{136}$$

for all A-series and B-series loading harmonics. From these now-known generalized displacements, one can compute the total (i.e., summed) strains and also the total stresses at all layers, sublayers, and θ-locations of a suitable number of axial stations. The stress state of the first material property sublayer is compared with the Mises-Hencky yield boundary for both the inner and the outer surface at appropriate z and θ locations. If yielding has not occurred anywhere, load incrementing and problem solution can be continued (alternatively, during the examination of the stress state for the first loading increment, one can readily apply a test to see how much larger the applied loading must be in order that the most critical stress state vector reach the Mises-Hencky yield surface, and loading up to that condition can be applied). For discussion, let it be assumed that N increments of applied loading have been employed to arrive just barely inside the yield surface for the most critical location.

2. For the first loading increment (N+1) in the plastic range, one proceeds as follows:

   a. First, note that the governing equations which are of the form

$$K^{(j)} \Delta q^{(j)}_{N+1} = \Delta F^{(j)}_{N+1} + \Delta F^{(j)}_{p_{N+1}} \tag{137}$$

contain as unknowns both $\Delta q^{(j)}_{N+1}$ and $\Delta F_p{}^{(j)}_{N+1}$. Hence an iterative procedure is needed to enable the correct $\Delta q^{(j)}_{N+1}$ to be determined.

b. As a first approximation ($\alpha = 1$) for finding $\Delta q^{(j)}_{N+1}$, solve

$$K^{(j)} \Delta q^{(j)\alpha=1}_{N+1} = \Delta F^{(j)}_{N+1} \tag{138}$$

for all A-series and B-series harmonics. Then sum the results to find the total strains and stresses at all control stations, θ-locations, and all ζ_i locations.

c. Then use the Mises-Hencky yield condition and flow rule to determine

$$\Delta \epsilon^{e\,\alpha=1}_{c_{N+1}} \quad \text{and} \quad \Delta \epsilon^{p\,\alpha=1}_{c_{N+1}}$$

at all of these locations.

d. Next compute ΔN_{p_c} at all θ-locations of each control station and then harmonically analyze these results to determine

$$\Delta N^{(o)\,\alpha=1}_{p_{c_{N+1}}}, \quad \Delta N^{(j)\,\alpha=1}_{p_{c_{N+1}}}, \text{ etc.}$$

at all control stations.

e. Next combine these equivalent plastic nodal loads to form

$$\Delta F^{(o)\,\alpha=1}_{p_{N+1}}, \quad \Delta F^{(j)\,\alpha=1}_{p_{N+1}}, \text{ and } \Delta \bar{F}^{(j)\,\alpha=1}_{p_{N+1}}$$

These values constitute a first estimate of the equivalent plastic nodal loads for load increment N+1.

f. A second approximation ($\alpha = 2$) to the correct solution for $\Delta q^{(j)}_{N+1}$ may be obtained by solving

$$K^{(j)} \Delta q^{(j)\alpha=2}_{N+1} = \Delta F^{(j)}_{N+1} + \Delta F^{(j)\alpha=1}_{p_{N+1}} \tag{139}$$

for all A-series and B-series harmonics.

g. This process is repeatedly carried out to find:

$$\Delta F_{p_{N+1}}^{(j)\,\alpha=2}$$

$$\Delta F_{p_{N+1}}^{(j)\,\alpha=3}$$

etc.

until these equivalent plastic forces converge. For example, one might require that

$$\left[\frac{\sum_{\text{all nodes}}\sum_{i=1}^{NPT}\left(\Delta F_p^{\alpha-1}-\Delta F_p^{\alpha}\right)_{N+1}}{\sum_{\text{all nodes}}\sum_{i=1}^{NPT}\left(\Delta F_{N+1}\right)^2}\right]^{1/2} < A \qquad (140)$$

where "A" is some suitable value like 0.1 perhaps.

3. One is now ready to proceed to the next loading increment N+2. This entire process is repeated until:

a. the deflections become too large for this small-deflection analysis to be valid or

b. the final load of interest has been reached.

ILLUSTRATIVE RESULTS

In Reference 28 elastic-plastic load-deflection analyses of an axisymmetrically-loaded spherical cap and of an asymmetrically-loaded flat circular plate are reported. In connection with the former, the effects of (a) various discrete element breakdowns, (b) load increment size, and (c) the use of various values of the convergence criterion,(A)are illustrated. It is shown that good accuracy is achieved and substantially less computer time is required when one uses comparatively large rather than small loading increments. Also, the deflections predicted at a given load level in the plastic range are not strongly affected by the value of A employed; values of A as large as 0.2 provide reasonably good results. Because of space and time considerations, only the asymmetrical-loading example is discussed in the following.

A 6061-T6 aluminum alloy plate which is depicted schematically in Figure 28 has been loaded asymmetrically in the laboratory as indicated also in Figure 28. Measurements were made of the apex deflection, deflection profiles, and both upper-surface and lower-surface meridional and circumferential strains.

Shown in Figure 29 is the discrete-element breakdown and model used to predict the load-deflection behavior of this assymmetrically-loaded structure. Also shown in Figure 29 are the control stations and θ-locations at which the $\Delta\epsilon^p$ and the ΔN_{p_c} have been computed. The asymmetric loading and its approximation by 9 Fourier series harmonics are indicated in Figure 30. Two representative uniaxial stress-strain curves for 6061-T6 material were taken into account and are shown in Figure 31.

Shown in Figures 32 through 40 are self-explanatory comparisons of measured vs predicted deflections and strains. For the purely elastic range (Figures 33 through 36) there is good agreement between measurements and predictions; this is regarded as confirming that the discrete-element modeling of the actual structure is reasonable. In the plastic range (Figures 32, and 37 through 40) at a total load level P of 11,000 pounds, the experimental-theoretical agreement while encouraging is not as good.

These predictions represent a first step and much remains to be done. Among items requiring further study are:

a. a faster convergence procedure

b. the effects and effectiveness of using various plastic strain-distribution functions G(s); in the present comparison, G(s) was taken to be the unit diagonal matrix,

c. means for automatically selecting load increment sizes ΔP to minimize computer time and to achieve rapid convergence, and

d. the inclusion and effects of transverse shear deformation and stress.

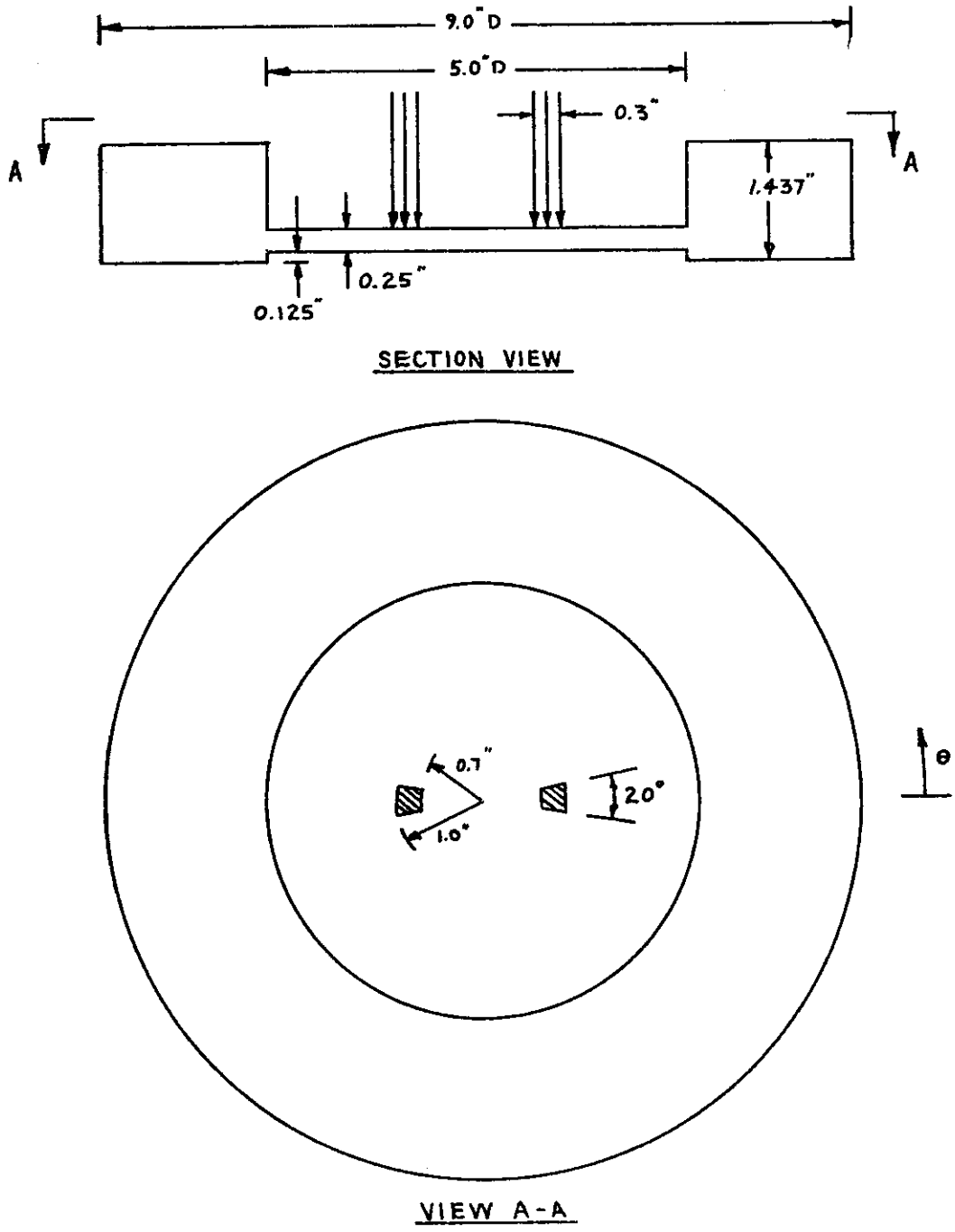

Figure 28. Geometry of Asymmetrically Loaded Test Specimen

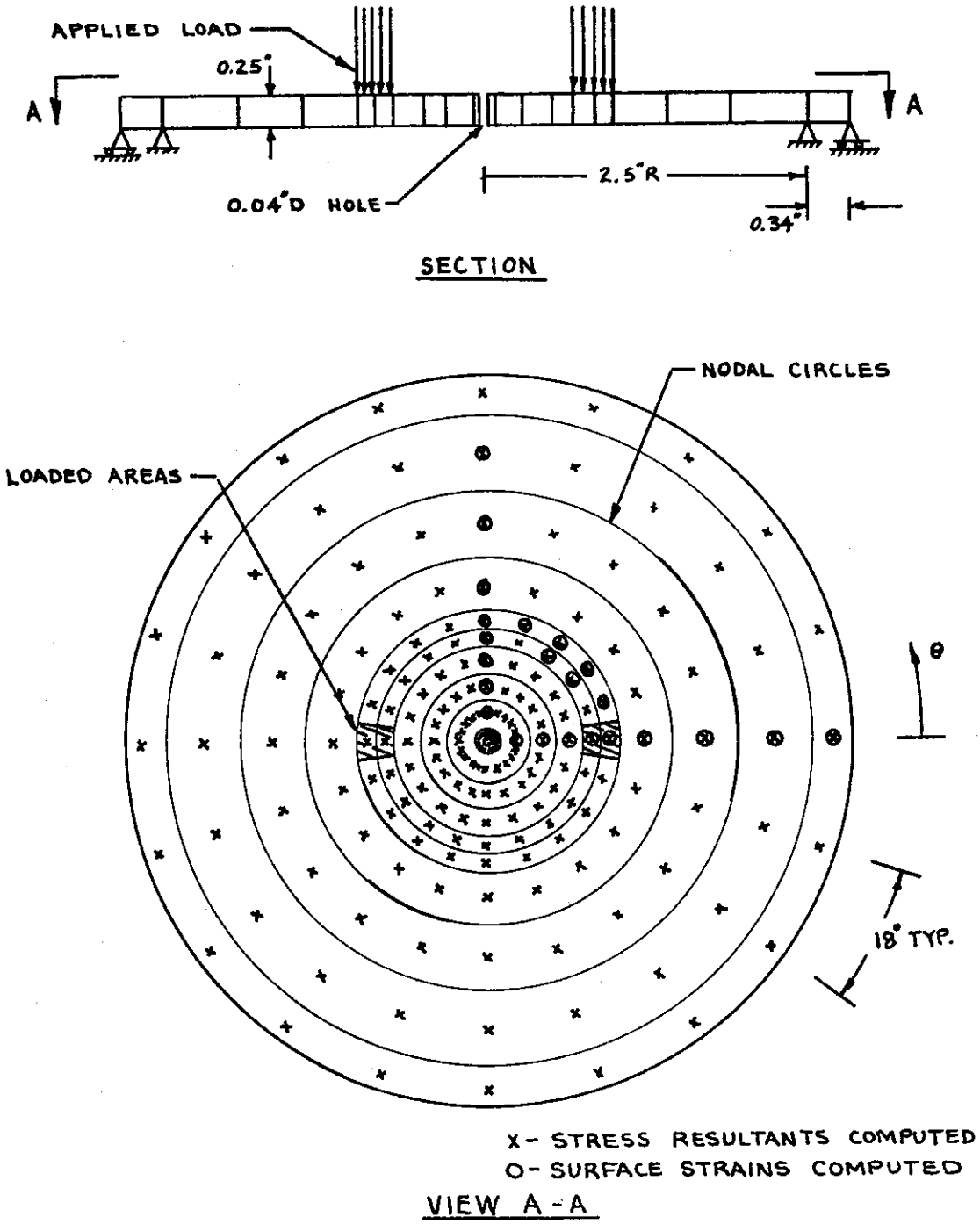

Figure 29. Geometry of Asymmetrically Loaded Discrete-Element Model

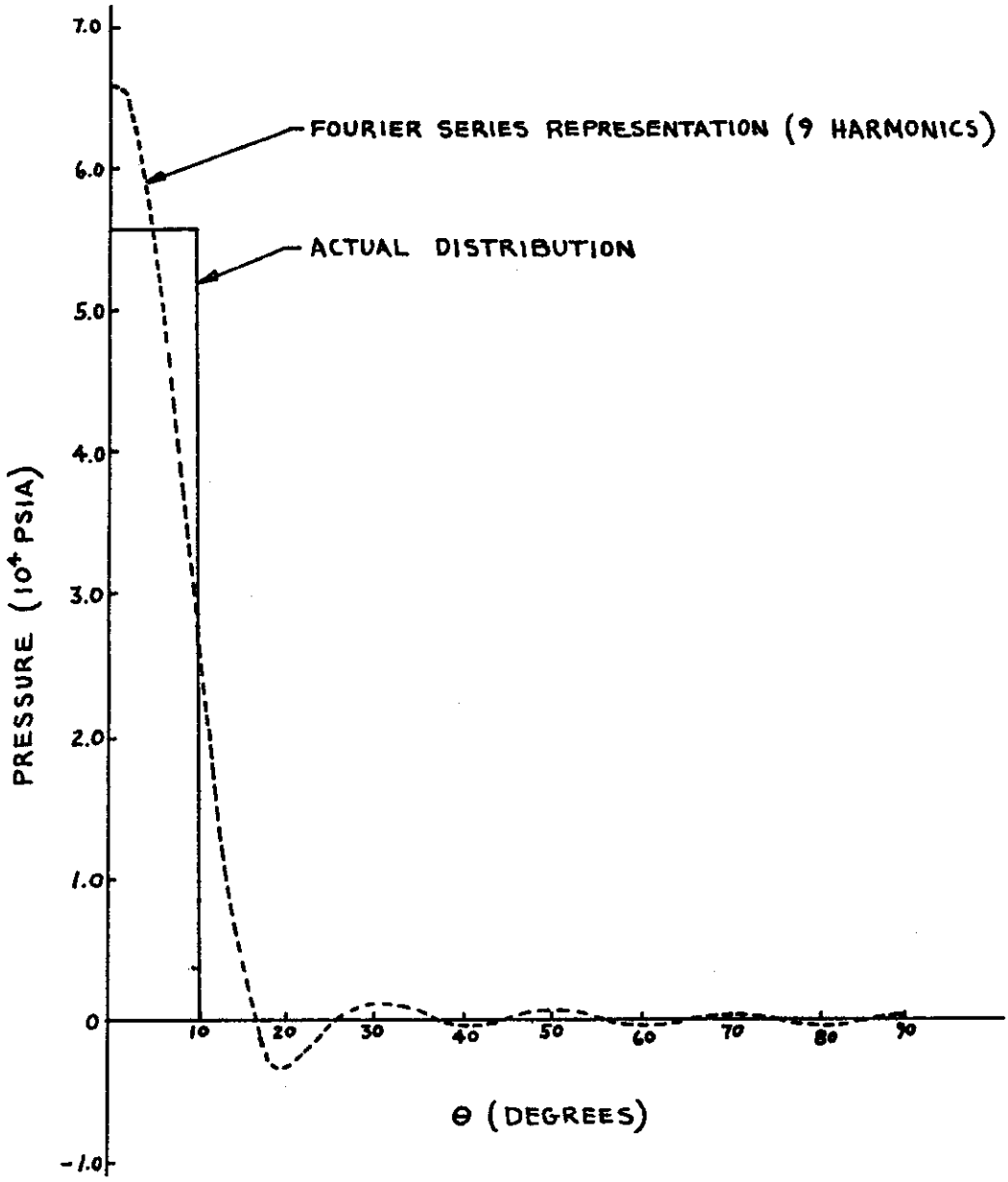

Figure 30. Circumferential Pressure Distribution Between Radii of 0.7 and 1.0 Inch

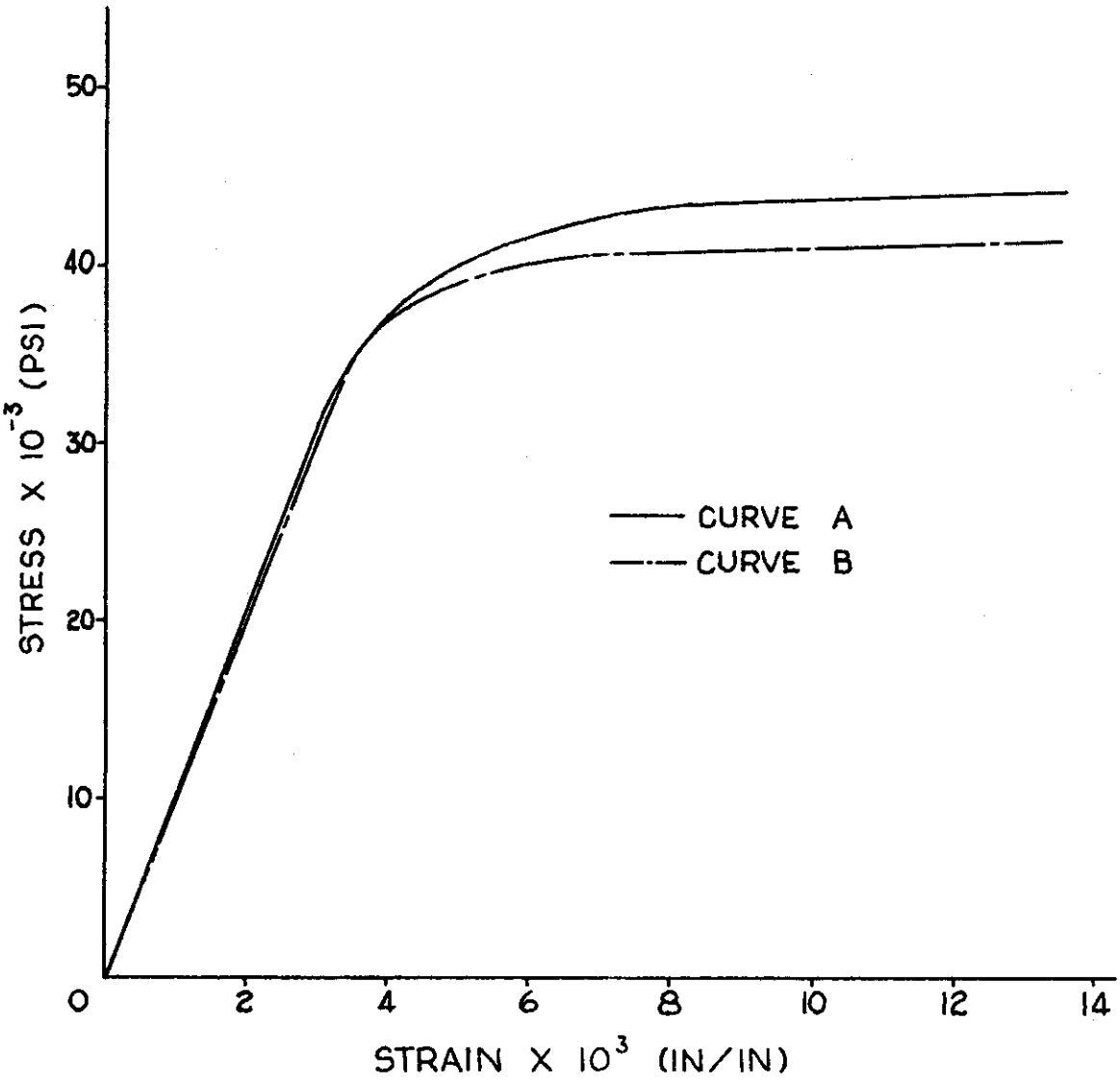

Figure 31. Idealized Stress-Strain Properties of 6061-T6 Aluminum Alloy

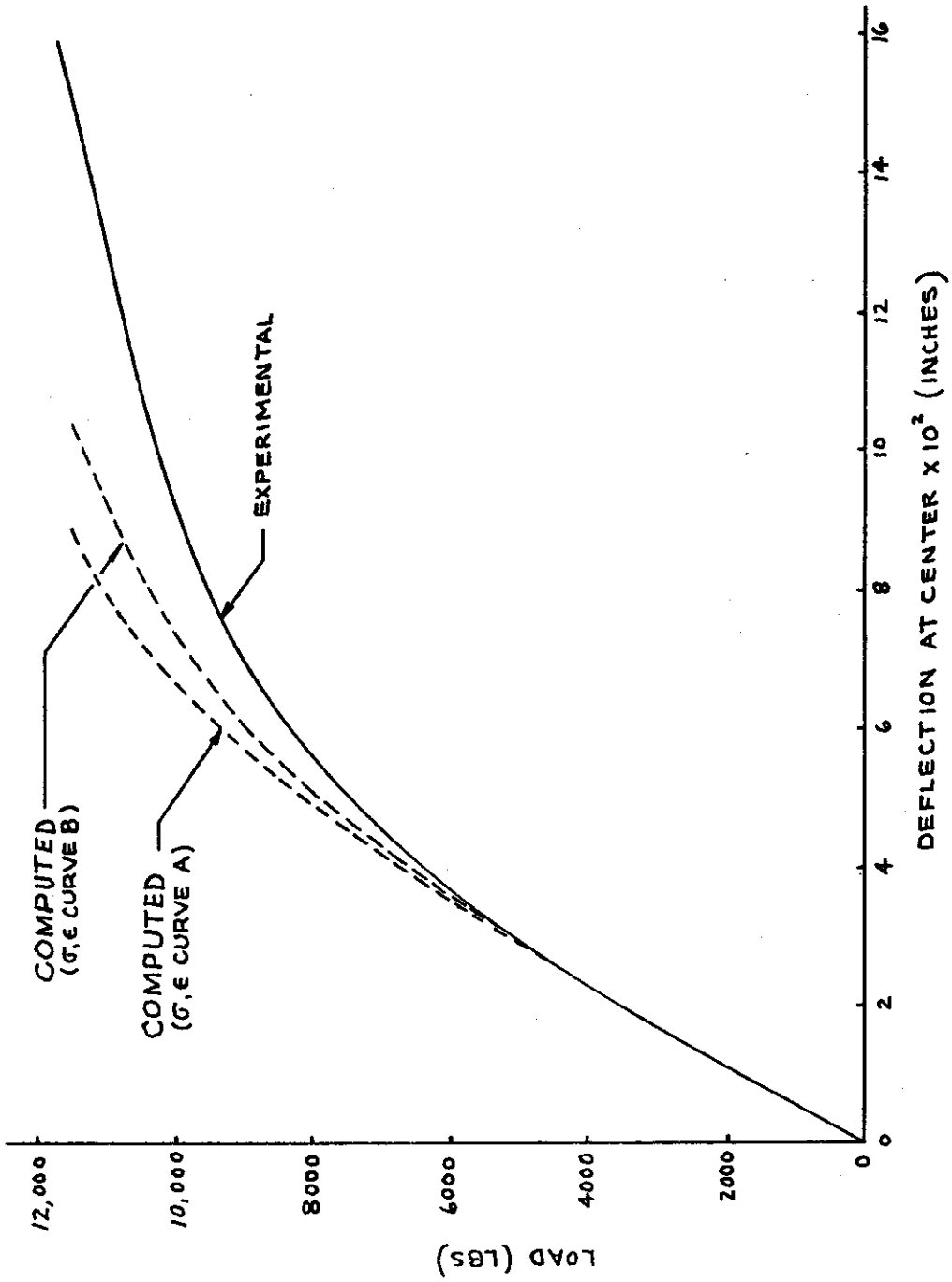

Figure 32. Asymmetrically Loaded Flat Plate Load Versus Deflection

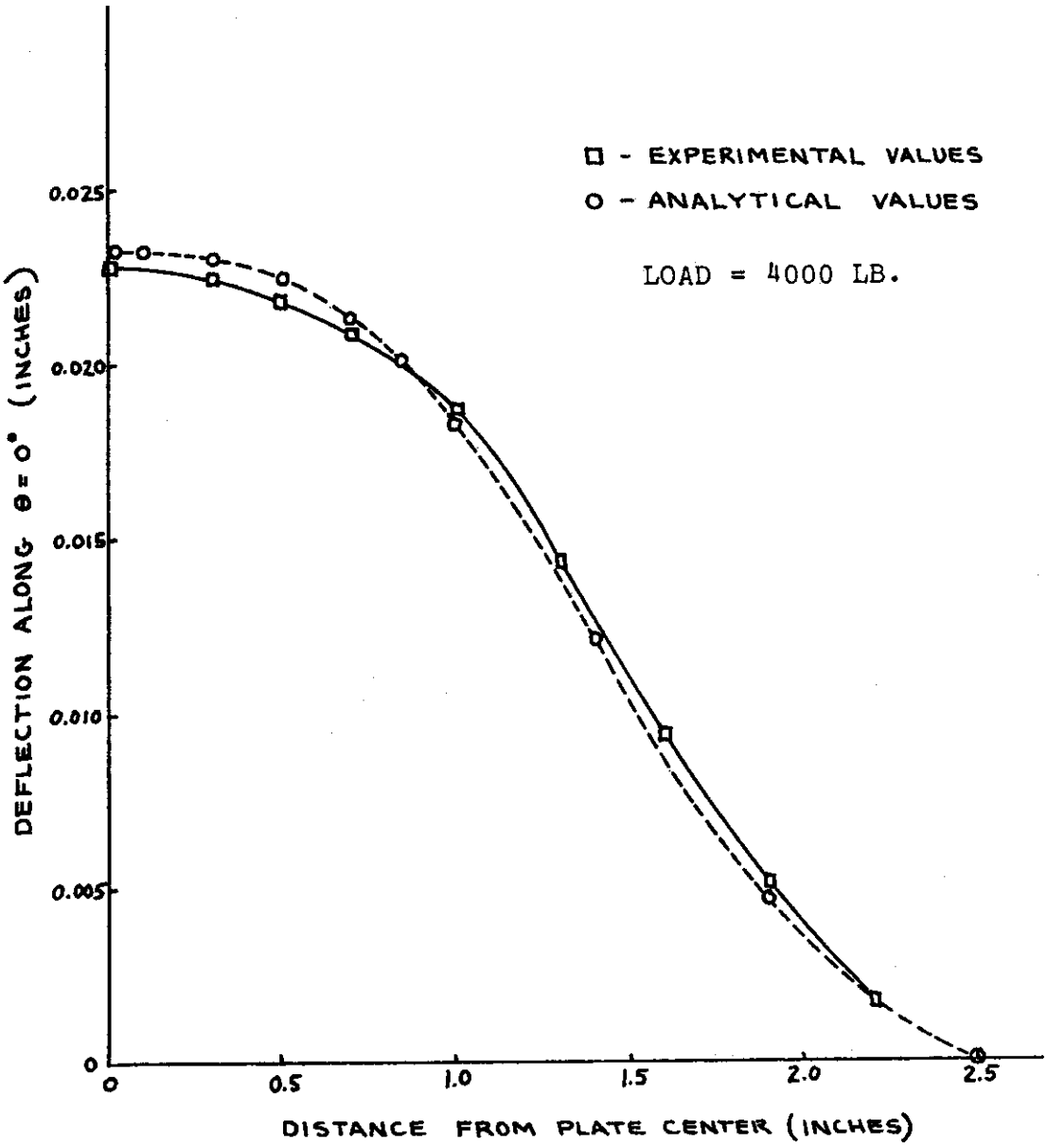

Figure 33. Meridional Variation in Deflection in the Elastic Range (θ = 0 Degrees)

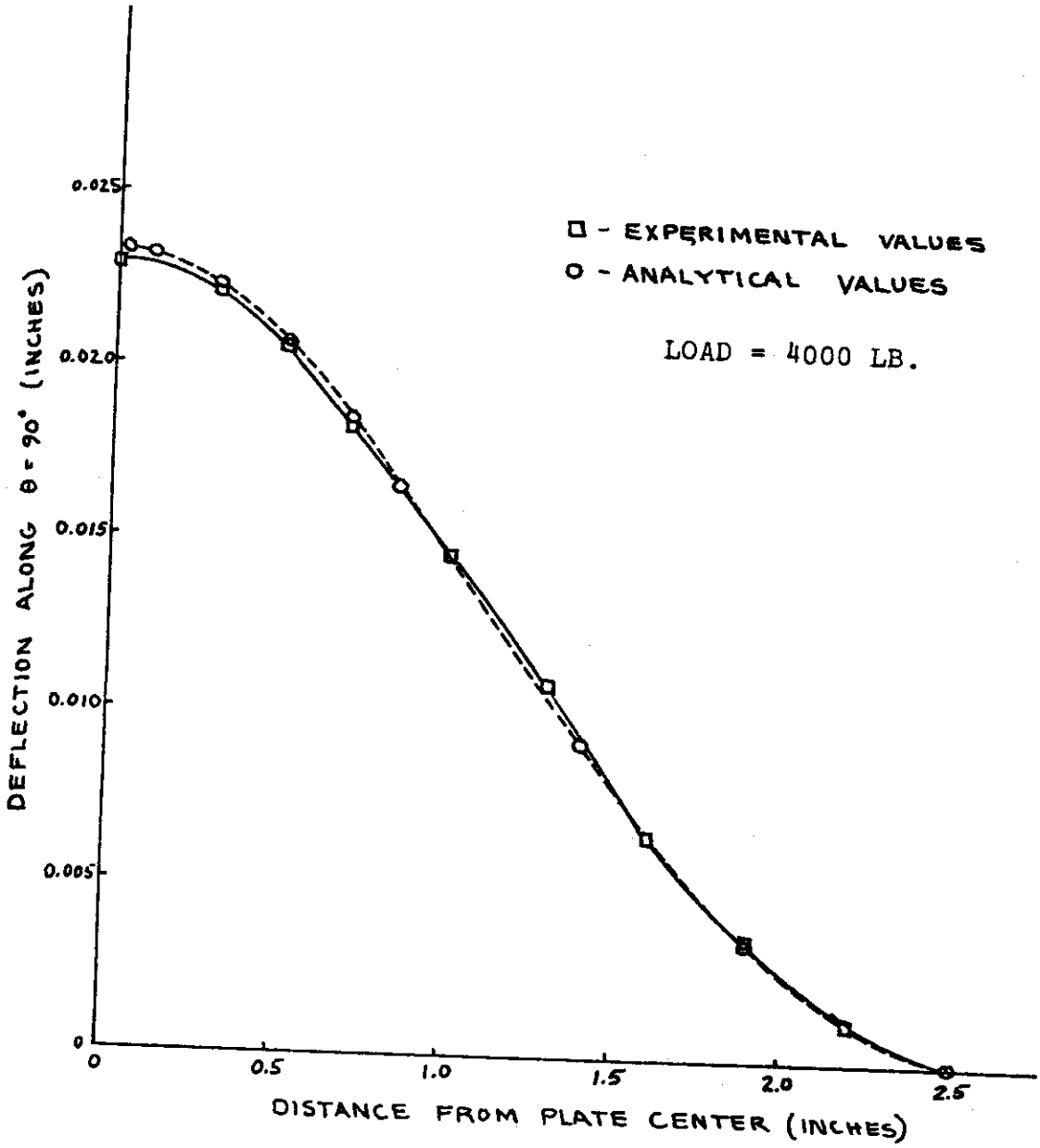

Figure 34. Meridional Variation in Deflection in the Elastic Range (θ = 90 Degrees)

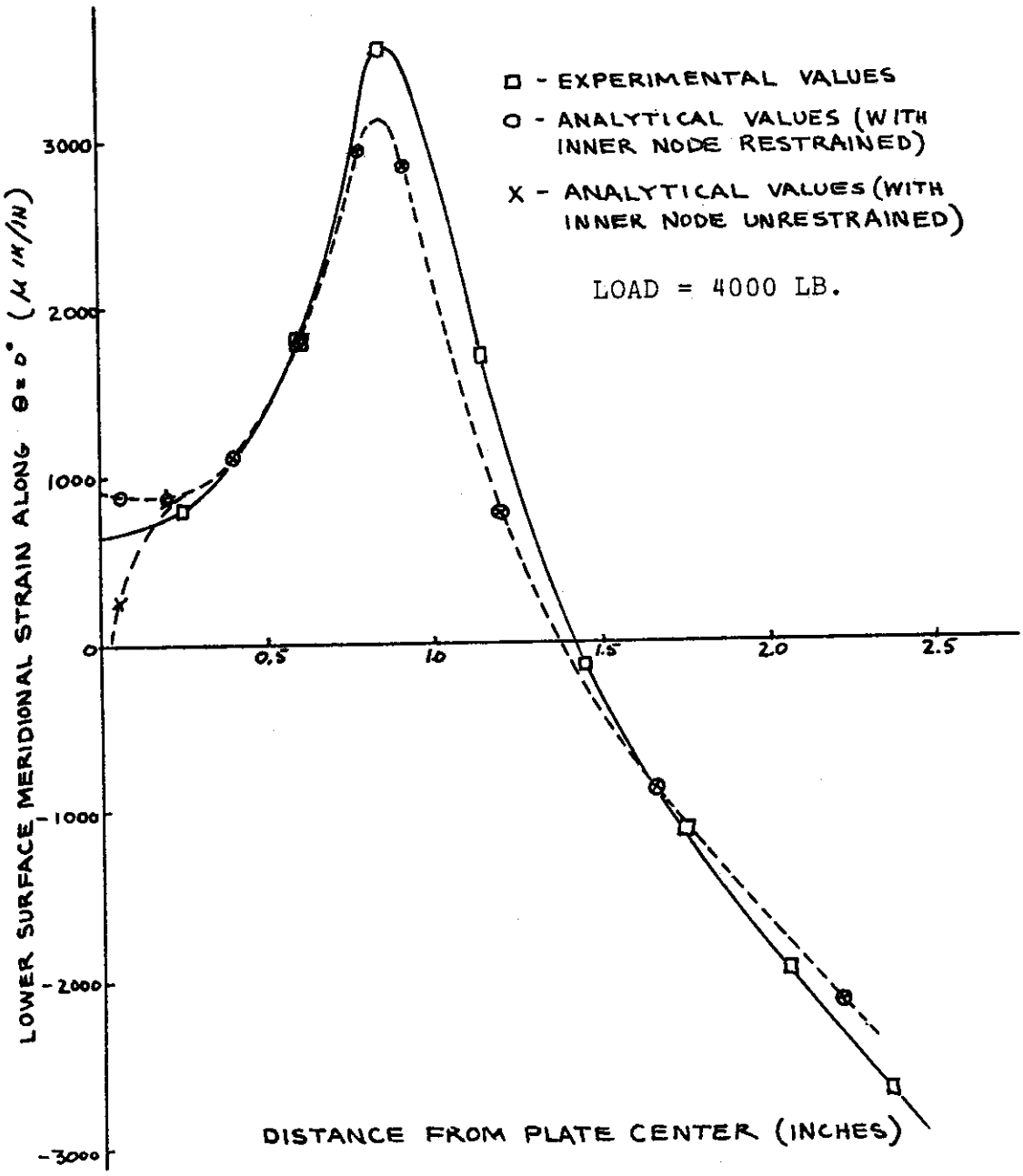

Figure 35. Meridional Variation in Lower Surface Meridional Strain in the Elastic Range (θ = 0 Degrees)

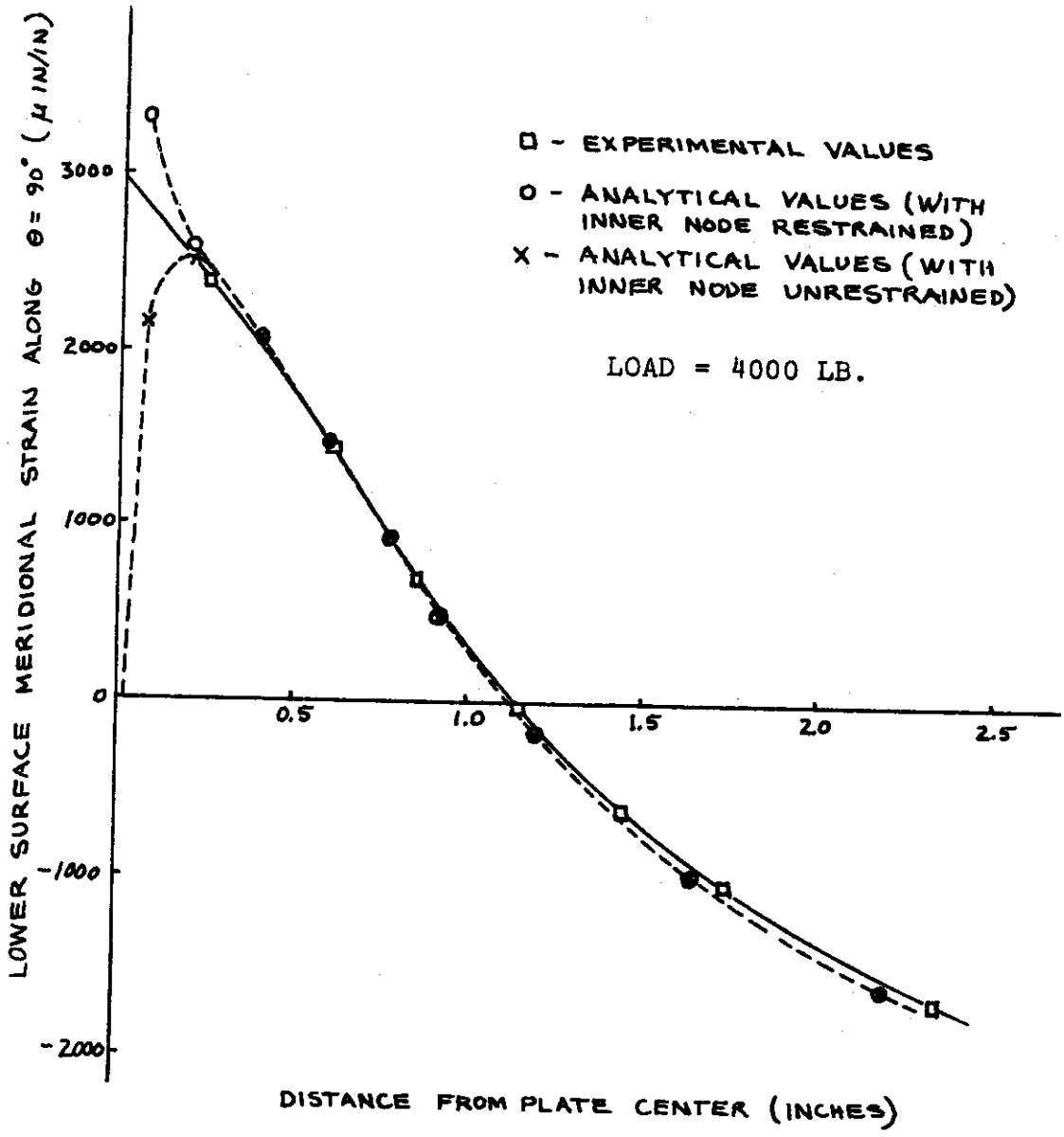

Figure 36. Meridional Variation in Lower Surface Meridional Strain in the Elastic Range (θ = 90 Degrees)

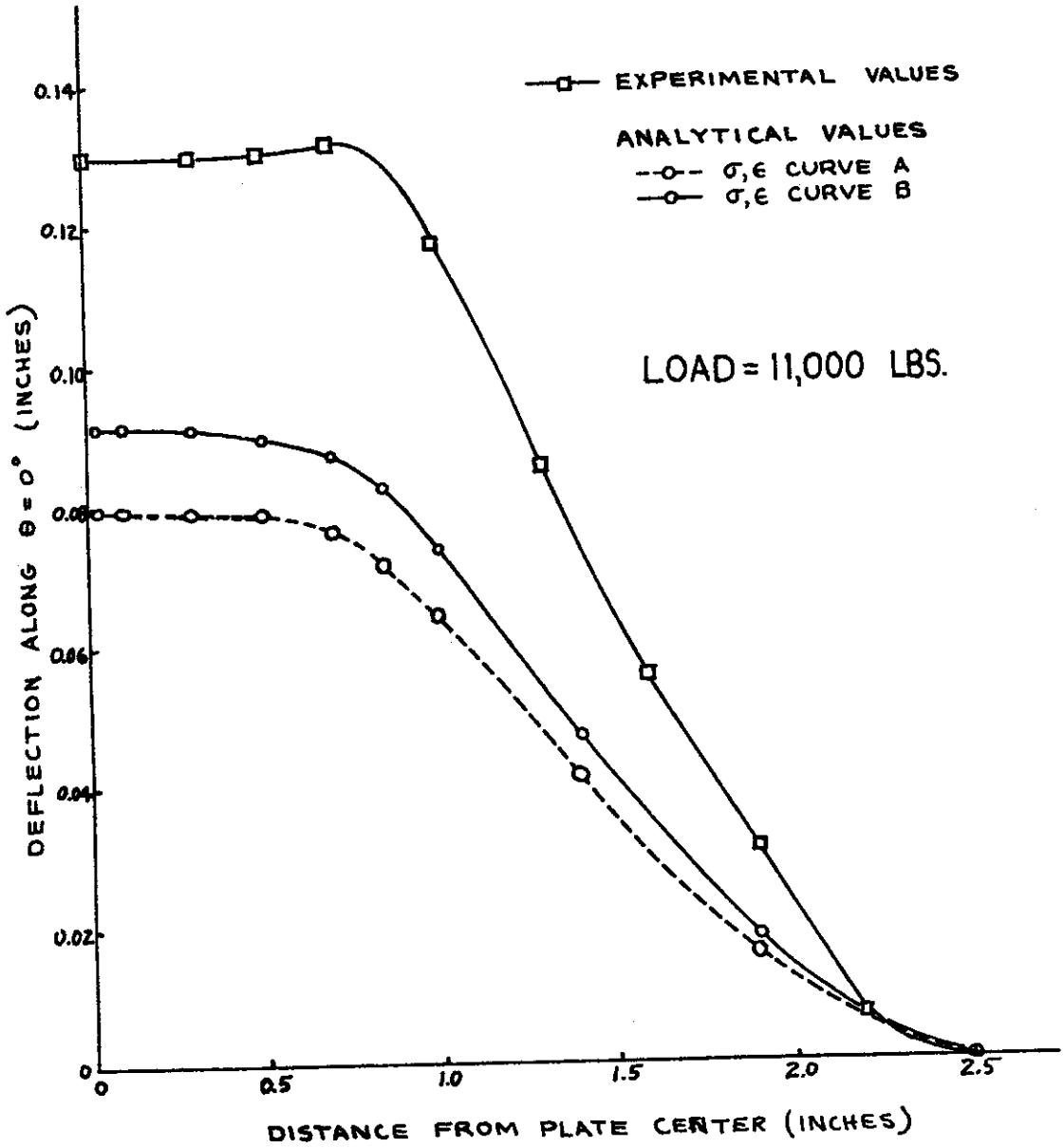

Figure 37. Meridional Variation in Deflection in the Plastic Range (θ = 0 Degrees)

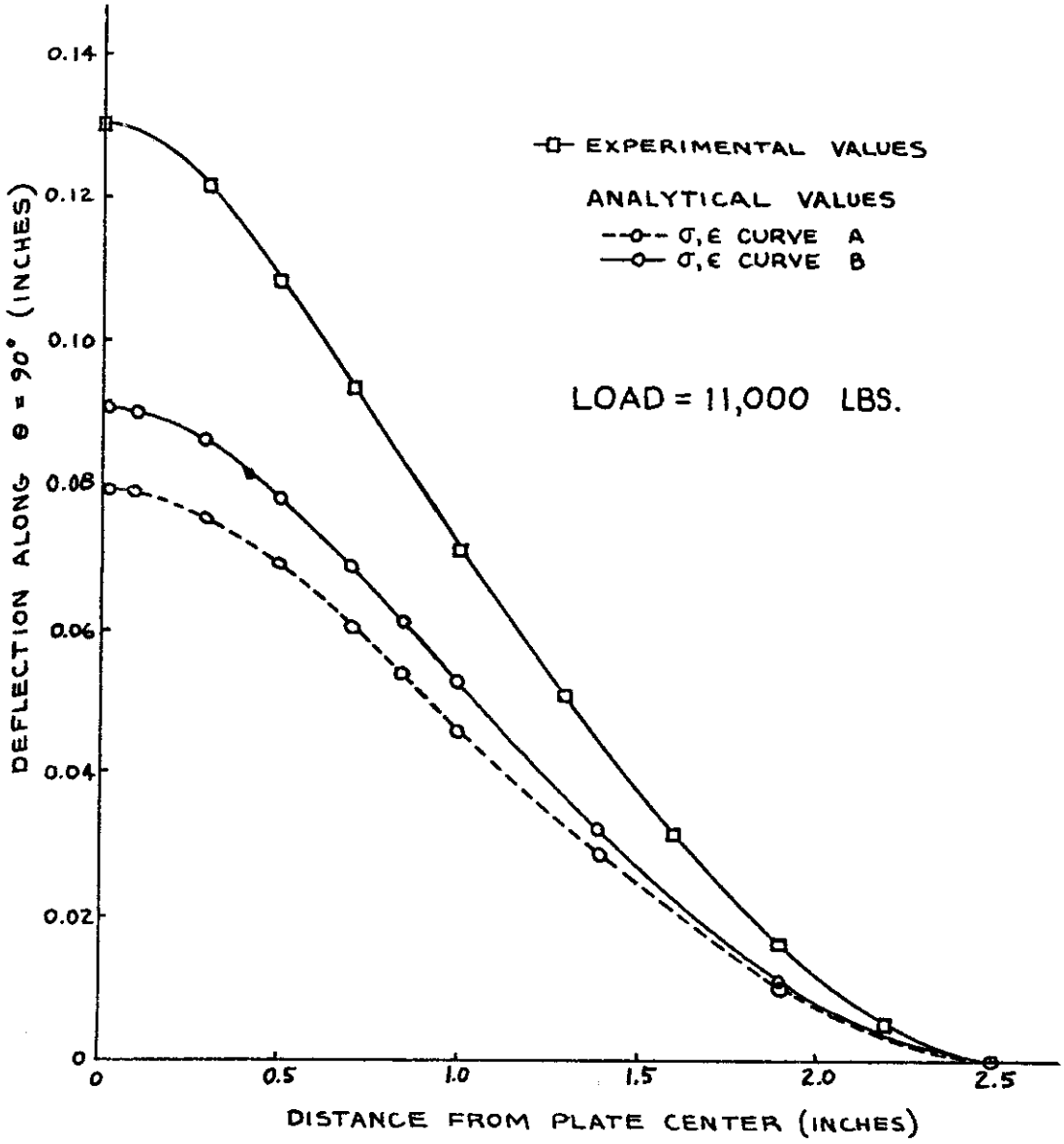

Figure 38. Meridional Variation in Deflection in the Plastic Range (θ = 90 Degrees)

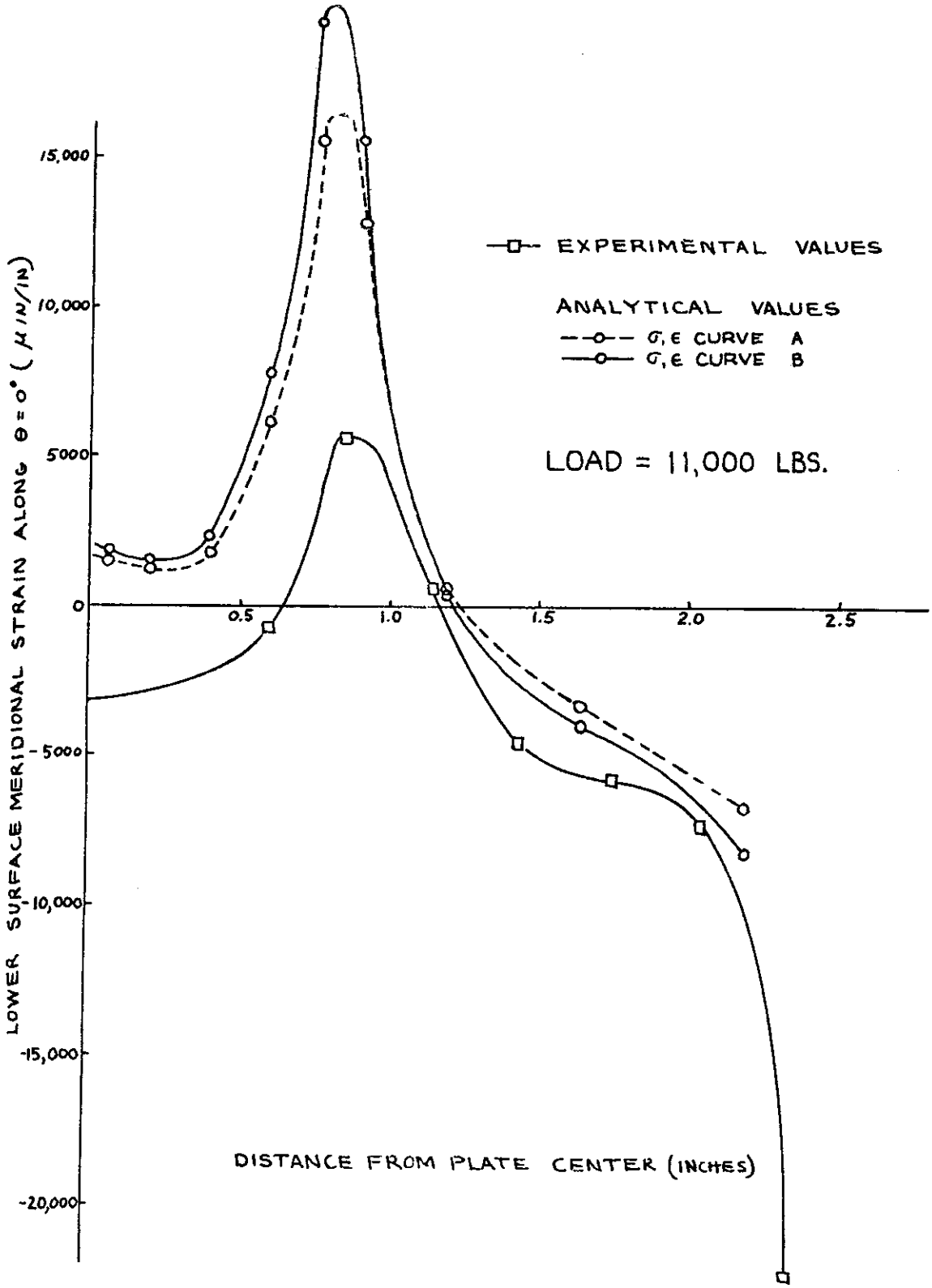

Figure 39. Meridional Variation in Lower-Surface Meridional Strain in the Plastic Range (θ = 0 Degrees)

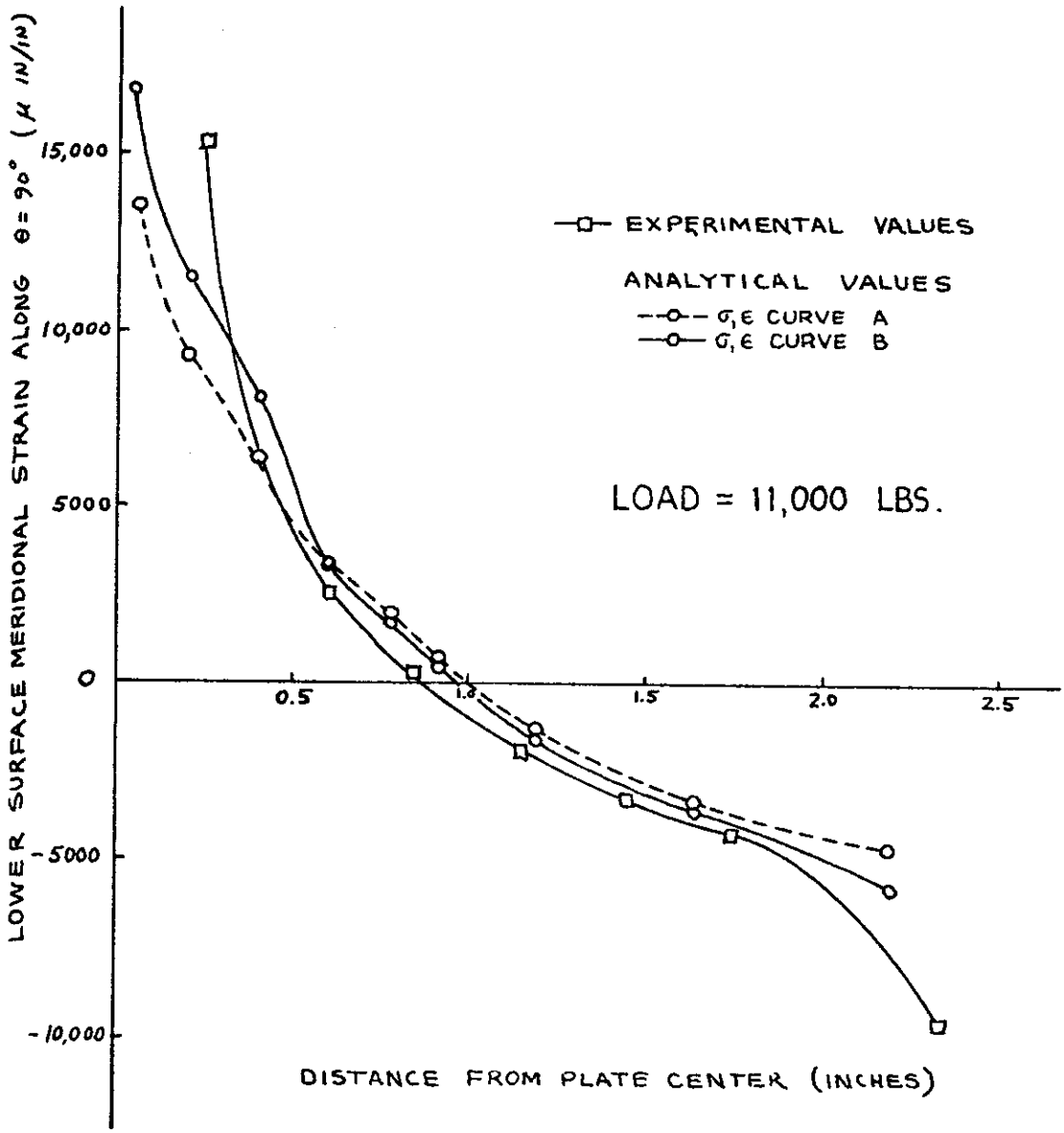

Figure 40. Meridional Variation in Lower-Surface Meridional Strain in the Plastic Range (θ = 90 Degrees)

Summary

The development of single-layer and bonded double-layer shell elements of revolution, solid elements of revolution, and a doubly-curved quadrilateral shell element has been reviewed, and their application to the linear elastic static analysis of a variety of axisymmetrically- and asymmetrically-loaded unheated and heated shells is presented. Comparisons with independent solutions show that the present discrete element predictions are reliable. An initial-strain formulation for the elastic-plastic small-deflection static analysis of axisymmetrically- and asymmetrically-loaded shells of revolution has been described, and the results of its application to an asymmetrically-loaded circular flat plate are compared with experimental data. Suggestions for improving the accuracy of these predictions are offered. Further details are given in the cited references.

Acknowledgments

In addition to the previously-acknowledged sponsorship of this research, we wish to acknowledge Mr. L. M. Boring of the MIT Aeroelastic and Structures Research Laboratory (MIT-ASRL) for his helpful assistance in preparing material for this paper. Former and current MIT-ASRL personnel who contributed to the studies reported herein include: Professor T. H. H. Pian, S. Atluri, Miss B. Berg, A. J. Cwiertny, Jr., J. N. Fowler, Mrs. S. French, S. Klein, W. M. Leveroni, Mrs. E. Mack, Mrs. P. Martz, R. B. McCallum, the late Dr. D. R. Navaratna, J. C. Speare, D. J. A. Stricklin, Jr., and F. Yin. The calculations were carried out largely at the MIT Computation Center.

SECTION V

REFERENCES

1. Meyer, R. R. and Harmon, M. B., "Conical Segment Method for Analyzing Shells of Revolution for Edge Loading", AIAA Journal, Vol. 1, No. 4, pp. 886-891, April 1963.

2. Grafton, P. E., and Strome, D. R., "Analysis of Axisymmetrical Shells by the Direct Stiffness Method", AIAA Journal, Vol. 1, No. 10, pp. 2342-2347, October 1963.

3. Klein, S., Matrix Analysis of Shell Structures, M. S. Thesis, Department of Aeronautics and Astronautics, Massachusetts Institute of Technology, Cambridge, Massachusetts, (also MIT-ASRL TR 121-12), June 1964.

4. Lu, Z. A., Penzien, J., and Popov, E. P., "Finite Element Solution for Thin Shells of Revolution", NASA Contract Report, University of California, Berkeley, July 1964 (also see J. Eng. Mech. Div., Proc. ASCE, pp. 119-145), Oct. 1964.

5. Percy, J. H., Pian, T. H. H., Klein, S., and Navaratna, D. R., "Application of Matrix Displacement Method to Linear Elastic Analysis of Shells of Revolution", AIAA Journal, Vol. 3, No. 11, pp. 2138-2145, November 1965.

6. Klein, S., "A Study of the Matrix Displacement Method as Applied to Shells of Revolution", AFFDL-TR-66-80, pp, 275-298 Conference on Matrix Methods in Structural Mechanics, W-P AFB Ohio, December 1965.

7. Klein, S. and Sylvester, R. J., "The Linear Elastic Dynamic Analysis of Shells of Revolution by the Matrix Displacement Method", AFFDL-TR-66-80, pp. 299-328, December 1965.

8. Pian, T. H. H. and Witmer, E. A., "Static and Dynamic Analysis of Re-entry Vehicle Shell Structures by the Finite-Element Method", Proceedings of the Oct. 19-21, 1965 DASA ABM Blast Vulnerability Conference, pp. 346-364, April 1966.

9. Jones, R. E. and Strome, D. R., "A Survey of Analysis of Shells by the Displacement Method", AFFDL-TR-66-80, December 1965, pp. 205-229 (Proc. Conf. on Matrix Methods in Structural Mechanics, W-P AFB, Ohio, Oct. 26-28, 1965).

10. Jones, R. E. and Strome, D. R., "Direct Stiffness Method Analysis of Shells of Revolution Utilizing Curved Element", AIAA Journal, Vol. 4, No. 9, pp. 1519-1525, September 1966.

11. Stricklin, J. A., Navaratna, D. R., and Pian, T. H. H., "Improvements on the Analysis of Shells of Revolution by the Matrix Displacement Method", Technical Note, AIAA Journal, Vol. 4, No. 11, pp. 2069-2072, November 1966.

12. Navaratna, D. R., "Computation of Stress Resultants in Finite Element Analysis", Technical Note, AIAA Journal, Vol. 4, No. 11, pp. 2058-2060, November 1966.

13. Witmer, E. A., Pian, T. H. H., Mack E. W., and Berg, B. A., "An Improved Discrete-Element Analysis and Program for the Linear-Elastic Static Analysis of Meridionally-Curved, Variable-Thickness, Branched Thin Shells of Revolution Subjected to General External Mechanical and Thermal Loads, Part 1 -- Analysis and Evaluation." SAMSO TR 68-310, Part 1 (also MIT ASRL TR 146-4, Part 1), March 1968. (AD 839242L)

REFERENCES (CONT)

14. Khojasteh-Bakht, M., Analysis of Elastic-Plastic Shells of Revolution under Axisymmetric Loading by the Finite Element Method, Department of Civil Engineering, University of California, Berkeley, SESM 67-8, April 1967.

15. Capelli, A. P., Nishimoto, T. S., and Radkowski, P. P., "The Analysis of Shells of Revolution Having Arbitrary Stiffness Distributions", Proceedings of AIAA/ASME 9th Structures, Structural Dynamics, and Materials Conference, Palm Springs, California, pp. 732-749, March 29-31, 1967.

16. Boring, L. M., Matrix Displacement Analysis of Shells with an Axisymmetric Midsurface but Having Circumferentially-Varying Structural Properties , MIT-ASRL TR 135-4, July 1968.

17. Klumpp, J. H., Lockheed Missiles and Space Co., Private Communication, December 1966.

18. Leveroni, W. M., Matrix Analysis of Bonded Double-Layer Shells of Revolution, BSD TR 67-153 (also MIT ASRL TR 121-13), July 1967.

19. Kotanchik, J. J., Discrete-Element Static Analysis of Bonded, Double-Layer, Branched, Thin Shells of Revolution. Part 1 -- Analysis and Evaluation. Part 2 --The SABOR 5 Program, MIT ASRL TR 139-6 (to be published).

20. Wilson, E. L., "Structural Analysis of Axisymmetric Solids", AIAA Journal, Vol. 3, No. 12, pp. 2269-2274, December 1965.

21. Becker, E. B. and Brisbane, J. J., Application of the Finite Element Method to Stress Analysis of Solid Propellant Rocket Grains, Rohm and Haas Co., Report No. S-76, Vol. 1, November 1965.

22. Wilson, E. L. and Jones, R. M., Finite Element Analysis of Axisymmetric Solids with Orthotropic Temperature-Dependent Properties, Aerospace Corporation TR-0158(53816-22)-1 (also BSD TR 67-228), September 1967.

23. Dunham, R. S. and Nickell, R. E., Finite Element Analysis of Axisymmetric Solids with Arbitrary Loadings, Dept. of Civil Engineering, University of California, Berkeley, Report No. 67-6, June 1967.

24. Yin, F.C-P., Discrete Element Analysis of Core-Stiffened Shells of Revolution, Massachusetts Institute of Technology, Aeroelastic and Structures Research Laboratory, TR 139-8, February 1967.

25. Speare, J. C., Discrete-Element Static Analysis of Core-Stiffened Shells of Revolution for Asymmetric Mechanical Loading, M. S. Thesis, Department of Aeronautics and Astronautics, MIT, June 1968.

26. Bogner, F. K., Fox, R. L., and Schmit, L. A., "A Cylindrical Shell Discrete Element", AIAA Journal, Vol. 5, No. 4, pp. 745-750, April 1967.

27. Utku, S., "Stiffness Matrics for Thin Triangular Elements of Nonzero Gaussian Curvature", AIAA Journal, Vol. 5, No. 9, pp. 1659-1667, September 1967.

REFERENCES (CONT)

28. Cantin, G. and Clough, R. W., "A Curved, Cylindrical-Shell, Finite Element", AIAA Journal Vol. 6, No. 6, pp. 1057-1062, June 1968.

29. Fowler, J. N., Elastic-Plastic Discrete-Element Analysis of Asymmetrically-Loaded Shells of Revolution, MIT, ASRL TR 146-3 (also BSD TR 67-193), July 1967.

30. Washizu, K. Variational Methods in Elasticity and Plasticity, Permagon Press Ltd., 1968.

31. Pian, T. H. H. and Tong, P., "Basis of Finite Element Methods for Solid Continua", Lecture notes of Professor Pian in the short course on "Finite Element Techniques in Structural Mechanics", College of Engineering, Cornell University, August 13-23, 1968.

32. Timoshenko, S. and Goodier, J. N., Theory of Elasticity, McGraw-Hill Book Co., Inc., New York, 2nd Ed., 1951.

33. Cwiertny, A. J. Jr., Thermal Stress Analysis of Single-Layer and Soft-Bonded Double-Layer Shells of Revolution, BSD TR 67-128 (also MIT ASRL TR 139-7), February 1967.

34. Novozhilov, V. V., Theory of Thin Shells, Noordhoff Ltd., Groningen, The Netherlands, 1959.

35. Greenbaum, G. A., "Comments on Numerical Analysis of Unsymmetrical Bending of Shells of Revolution", Tech. Note, AIAA Journal, Vol. 2, No. 3, pp. 590-592, March 1964.

36. Mack, E. W., Berg, B. A., and Witmer, E. A., "An Improved Discrete-Element Analysis and Program for the Linear-Elastic Static Analysis of Meridionally-Curved, Variable-Thickness, Branched Thin Shells of Revolution Subjected to General External Mechanical and Thermal Loads. Part 2 -- The SABOR 4 Program", SAMSO TR 68-310. Part 2 (also MIT ASRL TR 146-4, Part 2), March 1968. (AD 840614L)

37. Unpublished research in progress at the MIT Aeroelastic and Structures Research Laboratory by S. Atluri, T. H. H. Pian, J. Kotanchik, and E. A. Witmer.

38. Mar, J. W. and Wan, F., Lincoln Laboratory of the Massachusetts Institute of Technology, Private communications, 1966 and 1967.

39. Purdy, D., Air Force Flight Dynamics Laboratory, W-P Air Force Base, Ohio, Private Communications, 1966 and 1967.

40. Kalnins, A., "Analysis of Shells of Revolution Subjected to Symmetrical and Non-Symmetrical Loads", J. Appl. Mech. Vol. 31, No. 3, pp. 467-476, September 1964.

41. Bushnell, D. and Hoff, N. J., "Influence Coefficients of a Circular Cylindrical Shell with Rapidly Varying Parabolic Wall Thickness", AIAA Journal, Vol. 12, No. 12, pp. 2167-2173, December 1964.

42. McCallum, R. B. and Witmer, E. A., A Feasibility Study of the Analysis of Asymmetric Shells by the Discrete Element Method, MIT ASRL TR 135-5, September 1968.

REFERENCES (CONT)

43. Clough, R. W. and Tocher, J. L., "Finite Element Stiffness Matrices for Analysis of Plate Bending", Proceedings of Conference on Matrix Methods of Structural Mechanics, AFFDL-TR-66-80, pp. 515-546, December 1966.

44. Yao, J. C., "Bending Due to Ring Loading of a Cylindrical Shell with an Elastic Core", Journal of Applied Mechanics, pp. 99-103, March 1965.

45. Mendelson, A. and Manson, S. S., Practical Solution of Plastic Deformation Problems in the Elastic-Plastic Range, NASA TR R28, 1959.

46. Padlog, J. Huff, R. D. and Holloway, G. F., The Unelastic Behavior of Structures Subjected to Cyclic, Thermal, and Mechanical Stressing Conditions, WADD TR 60-271, 1960.

47. Percy, J. H., Loden, W. A., and Navaratna, D. R., A Study of Matrix Analysis Methods for Inelastic Structures, RTD-TDR-63-4032, 1963.

48. Pope, G. A Discrete Element Method for the Analysis of Plane Elastic-Plastic Stress Problems, RAE TR 65028, 1965.

49. Swedlow, J. L. and Yang, W. A., Stiffness Analysis of Elastic-Plastic Plates, GALCIT SM 65-10, 1965.

50. Argyris, J. H., "Continua and Discontinua", Conference on Matrix Methods in Structural Mechanics, Wright-Patterson AFB, Ohio, October 26-28, 1965.

51. Marcal, P. V., "A Comparative Study of Numerical Methods of Elastic-Plastic Analysis", AIAA/ASME Palm Springs Conference April 1967.

52. Armen, H., Jr., Isakson, G., and Pifko, A., "Discrete Element Methods for the Plastic Analysis of Structures Subjected to Cyclic Loading", AIAA/ASME Palm Springs Conference, April 1967.

53. Khojasteh-Bakht, M., Analysis of Elastic-Plastic Shells of Revolution under Axisymmetric Loading by the Finite Element Method, U. of C. Berkeley, Dept. of Civil Engineering, SESM Rept. No. 67-8, April 1967.

54. Bohnenblust, H. F. and Duwez, P., "Some Properties of a Mechanical Model of Plasticity", J. Appl. Mech. Vol. 15, No. 3, pp. 222-225, Sept. 1948.

55. White, G. N., Jr., Application of the Theory of Perfectly Plastic Solids to Stress Analysis of Strain-Hardening Solids, Graduate Division of Applied Mathematics, Brown University, TR No. 51, August 1950.

56. Prager, W. and Hodge, P. G., Theory of Perfectly Plastic Solids, John Wiley and Sons, Inc., New York, pp. 608, 1951.

57. Besseling, J. F., A Theory of Plastic Flow for Anisotropic Hardening in Plastic Deformation of an Initially Isotropic Material, National Aero. Research Institute, Amsterdam Report S. 410, 1953.

REFERENCES (CONT)

58. Balmer, H. A. and Witmer, E. A., Theoretical-Experimental Correlation of Large Dynamic and Permanent Deformations of Impulsively-Loaded Simple Structures, FDL-TDR-64-108, July 1964.

59. Leech, J. W., Finite-Difference Calculation Method for Large Elastic-Plastic Dynamically-Induced Deformations of General Thin Shells, AFFDL-TR-66-171, December 1966.

60. Prager, W. An Introduction to Plasticity. Addison-Wesley Publ. Co., Inc., 1959.

UNCLASSIFIED

Security Classification

DOCUMENT CONTROL DATA - R & D

(Security classification of title, body of abstract and indexing annotation must be entered when the overall report is classified)

1. ORIGINATING ACTIVITY (Corporate author)	2a. REPORT SECURITY CLASSIFICATION
Air Force Flight Dynamics Laboratory Wright-Patterson Air Force Base, Ohio 45433	Unclassified
	2b. GROUP N/A

3. REPORT TITLE

PROCEEDINGS OF THE SECOND CONFERENCE ON MATRIX METHODS IN STRUCTURAL MECHANICS

4. DESCRIPTIVE NOTES (Type of report and inclusive dates) Proceedings of the Air Force Second Conference on Matrix Methods in Structural Mechanics held 15-17 October 1969 at WPAFB, Ohio.

5. AUTHOR(S) (First name, middle initial, last name)

None

6. REPORT DATE	7a. TOTAL NO. OF PAGES	7b. NO. OF REFS
December 1969	1464	

8a. CONTRACT OR GRANT NO.	9a. ORIGINATOR'S REPORT NUMBER(S)
b. PROJECT NO.	AFFDL-TR-68-150
c.	9b. OTHER REPORT NO(S) (Any other numbers that may be assigned this report)
d.	

10. DISTRIBUTION STATEMENT

This document has been approved for public release and sale; its distribution is unlimited.

11. SUPPLEMENTARY NOTES	12. SPONSORING MILITARY ACTIVITY
	AF Flight Dynamics Laboratory AF Institute of Technology

13. ABSTRACT

The Air Force Second Conference on Matrix Methods in Structural Mechanics, held at Wright-Patterson Air Force Base, Ohio on 15-17 October 1969, was sponsored jointly by the Air Force Flight Dynamics Laboratory, Air Force Systems Command, and the Air Force Institute of Technology, Air University. The purpose of the conference was to discuss the recent developments in the field of matrix methods of structural analysis and design of aerospace vehicles. The forty papers presented were arranged into seven sessions: Structural Weight Optimization, Dynamics, General Elements, Curved Elements, Applications, General Methods, Nonlinear Analysis.

DD FORM 1 NOV 65 1473

UNCLASSIFIED

Security Classification

14. KEY WORDS	LINK A		LINK B		LINK C	
	ROLE	WT	ROLE	WT	ROLE	WT
Structural Analysis Methods Finite Element Methods Discrete Element Methods Matrix Structural Analysis Structural Dynamics						